Politecnico di Milano

SCHOOL OF INDUSTRIAL AND INFORMATION ENGINEERING

Master of Science – Energy Engineering

Techno-Economic Analysis of Multi-Tower Solar Thermal Power Plants

Supervisor:

Prof. Marco Binotti

Kilian Cooreman Magnus

916452

Academic Year 2020-2021

Acknowledgment

First, I would like to show my gratitude to Professor Marco Binotti for giving me the opportunity to work on this thesis and guide me through it, for all the support and patience during this long period.

I would also like to give a special thanks to Belen Rivas for being there with me every step of the way during my master’s degree and for overcoming together all the challenges that came along the way.

Thanks to my family for supporting me and pushing me to work harder and to always aim higher and challenge myself.

I want to also thank all my friends who have accompanied me and helped me overcome all my issues.

Abstract

With the technology innovation boom than renewables are experiencing new challenges arise, one of those is the dispatchability of the cheaper renewable option (PV and Wind), for this reason CSP poses a solution with its thermal storage and stabilizing the grid from intermittent sources like PV and Wind, what has been limiting the evolution of CSP is its high cost and LCOE that comes with it, which leaves CSP out of the competitive range of renewables.

The present study makes use of technological improvements within the CSP world, like the use of Sodium as a heat transfer fluid for high temperature applications and complemented with a sCO_2 cycle which has smaller size and higher efficiency than the Rankine cycles.

The focus of this work is to study a multi-tower approach regarding CSP in order to improve its efficiency and allow for easier implementation of the technology, since now a days CSP is known to be complex and requires a lot of invested hours for projects, while PV and Wind implemented a modular approach reducing the complexity of investing and engineering of power plants.

Multiple towers and thermal powers were simulated for comparison between them in a modular plant, starting from the modular towers up to simulating central receivers with high thermal powers, and then a performance and economic assessment of the different layouts and thermal targets was made.

For the implementation of multi-tower or modular approaches a very important factor rises, the piping for the plant, like parabolic trough the piping is very relevant in modular CSP and is further studied, from the designing up to the performance during operation of the plant.

The rest of the plant components were estimated from literature and used for modeling the complete plant.

Table of Content

List of Figures

List of Tables

1. Introduction to Solar energy and generating systems.

Solar energy can be dated as back as $(287 - 212\ BC)$ to Archimedes the famous Greek Mathematician and Philosopher, when he used reflective surfaces to focus the sun radiation into some Roman fleets burning them down [1], Although it sounds cool it was later proven by MIT students and MythBusters that it was provably unpractical and unlikely to have happened due to the moisture in the wood making it much harder to ignite and start a fire. [2]

Another early application of solar energy is in the orientation of the houses where Socrates described that the best layout would be with the main room aiming at the south [1], which holds true for the northern hemisphere, and this comes to show that solar energy has being there in our thoughts since the beginning of times in simple applications such as house orientations, nowadays apartments orientations can even increase the value of the apartment and all of this due to the solar energy.

During the early Renaissance, studies and applications were aimed at steam production mainly by reflecting surfaces. The famous inventor Leonardo Da Vinci performed experiments regarding parabolic mirrors for thermal energy for a dyeing industry. [1]

At the dawn of the Industrial Revolution, Solar Energy was no longer pursued due to lack of practical application since fossil fuels were abundant and cheap, and only experiments regarding its feasibility where conducted. [1]

It is like the old saying goes “You Reap What You Sow.” And that is exactly what is happening right now, due to the abuse of fossil fuels without consideration of the externalities we are now facing a huge climate change that most scientist are trying to figure out how to stop, and it will take world collaboration to stop it without risking economic recession and grid reliability. Renewables are now taking over with huge expansion in terms of installed capacity and energy produced due to different incentives from governments making it more feasible to invest in them, even for self-consumption at home with PV modules.

As we can see Solar Energy, specifically concentrating solar energy has been there for a while and has had ups and downs regarding technological improvement, it was fossil fuels which slowed down its development during the industrial revolution and now CSP technology is looking to replace fossil fuels with clean energy production, mainly due to the contamination and the fact that renewable technologies are as its implied in its name renewable while fossil fuels are the opposite.

1.1. Solar Energy

The Sun behaves as a Blackbody at the temperature of $5777\ [K]$, inside of it its fusion process occurs where Hydrogen combines until it forms Helium, Figure 1-1 shows the process called Proton-Proton Chain Reaction, this process generates energy, and this energy goes from its core to its surface and then its emitted towards the universe in the form of radiation. [3]

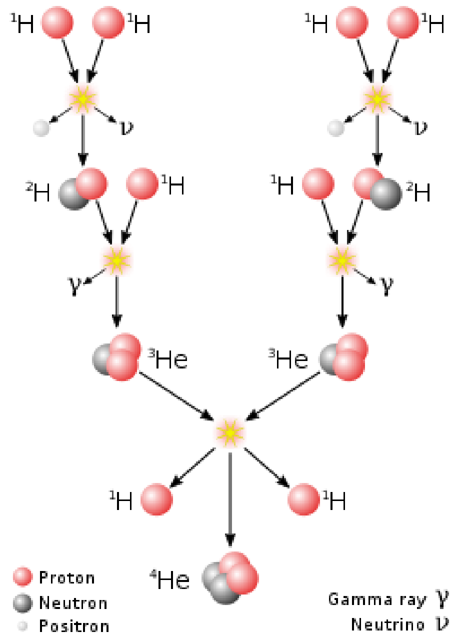

Figure 1-1: Proton-Proton Chain Reaction of the Sun. [3]

The sun irradiates a total of $3.8 \times 10^{14}\ [TW]$ to the whole universe, but only a fraction of that energy is caught by the Earth, this is due to the distance between the Sun and the Earth $(1.495 \times 10^{11}\ [m])$ (Figure 1-2).

The fraction reaching the outside atmosphere of Earth is $175000\ [TW]$, while the one reaching ground level is $89000\ [TW]$, while the world net consumption of electricity in 2018 was of $23400\ [TWh]$ [4].

This comes to show the potential of the solar energy, although the value is overestimated since we cannot physically use all the available space for solar energy, but it does give a rough estimate of its power.

If we look at Chile, it has a solar energy potential of $1340\ [GW]$ [5]:

- By adding 25-30 $[GW]$, supplies the whole electricity consumption of Chile. [5]
- By adding 200 $[GW]$, its able to supply 30% of South America's demand. [5]
- With 2.5 $[GW]$ its able to supply 30% of the demand for green hydrogen of Japan by 2030. [5]

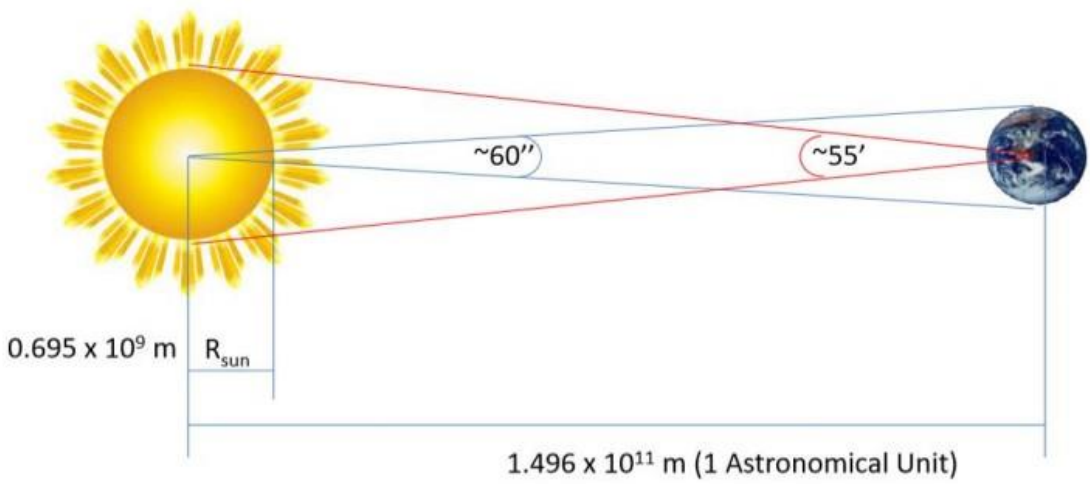

Figure 1-2: Sun and Earth distance and angles. [6]

The Direct Normal Irradiance (DNI) is the amount of solar radiation received in a collimated beam on a surface normal to the sun at its current position in the sky, it is measured in $[W/m^2]$ and its values ranges in between $(0\ and\ 1000\ [W/m^2])$, while the Direct Normal Irradiation measures the energy over a 60-minute period of the Irradiance and its measured in $[Wh/m^2]$. [6]

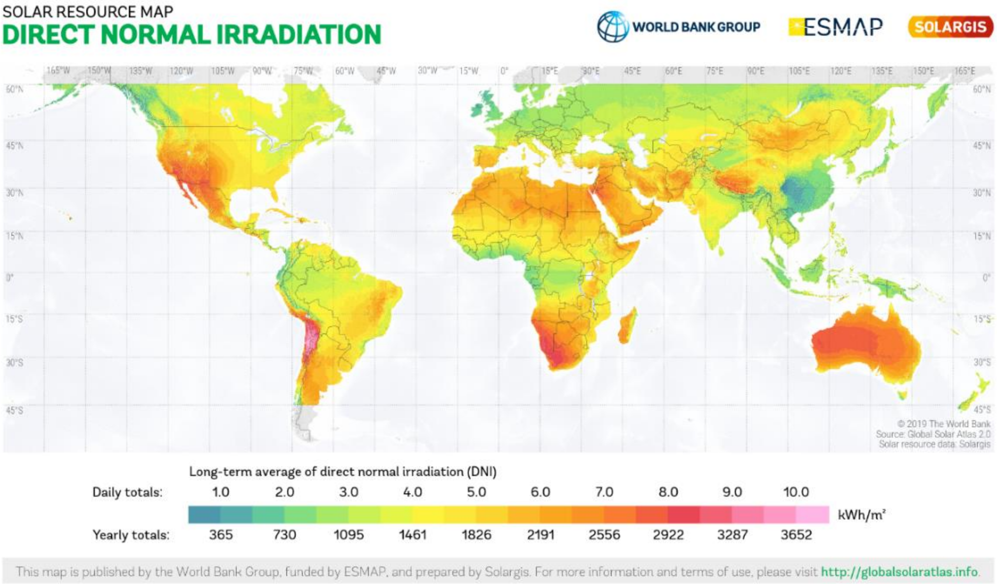

Figure 1-3: Direct Normal Irradiation (DNI) World Map [7]

The yearly sum of DNI is measured in $[Wh/m^2y]$ and good values for the implementation of solar plants are ($> 1800[Wh/m^2y]$) [8], so looking at Figure 1-3 we see that the potential for solar plants is huge, with outstanding performance in the north of Chile, and very good performance on Australia, USA and Africa.

Another way of measuring the radiation reaching the Earth is the Global Horizontal Irradiance (GHI). This value is useful for PV since it considers DNI and Diffuse Horizontal Irradiance (DIF) [9], and PV can harness diffuse radiation while CSP cannot. Figure 1-4.

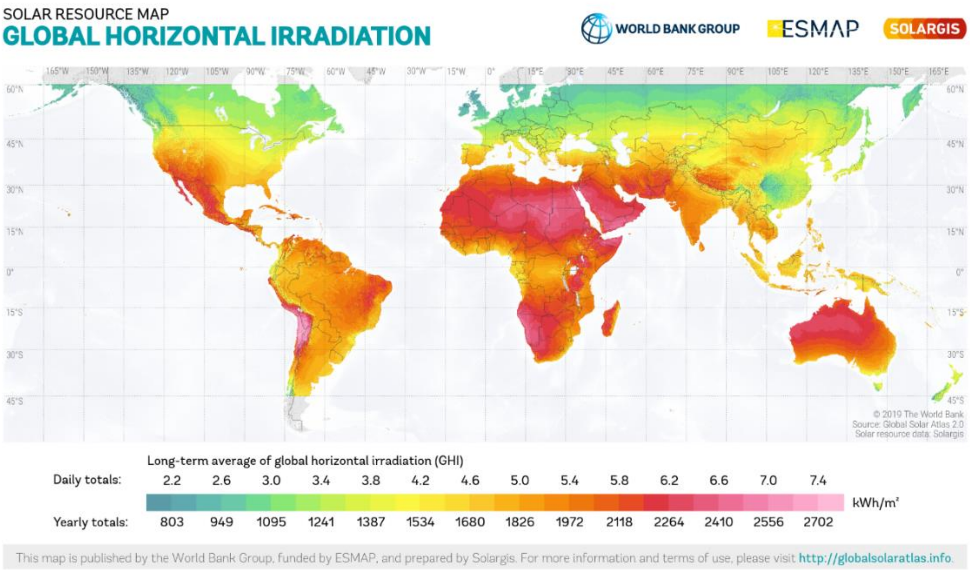

Figure 1-4: Global Horizontal Irradiation (GHI) World Map [7]

One important value in terms of generation is the Levelized Cost of Electricity (LCOE), which is calculated by setting the net present value of the power plant to zero over its lifetime [6], it is the most common tool used for comparing different plants and technologies and it can be calculated by:

$$LCOE\left[\frac{\$}{MWh}\right] = \frac{Total\ plant\ costs \cdot CRF + Fixed\ O\&M}{Yearly\ Electricity\ Production} + variable\ O\&M \qquad \text{Eq. 1}$$

On Figure 1-5 we see the improvement of different renewable technologies in terms of LCOE where solar technologies PV and CSP have shown the greatest decrease on costs compared to other renewables, where PV now competes with fossil fuels costs whereas CSP still has some way to go to be more competitive with current technologies.

Another tool which is not as common as the LCOE is the Life Cycle Assessment (LCA) which is used to estimate the environmental impacts of the whole process of a products life, from production up until finishing its life cycle [6], this is an important tool since renewable technologies are aimed at reducing the environmental impacts of fossil fuels. But for the scope of this thesis the LCA will not be considered, but for further studies it should be noted.

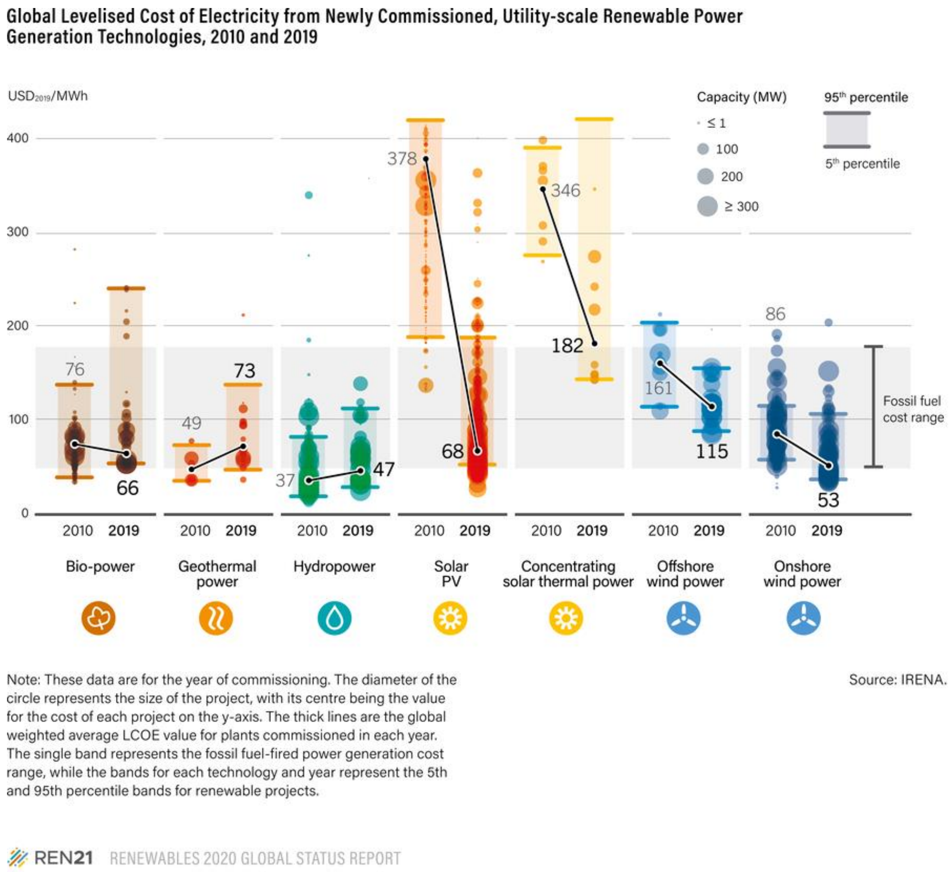

Figure 1-5: LCOE variation of different renewable technologies from 2010 to 2019, from REN21. [10]

1.2. Photovoltaic Systems

Photovoltaic systems convert the radiation from the sun into electricity using the photovoltaic effect which generates a Voltage and an electric current by absorbing the energy from the photons. PV modules consist of usually 60-96 solar cells connected in a series configuration, this modules and cells are made of semi-conductors with the one most used (Si), different technologies have emerged like, Mono and Poly crystalline silicon, bifacial modules and thin film technologies, each of those with its advantages and disadvantages, for example bifacial modules can absorb direct diffuse and albedo irradiance, while CSP can only make use of the direct sunlight.

This technology is highly modular, with modules having the same size and a very simple installation process, modules keep on improving their efficiencies as installation become more and more common, due to this repetitive process of installation and production overall costs related to this technology can be scaled down, simplicity can go a long way if well applied.

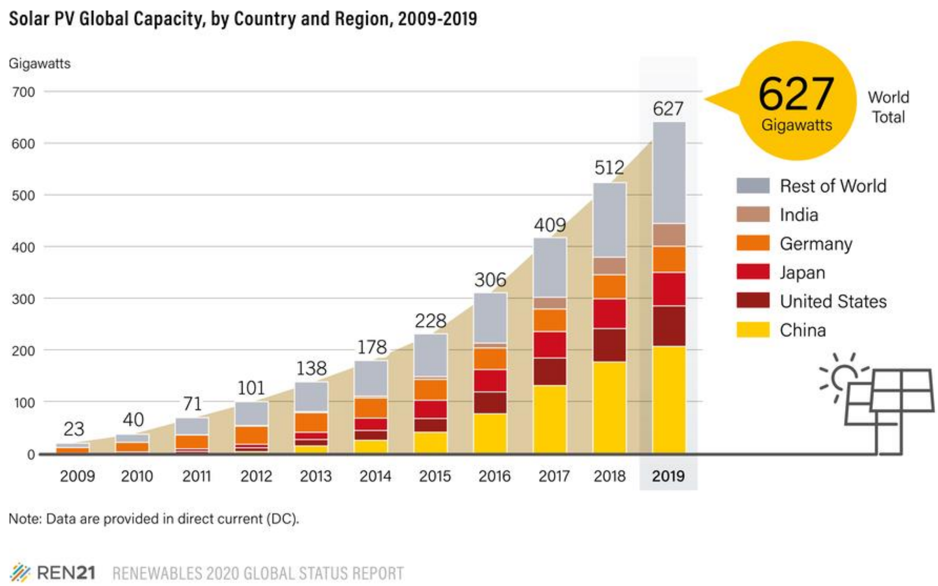

Figure 1-6: Solar PV Global Capacity, taken from REN21 trends report. [10]

PV modules have shown that they are flexible in terms of applications, where it can be applied to utility scale plants up until small scale residential application due to its modularity, this flexibility has helped its pursue and cost scaling to competitive ranges, on Figure 1-6 we see the increase in installed capacity with an exponential curve starting at around 2013 where in 6 years the installed capacity went from 138GW to 627GW, comparing it with 2010 where it only had 40GW its 15-16 times more than in that year, if we compare this with Figure 1-5 we understand the extreme reduction in terms of costs for PV installations, this gives us a sense of the power that simplicity, modularity and wide range of applications can do to a technology.

1.3. Concentrated Solar Power Systems

Concentrated Solar Power or also known as CSP, concentrate the incoming solar radiation into a Heat Transfer Fluid (HTF) which usually consists of Water/Steam, Oil or Molten Salts depending on the type of technology used. CSP usually generate electricity ranging from 10kW up to several 100MW [11]. The main advantage of this technology is its ability to store thermal energy, and with this it can ensure production when the sun is not shining, so the comparison between CSP and PV comes up, we should be considering PV-Battery system and not a PV-Only system for comparison, because only then we would be considering similar conditions.

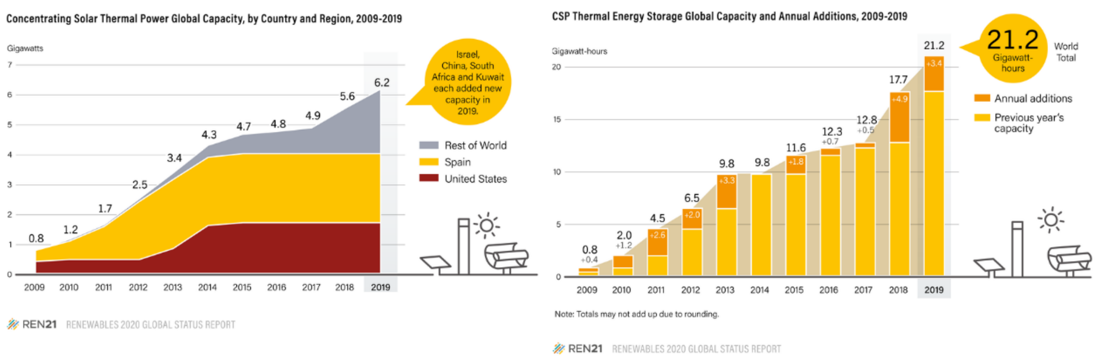

Figure 1-7: CSP Global Installed Power and Storage Capacity, taken from REN21 trends report. [10]

If we look at Figure 1-7, we see that CSP technology has been exploited mainly by USA and Spain on the past but it was no longer pursued by them, nowadays its China who is focusing on renewable technologies increasing its installed capacity and with that investing in CSP technology, this could be a tipping point for scaling up the costs of CSP and making it cheaper and more feasible.

By looking at Figure 1-7, we can see the amount of energy storage installed over the world and the newly installed capacity, from 2018 we see an increase of interest in this technology and a study from 2019 showed that the LCOE global average of CSP lowered 26% in 2018 compared to 2017, and 46% compared to 2010, achieving even lower LCOE values than natural gas peaking plants (under certain conditions). [10]

Some plants include PV or Wind with CSP, like “Cerro Dominador” in Chile which combines CSP with PV. Another option for CSP plants is the application of a Combined Heat and Power (CHP) cycle to increase the efficiency of the plant by making use of the remaining thermal power after the power block cycle. Table 1-1 shows performances of CSP technologies, these values are for reference since the location and tracking method will influence the value.

Table 1-1: Different CSP Technologies Performances. [6]

	Linear Focus		Point Focus	
	Parabolic Through	Linear Fresnel	Solar Dish	Solar Tower
Concentration Ratio	~ 90	~ 160	> 2500	$\sim 500 - 800$
Nominal Optical Efficiency (%)	~ 76	~ 64	~ 80	$\sim 65 - 75$
Yearly Average Optical Efficiency (%)	$\sim 50 - 55$	$\sim 35 - 40$	~ 70	$\sim 57 - 65$

1.3.1. Parabolic Trough

Parabolic Trough (PT) systems consist of parabolic shaped mirrors which concentrate the sun rays into the focal length of the mirror shape, at this focal length a tube containing the heat transfer fluid is located, covered by a steel pipe with a coating and placed inside an evacuated glass tube, this glass tube and the coating are meant for reducing the convective and the radiative losses, respectively. [11]

This technology is nowadays the most mature technology of CSP, on 2018, 90% of all CSP plants were Parabolic Trough. [12]

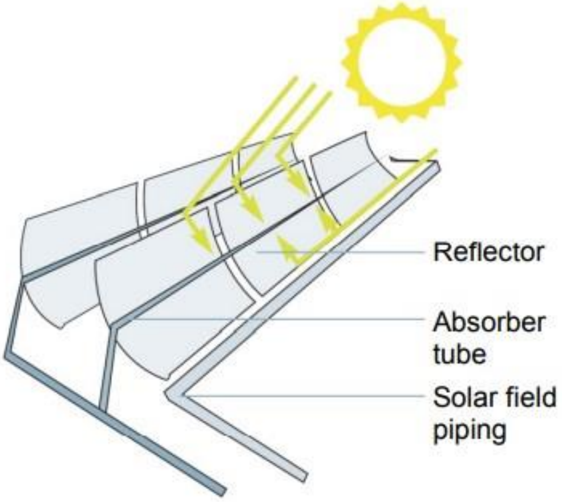

Figure 1-8: Parabolic Trough Concept. [10]

The most used fluid for this application is thermal oil, which is usually increased from 293 ℃ up to 393 ℃ [12], then this heat is transferred to the power block usually a steam generator or to the storage systems depending on whether it has one or not.

This type of system counts with a one axis tracking system which can be N-S or E-W, where N-S oriented has the highest electric production but has high variations from month to month, while E-W configuration has a more stable production but with a lower yearly production, so N-S is usually chosen due to higher production. [6]

One advantage of Parabolic Trough is its modularity where one plant can be scaled up accordingly to energy demand needs, one example of this is the SEGS complex in California, USA, where the first plant was inaugurated in 1984, and over the years it was scaled up to 354 MW of installed capacity [13]. Modularity also helps in terms of production where one system can be fitted to different places or locations, increasing the production of one type of process scaling down the costs of production and engineering. Figure 1-9 shows an installed plant using PT.

Figure 1-9: Parabolic Trough Plant, CSP Spain Orellana. [14]

1.3.2. Linear Fresnel

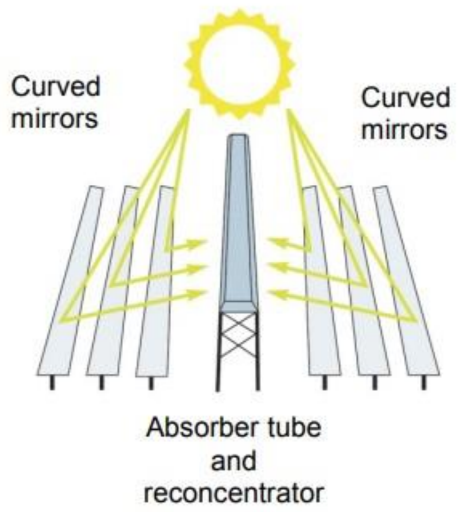

Figure 1-10: Linear Fresnel Concept. [10]

Linear Fresnel as its name suggests is another type of CSP linear focus system, it is named after the Fresnel lens which has multiple refracting lens, this type of technology is a mixture between Parabolic Trough and Solar Tower, since its still a linear tube receiving the heat but instead of the parabolic mirror moving with the tube in this case there are sets of mirrors which reflect the sun rays independently onto the receiver, like the Solar Tower heliostats. [15]

Usually, a secondary concentrator is placed at the top of the receiver to improve the optical efficiency of the system, they are more space efficient since the mirrors are placed on the ground unlike PT, which creates bigger shadows, so more space needs to be used, in terms of convective heat transfer PT is better since Linear Fresnel does not use glass to reduce these losses.

If we look at Table 1-1, Linear Fresnel can achieve higher concentration ratios than PT, making it more suitable for working with higher temperatures, and by operating at higher temperatures you can use higher efficiency power block cycles improving the thermal to electricity efficiency.

1.3.3. Parabolic Dish

Parabolic Dish is a type of point focus CSP technology, it uses its parabolic geometry to concentrate the incoming rays into a single focal point unlike PT which concentrates rays into a line, due to this point focus its able to achieve higher much higher concentration ratios than other technologies, it is also the most efficient of CSP in terms of optical efficiency and its modular, so a plant can consist of multiple dishes or for small scale applications a single dish, this makes the technology flexible and efficient. [16]

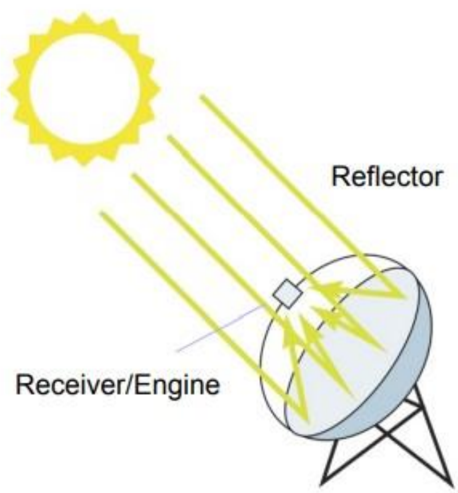

Figure 1-11: Parabolic Dish Concept. [10]

They use 2-axis tracking systems usually driven by an electric motor, and they heat up a heat transfer fluid reaching temperatures of around 750 ℃ integrated in a Stirling Engine to produce electricity, this technology has the potential to become the least expensive source of renewable energy. [17] [11]

1.3.4. Solar Tower

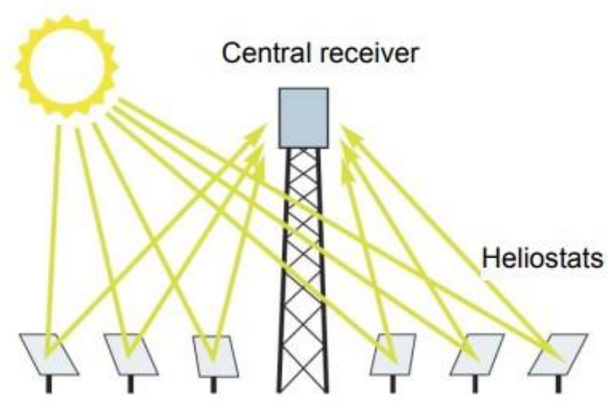

Figure 1-12: Central Receiver Concept. [10]

Solar Towers are also known as central receivers, this system consists of a solar field of mirrors (called heliostats) which reflect the incoming radiation onto a Receiver at the top of the Tower, through the receiver the thermal energy is absorbed by the HTF which goes then moves along the piping system into a Power Block (PB) or to the Thermal Storage, each of these components are explained more in depth later, since the scope of the study is related to this technology.

The Heliostats have a 2-axis tracking system to better follow the sun path and aiming strategy onto the receiver, there are different sizes of heliostats depending on the capacity and size of the plant, where increasing its size brings some benefits and some disadvantages compared to smaller size heliostats. For example, at Jemalong Solar Plant they use heliostats with an area of $3.6\ [m^2]$ while at Cerro Dominador they have $140\ [m^2]$, these plants operate a $1\ [MW_e]$ and a $110\ [MW_e]$ respectively [18] [19], highlighting the difference in heliostat sizes.

For the Receiver there are different sizes and types all dependent on the capacity of the plant, the higher the capacity usually the bigger the receiver size, the size is also influenced by the piping material and the HTF since they impose a limit on the maximum temperature and peak flux over the receiver. While the tower height is also dependent on the plant capacity having higher tower heights for higher fields, this is because the optical efficiency for large solar fields is heavily influenced by the tower height.

Different HTF are being investigated for Solar Tower applications, but the commonly used one is Molten Salts or Water, being the first one more common, Molten Salts limit the maximum temperature to about $565\ ℃$, also limiting the power block operating temperature, nowadays the path for increasing the efficiency is the use of supercritical power cycles which operate in the range of $600℃ - 800℃$, so better materials and fluids must be investigated in order to achieve this range, a promising HTF is Sodium which has some technical barriers but good performance for CSP applications. [18]

Some Solar Towers use Thermal Storage systems to improve its capacity factor, while direct steam generators face complexity and costly methods for thermal storage, while molten salts became the leading technology for thermal storage due to it being cheap with high heat capacity [18], if we take Sodium as a thermal storage it becomes economically unfeasible due to its cost compared to molten salts, a study determined that Sodium was more feasible only for low storage systems of $(< 3\ h)$. [20]

2. State of the Art

A careful review of the State of the Art of the technology is fundamental for a good investigation on a given topic, in this case a general review of the CSP state is investigated and a more detailed study is given to some modular technologies that have emerged in the CSP industry to have knowledge on what is available and what is the focus of today's research activity regarding CSP's future.

The four technologies mentioned before are the one generally looked at in the CSP industry, Parabolic Trough and Linear Fresnel have fundamental limits due to limits in their concentration ratio, while Solar Tower and Parabolic Dish can achieve much higher concentration ratios, but on the same time they require a more complicated tracking system and a higher degree of complexity. [21]

In the past (2013) Parabolic Trough was the go-to option regarding CSP, it was cheaper and easier to implement than the other technologies, while now a day's PT and Solar Tower are the one dominating the CSP market, Linear Fresnel and Parabolic Dish are still not widely popular with some small plants under construction or development. [21]

2.1. Multi-Tower Approaches

The main goal from Multi-Tower approaches is to increase the overall optical efficiency of the plant, which currently is a big issue for very large field which reach much lower optical efficiency than the smaller fields, so to solve this issue multiple approaches have been looked at, the main two approaches regarding multi-tower are:

1) "Multi-Tower Multi-Aiming": This one consists of multiple towers and heliostat fields, but the heliostats can aim at multiple towers depending on the sun position (searching for a better optical efficiency). [22]
2) "Multi-Tower Assigned-Aiming": While this one consists of multiple towers and heliostats which are somewhat independent, and the heliostats have a single receiver aiming point for each module. [22]

From now on, the second one will be called modular approach because of its modularity where each module is independent from the others.

Research on the topic of "Multi-Tower Multi-Aiming" has been there since 2002 with [23] where the idea of that research was to overlap heliostat fields from multiple towers to make better use of the ground, because the farther the heliostats are the more space in between there is to avoid shading losses, so in this research that unused space is used by another heliostat aiming at another tower, Figure 2-1 shows the layout of the towers and Figure 2-2 shows a simple view of two overlapping towers with their heliostat fields, while it is true that most of the heliostats have single point aiming like the modular type, there are sections where the field from more than two towers overlap and in that case it was more complex and a multi-aiming strategy was adopted. This layout saw improvements on the ground usage but has never been employed.

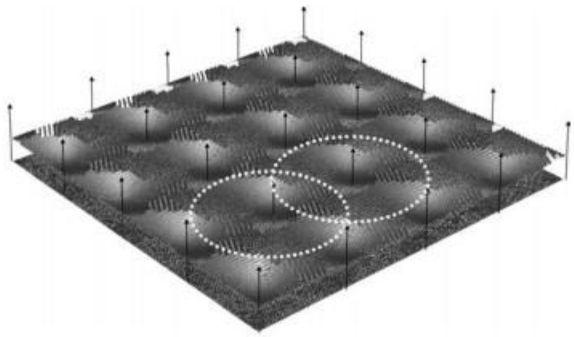

Figure 2-1: Layout of multi-tower arrangement with overlapping heliostat fields. [23]

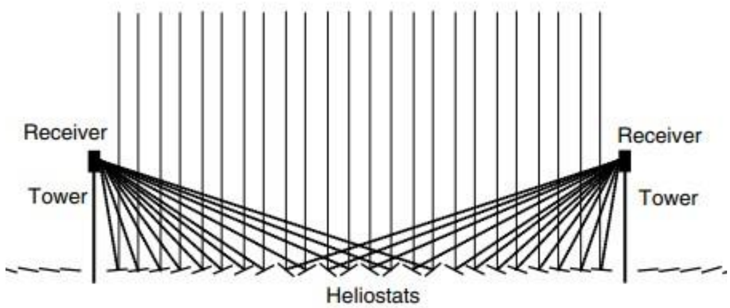

Figure 2-2: Two towers with the overlapping heliostat fields. [23]

Later, in 2011 more research multi tower where conducted, now using a more modular approach but with and without a multi-aiming strategy, where it used similar layout than those of Sierra Sun Tower but on a smaller scale using towers of only 16.7 meters high and a plant layout very similar to parabolic trough as can be seen in Figure 2-3, the results showed an improvement regarding the annual optical efficiency, where having multi-aiming strategy on the heliostats proved to have an even higher impact than the one with no sharing, but sharing the whole set of heliostats from NSEW showed only a little improvement over sharing only EW heliostats. [24]

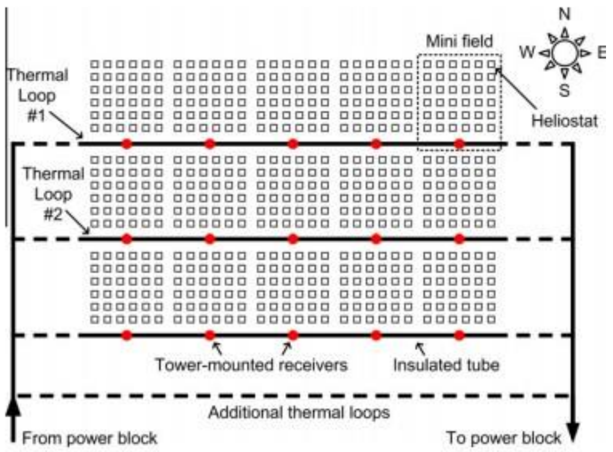

Figure 2-3: Field layout for proposed for research, using mini SierraSun towers and heliostat fields. [24]

More recently two studies regarding “Multi-Tower Multi-Aiming” have been conducted, focusing on the simulation and design considerations of implementing a second tower to improve the optical efficiency of a large solar field for a single tower.

One of those studies simulated two towers which were on the same horizontal line and the heliostats which were in between changed the tower to which they were aiming depending on the sun position, different distances between towers where simulated to find the optimal distance for better optical efficiency, the main conclusion from this paper was that there was an optical efficiency improvement of up to 8% when comparing to a single tower but when compared to two independent fields the improvement was less than 1%. [25]

While the other study also involved a second tower, in had a different approach by selecting the place of the second tower in a more convenient place improving the worst heliostats from the initial single tower field, Figure 2-4 shows the single tower and the multi tower simulations where there is a clear evidence of optical improvement on the south heliostats. The study went further and simulated different thermal targets and concluded that for targets higher than $400\ MWth$ a multi tower approach yielded a better LCOH when compared to single tower [26]. This is due to that higher power require larger heliostat fields which in turn yield lower optical efficiencies, and this is where multi tower and modular approaches come in handy.

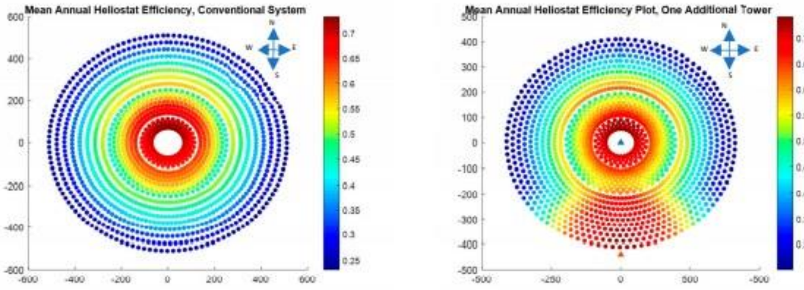

(a) (b)

Figure 2-4: (a) Conventional Single Tower Field. (b) Multi-Tower Field. [26]

Small fields have shown to improve the optical efficiency and allow for an easier flux control over the receiver, whereas big fields have higher attenuation and spillage losses, and increases the complexity of controlling the flux distribution over the receiver. [22]

Regarding modular technologies, different companies have worked on modular approaches which we will discuss later, but so far it seems that the one from Vast Solar has had the best success, while in terms of research there is a relevant chapter from the book Green Energy and Environment which simulates multiple plant layouts and compares the obtained LCOE and performance, figure xxx shows results in terms of LCOE for the different single tower plants and multi-tower plants, where we can see that not always the best solution is given by a single tower. For a 306 $MWth$ plant a multi-tower consisting of 6 towers each with a thermal power of 51 $MWth$ was the best solution, achieving an LCOE of 115 [$\$/kWh$] [22].

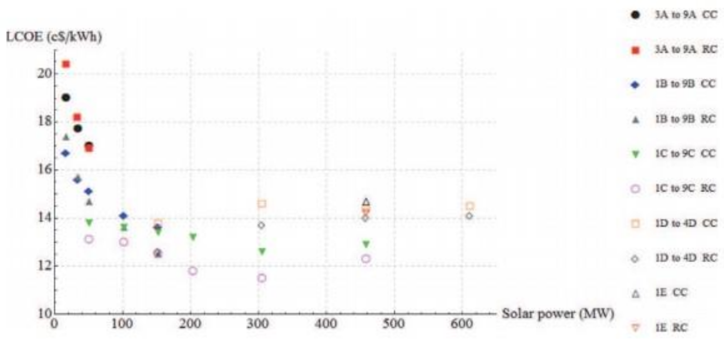

Figure 2-5: LCOE for the different plant configurations. [22]

One limiting factor of small-scale power plants is the lack of cost-effective and efficient power cycles for low capacity, where the higher the capacity the lower the specific costs related to the power block components. [22] This is a very important factor to consider when employing modular approaches or small-scale power plants for developing countries or cities where you could start small and increase with time the modules and capacity, because right now the high capital required, and the risk associated will not allow for the development of those type of projects.

Main research regarding Multi-Tower technologies have been in the form of heliostats having the choice to aim at two or more towers at different points in time, while in practice a modular approach is used where each set of heliostats aims at a certain tower independent from other modules, moving forward the modular choice is the one investigated in this work for the multi-tower approach due to its simpler and more practical approach.

2.2. Modular Technologies

One big disadvantage of Solar Towers is that they lack modularity and simplicity, if we take for example PV and Parabolic Trough they are modular, which has allowed these technologies to create economies of scale on the production of materials and reduce their costs making it more economically attractive, PV technologies is a very clear example of this where all modules are similar in size and can be easily implemented on different situations, from residential applications to large scale generation, and we see that PV technologies have decreased significantly its costs and LCOE over the years as seen in Figure 2-6.

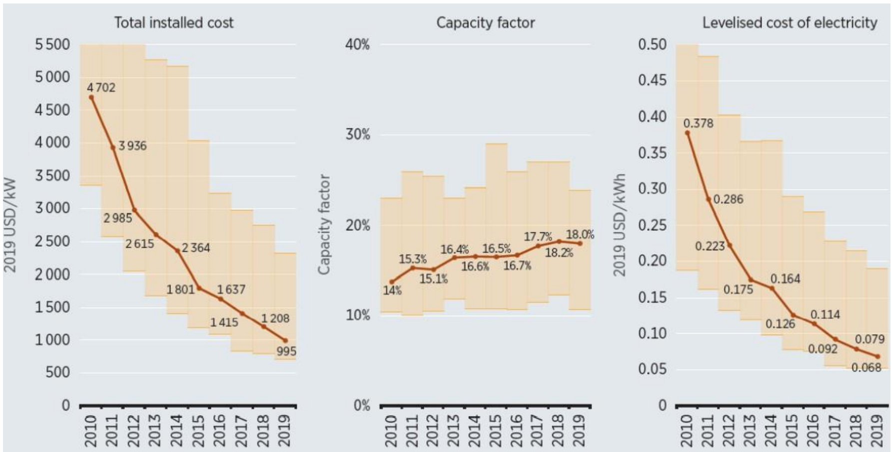

Figure 2-6 PV Technology Improvement Over the Years. [27]

Therefore, a possible approach on decreasing the costs of Solar Towers is to implement a modular technology which can be implemented for small applications and then scaled up for bigger applications, it can start small and over the years increase its capacity with an increase in demand or it could even start on a big scale for developed countries which require a big plant, delivering the same capacity but with the advantage of modularity and simplicity.

There have been different approaches to modularity of Solar Towers, each with its unique solution but most of these have a common Solar Field approach which is a Polar Field, this means North Oriented if we are on the Northern Hemisphere, while South Oriented for the Southern Hemisphere, the reason behind this is to increase the optical efficiency by means of increasing the Cosine efficiency of the heliostats, which can be explained by Figure 2-7 where the Effective reflector area is higher for heliostats which are opposite to the sun with respect to the Tower.

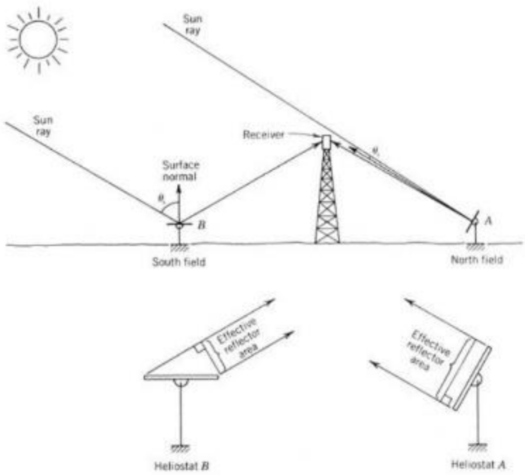

Figure 2-7 Illustration of the Cosine Efficiency on the Heliostats [35]

Table 2-1: Summary from small CSP towers investigated.

	Aora Solar	**eSolar**	**Solarstor**	**Vast Solar**
Location	*Ethiopia*	*California*	*Lake Cargelligo*	*Jemalong*
Power $[MW]$	0.1	5	3	1.2
Heliostat Number $[-]$	$1x52$	$2x12000$	$8x100$	$5x700$
Heliostat Size $[\mathbf{m^2}]$	$-$	1.136	9.8	3.6
Storage	*None*	*None*	*Graphite*	*Sodium*
Tower Height $[\mathbf{m}]$	30	55	24	27
Receiver Type	*Cavity*	*Cavity*	*Cavity*	*Billboard*
Receiver Size $[\mathbf{m^2}]$	$-$	$-$	$-$	2.25
HTF	*Air*	*Steam*	*Steam*	*Sodium*

2.2.1. Aora Solar

Aora Solar "The Tulip" consists of a solar-hybrid plant which heats air into a micro-gas turbine to produce 100 $[kW]$ of electricity and in addition to the electricity it produces 170 $[kWt]$ of thermal energy as a by-product functioning as a Combined Heat and Power (CHP) plant [28]. The name comes from its design which resembles a Tulip as we can see in Figure 2-8.

Figure 2-8: Aora Solar, Pilot CSP plant with a Solar-Hybrid micro-gas Turbine [29]

A more detailed look at the components and the flows can be seen in Figure 2-9, where all the components of the plant are shown illustrating its operation. This system has 3 operating modes depending on the solar radiation at the time, these modes are:

1. Solar Only Mode
2. Hybrid Mode
3. Fuel Only Mode

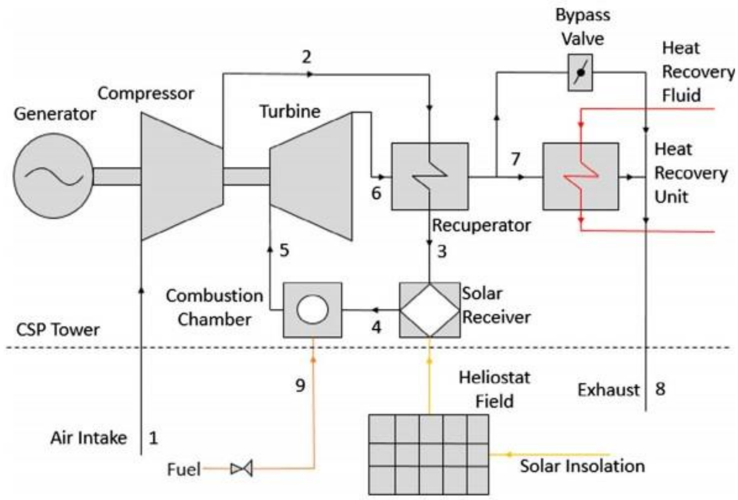

Figure 2-9 Component diagram and stream flows for CSP system with solarized CHP microturbine [30]

Aora Solar estimated that this technology has some benefits that are well suited for Africa due to its 24 hours supply of electricity and heat that make this technology a good choice for off-grid applications and its modularity which allows for a scaling up by adding more towers and mirrors once the community needs start outgrowing the energy output from one single tower. It also has a small installation time of around 6 months and use $3.500\ m^2$ of land which compared to PV is better. [28]

A study from the State University of Arizona showed that with this system the annual fuel usage could be reduced by 26.0% comparing it to a traditional micro-gas turbine and that the annual operating time of the 3 different modes would be around 59.8% for fuel only, 12.4% hybrid and 27.8% solar only which could be improved if the requested power for the system could be reduced. [30]

The implementation and optimization of the solar field with the use of a secondary concentrator (CPC) was also studied by the University Politecnico di Milano with an energy and economic analysis. The results of this study determined an overall optical efficiency of 77.9% for design conditions and a 66.9% for its annual operation with the secondary concentrator, while on the economic side it showed that a reduction of design Effective Direct Normal Irradiation (EDNI) from $700\ W/m^2$ to $550\ W/m^2$ allowed for a reduction on the LCOE of the plant to $158\ €/MWh$ which is competitive to large scale tower plants [31], PV reference value is $158\ €/MWh$ but PV can't supply its energy on demand or at night without batteries which increase the cost of the plant.

2.2.2. Solastor

An innovative approach for CSP technology was presented by Solastor in terms of thermal storage and modularity, the approach was to have a modular system with a surrounded heliostat field concentrating the sun into a cavity receiver aimed downwards, at the top of the tower a graphite receiver collects the energy from the sun and stores it. Then water is pumped through the tower and through the graphite receiver exchanging energy and generating "Dry" steam which generates electricity by means of a steam turbine. Figure 2-10 Figure 2-10 Basic Diagram of Solastor's Graphite Receiver System shows a simplified diagram of the system:

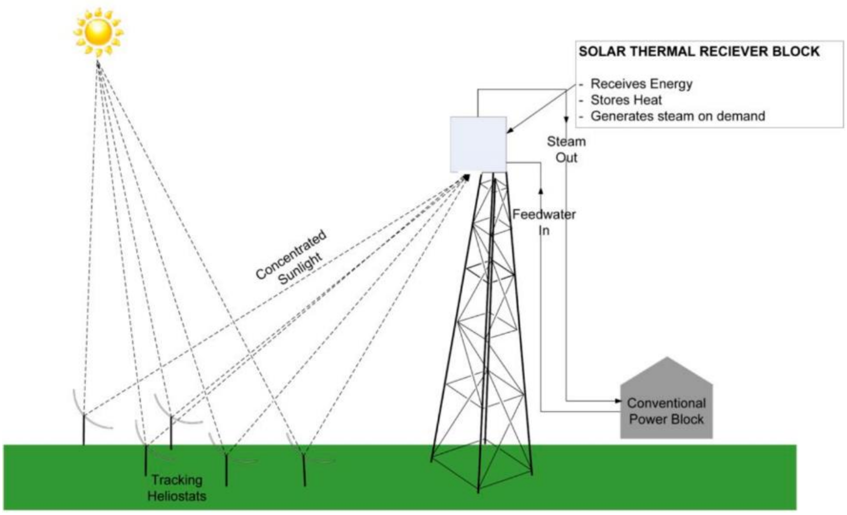

Figure 2-10 Basic Diagram of Solastor's Graphite Receiver System [32]

The system consists of a Tower which is 24 meters high and surrounded by a Solar Field of up to 100 Toroidal Heliostats, this type of heliostats was chosen due to the higher efficiency compared to normal heliostats. The receiver mounted at the top contains the Solar Thermal Receiver (STR) which has 10 tonnes of high purity graphite allowing for up to 800℃ operating receiver temperature. This system can produce steam at 530℃ and each module can hold 3MWh of thermal energy. [32]

Further technical information can be found regarding one of the systems implemented by Solastor at the Final Public Report to the Commonwealth of Australia [33]. Also, a more detailed study of the optical efficiency by passive adjustment is implemented on the paper [34] but for the aim and scope of this thesis will not be considered.

Solastor's graphite system has been implemented on a low scale at Australia (Lake Cargelligo Plant) Figure 2-11, and at China (Jiangyin Plant) Figure 2-12. The plant in Australia consists of 8 modules feeding a 3MW steam turbine while the China plant has 6 modules feeding a 500kW steam turbine, these differences come to show how modular systems can be fitted for different kind of needs.

Figure 2-11 One Module of Solastor's Graphite Receiver at Lake Cargelligo During Construction. [32]

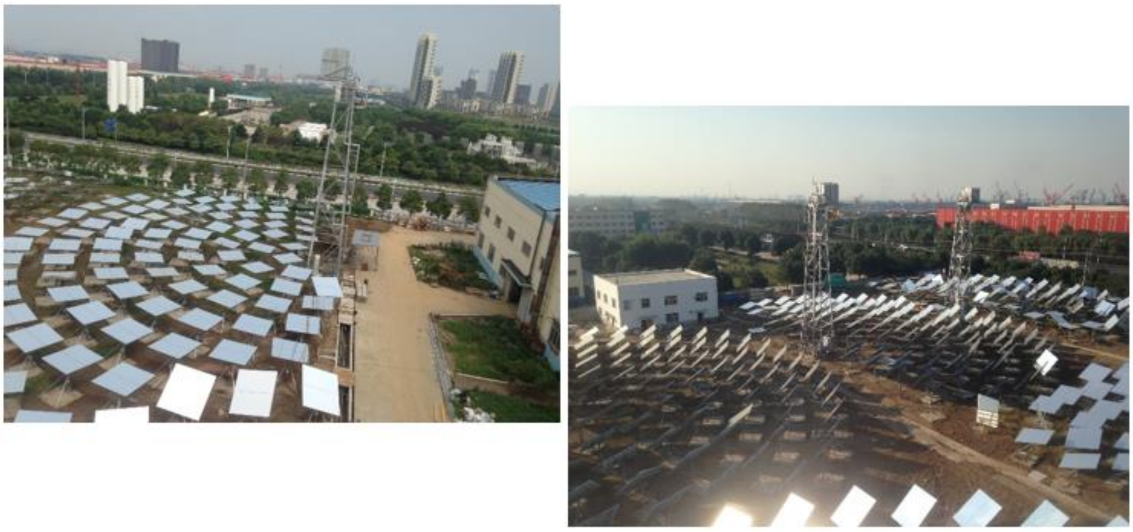

Figure 2-12 Jiangyin, China Solastor's 6 Module Plant [32]

Future plans for this technology are aimed at Cyprus after the approval of a 50MW capacity project by the European NER300 funding, this system will consist of 300 modules with a single 50MW steam turbine and an expected annual output of 172 GWh. [35]

2.2.3. eSolar

eSolar built a CSP plant called Sierra SunTower in 2009, which consisted of two towers and fours sub fields of heliostats, having 24.000 heliostats aiming at the 55 meters high towers, they used very small heliostats of 1.136 [m2] and had a direct steam Rankine cycle producing 5 MW of electricity. [36]

The fields where oriented to the north and to the south, and have a very different layout than common central towers, this distribution can be seen in Figure 2-13, this distribution provided an annual cosine, blocking and shading efficiency of 70.1% [37].

Figure 2-13: Sierra SunTower plant layout. [37]

Later they proposed a Molten Salts modular system, which could be chosen accordingly to the energy needs and convenience, the modular tower consisted of $50\ [MWth]$ modules which could be replicated to create plants from $50\ [MW]$ up to $200\ [MW]$, two different $100\ [MWe]$ plant configurations are shown in Figure 2-14, having different capacity factors, which range from 20% to 75% [38].

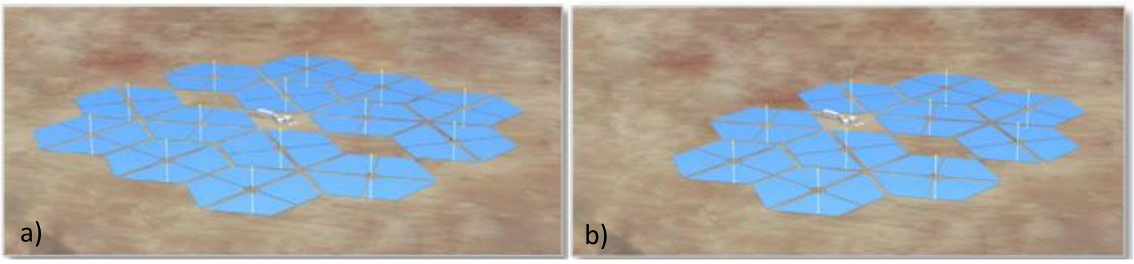

Figure 2-14: Conceptual Layouts of $100\ MWe$, a) 75% Capacity Factor, b) 55% Capacity Factor [39].

The plant components considerations were, as follow [38]:

- **Solar Collector:** A hexagonal field was chosen because it had a good optical efficiency and allowed for a better combination between different modules. Also, a dense configuration was chosen to decrease wind loads and choose lower cost heliostats.
- **Receiver and module size:** $50\ [MWth]$ was chosen due to it being able to be shipped pre-assembled without overcomplicating the shipping and costs related.
- **Tower configuration:** Between lattice, concrete, and steel monopole, the later was chosen due to it being lowest cost configuration for that size.

2.2.4. Vast Solar

Vast Solar proposed a pilot plant which employs a modular configuration of 5 independent towers, each producing 1.2 $[MWth]$ and using a Polar array with Sodium as a HTF, these towers are connected to one supercritical carbon dioxide power block (sCO_2) of 1.1 $[MW]$ [18] which produces electricity from the thermal input power, on *Figure 2-15* we have an aerial view of the pilot plant with its components for a better understanding of its operation.

Figure 2-15: Vast Solar Jemalong Power Station [18]

By using Sodium as a HTF, Vast Solar's plant manages to have a wider range of operating temperature because Sodium has a stability limit of 882°C, while Solar Salts has 600°C [40], due to this wider temperature Vast Solar can improve the Power Block efficiency because of the higher temperature which allows for an improvement on the cycle efficiency and also improving the TES power density [18], on the other side this higher temperature improves the thermal losses and thus reducing the thermal efficiency of the receiver and the piping thermal efficiency.

While the use of a polar array allows for an improvement on the optical efficiency of the heliostats, by improving the Cosine, block and shading efficiencies which was estimated by Vast Solar to be an improvement of 17% [18] in coefficient of performance which in turn allows for more energy per m^2 to be reflected to the receiver.

Vast Solar's technology uses an Air-cooled condenser, it uses the MACCSol air cooled condenser, and it was one of the first in the world to deploy it, since this system uses no water in the cooling cycle it is very practical for the operation of plants which are in areas where water is in short supply. [41]

After the success story of Jemalong Power Station, Vast Solar is looking to develop a 50 $[MW]$ power plant in Mount Isa, North West Queensland in Australia. Which will make use of a solar PV system with batteries and a gas engine powered by Vast Solar's CSP technology in a $\$600m$ total investment project. [42] [43]

3. Methodology

In this section there is the description of the process, models, and assumptions regarding the simulation of different configurations for CSP plants, the aim of this work is to analyze the best choice in terms of energy efficiency and in terms of economic feasibility for a Modular Solar Towers System compared with a Central Receiver Tower System so considering this the methodology will follow this aim, the step-by-step process is:

Firstly, an analysis on the tower, receiver and solar field is made with SolarPILOT which is an Open-Source software from NREL [44], two types of simulations are made, 1) with a Polar Solar Field and a billboard type receiver and 2) with a typical cylindrical receiver and a Surrounded Solar Field, and for both cases a parametric analysis is made searching for the best choice for the given thermal power.

SolarPILOT uses an analytical Hermite polynomial model to calculate the performance of the solar field, delivering the optical efficiency the different powers computed and the flux distribution onto the receiver, for this the user must give the assumptions, properties and geometry of the components.

The location chosen for the simulations is Antofagasta (Lat. -23.4°; Long. -70.4°) because the north part of Chile is considered to have a high flux of irradiation as can be seen in Figure 1-2, and currently "Cerro Dominador" is becoming operational (A Molten Salt Central Receiver Tower CSP) so it would be interesting to consider the application of modular towers in the northern part of Chile, the weather data was downloaded from NREL's website.

Secondly, the complete plant is simulated at design conditions, with the number of towers required for the modular approach and the Receiver and Piping models for the whole plant, this is done by means of a target thermal power which is required and the layout of the whole plant which is further explained in the following pages.

For this second part, a MATLAB model was developed and used, which uses as input the SolarPILOT results and computes the piping and other components of the plant to calculate the performance at design conditions.

Lastly, the complete plants are simulated in off design conditions, simulating the yearly performance of the different configurations, obtaining the different efficiencies, the energy output and the LCOE of the plants for comparison in order to see which would be the best choice moving forward.

The MATLAB code is further developed to include the annual performance of the plant, using as input the design conditions and the yearly weather data.

A simplified flow diagram is shown in Figure 3-1, SolarPILOT is a tool used for obtaining the single tower performance and the Plant Design and Plant Annual are models developed on MATLAB which use the piping models later explained to obtain the plant performance.

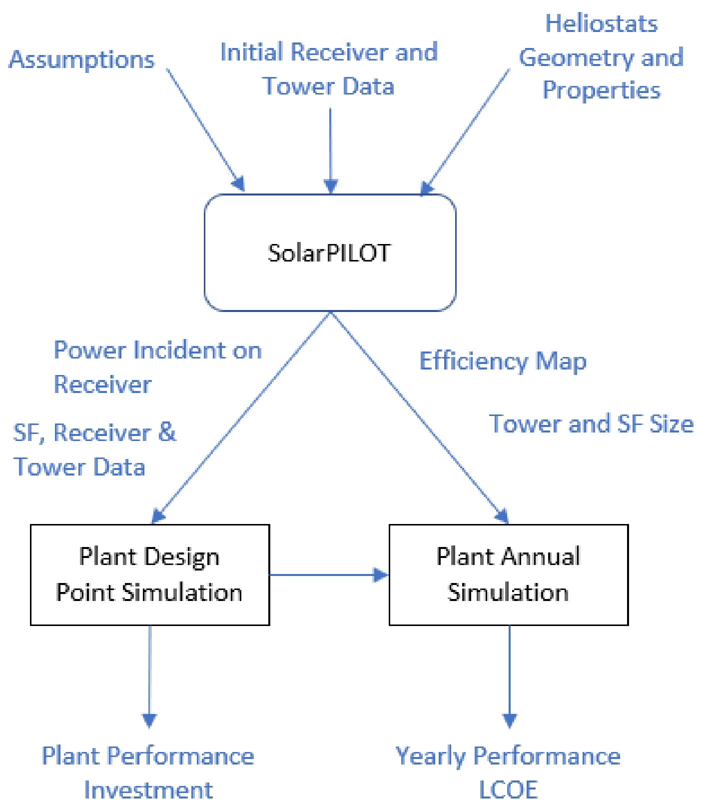

Figure 3-1: Flow diagram showing the summarized steps regarding the work done.

Further explaining of the design and annual assumptions are made in the following sections which are specific to each model developed.

3.1. Design Conditions

The considerations made regarding the on-design operation of the plant are made here, considerations such as the thermal target, the layout distribution, the operating conditions of the fluid and the piping.

The initial setting is to choose the module for the analysis, with its respective performance and physical distribution of heliostats, tower and receiver dimensions, the performance will be used to calculate the number of modules required for a certain thermal target.

For the thermal target, a variety of multiples of $Q_{abs\_HTF} \cdot 4$ is taken, this is to have a symmetrical layout in the 4 quadrants, then once we have the amount of modules required for the plant, the layout considerations have to be made, this is setting the maximum allowable towers for each row in order to compute the amount of rows required, it is important to set a number which allows for "full" rows because the program calculates full rows.

While for the operating conditions of the fluid, the pressure and type of fluid is set, and for the temperature an inlet temperature to the cold side of the piping through the field is set and a ΔT at the receiver is also set, with this the mass flow of sodium is computed for each module and for the whole plant.

For the piping, the properties of the steel and insulating layer are set and the desired outlet temperature of the piping, this desired outlet temperature is given by safety considerations, the maximum temperature of the insulating layers is set for computing the thickness of each layer and not overpass the operating temperature of the layer.

With the previous information the plant performance is obtained, temperature distribution, pressure and thermal losses, piping dimensions and plant layout, but there are still some components missing such as the power block and thermal storage, for choosing these components three important parameters have to be set as well, the solar multiple, the storage hours and the power cycle efficiency, with the solar multiple and power cycle efficiency the rated power of the sCO_2 cycle is computed, and for the storage the inlet power required by the power block times the storage hours are used for computing the storage capacity.

While for the solar multiple and storage, a value of 2.5 is chosen for the solar multiple in order to supply energy outside the sun hours and have a higher capacity factor, while for the storage hours Figure 3-2 shows the LCOE trend of different storage hours and the lowest one for 2.5 SM is chosen, obtaining 9 hours of thermal storage.

Finally with all the previous considerations the performance at design conditions is computed, together with the investment costs and the specific costs ($\$/kWth$ and $\$/kWe$), this information is important and will later be used for the off design of the plant.

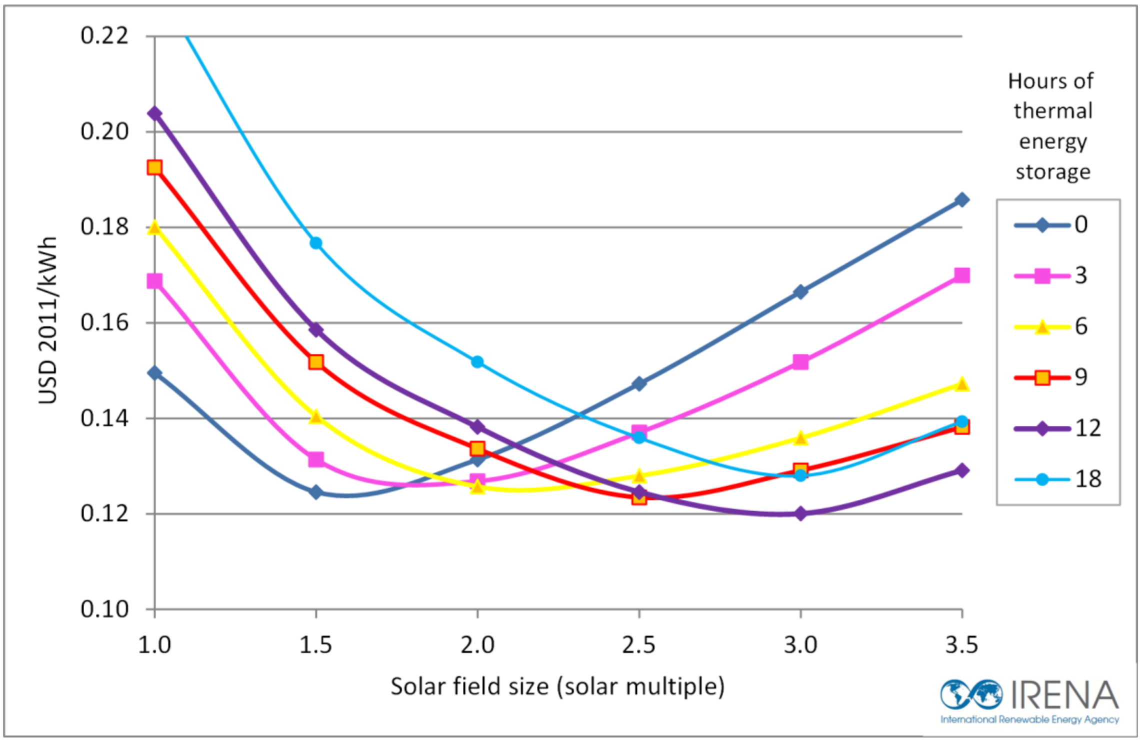

Figure 3-2: Optimum storage hours depending on the Solar Multiple Chosen. [27]

3.2. Off-Design Conditions

For the off-design operation of the plant the thermal losses through the piping and receiver are assumed to be always the same value, but not the same efficiency, since different thermal power flows through the piping at off-design conditions, this assumption is not completely real but can be considered true for practical effects, the main change would be in the internal convection with the different flow conditions.

While for the power block operation an assumption is made that it operates at full load all the time, so the efficiency is constant throughout the year. Thermal losses regarding the storage are neglected but further study should take it into account, a reasonable value of $(98-99\%)$ could be taken.

The last considerations made are the operating conditions at which the plant operates and does not operate, for this the thermal losses of the receiver and piping are considered, so the HTF fluid will only flow onto the receivers when the energy arriving at the receiver is higher than the energy lost at the receiver and piping, which would make it inconvenient for operation of the plant.

Lastly, an annual simulation is performed considering the conditions described above, this simulation starts with information regarding the radiation at the field on an hourly basis using the incident DNI at that given hour to calculate the energy arriving at the solar field.

$$E_{SF} = DNI \cdot A_{helisotats} \cdot n_{heliostats} \cdot 1\ hour\ [MWh_{th}] \quad \textit{Eq. 2}$$

Then the optical efficiency is calculated by means of the efficiency map from the single tower results, this value is interpolated with the sun position at that time and the efficiency map to find the optical efficiency at that time, for this the zenith and azimuth angle are used. The energy arriving at the receiver will be the product of the energy at the field times the optical efficiency.

$$E_{Receiver_{incident}} = E_{SF} \cdot \eta_{optical} \; [MWh_{th}] \qquad \textit{Eq. 3}$$

For the thermal efficiency of the receiver two parts are considered, the reflectivity losses firstly and then the convection and radiative losses, for the energy absorbed by the receiver the reflectivity is considered to be constant at 94%, while for the receiver losses the value from the design point considering the convection and radiative losses, this value is assumed to be always the same when operating the receiver (same temperature distribution so similar losses).

$$E_{Receiver_{absorbed}} = E_{Receiver_{incident\,SF}} \cdot \eta_{reflectivity} \; [MWh_{th}] \qquad \textit{Eq. 4}$$

$$E_{HTF_{absorbed}} = E_{Receiver_{absorbed}} - E_{Receiver_{losses}} \; [MWh_{th}] \qquad \textit{Eq. 5}$$

Then the piping losses are considered to calculate the energy arriving at the inlet of the power block and thermal energy storage, as mentioned before, these losses are considered to be the same as at the design point.

$$E_{PB_{inlet}} = E_{HTF_{absorbed}} - E_{Piping_{losses}} \; [MWh_{th}] \qquad \textit{Eq. 6}$$

The electricity produced is calculated assuming full load conditions at the power block, so a constant efficiency of the cycle is assumed equal to the one obtained at the design of the plant.

$$E_{el_{produced}} = E_{PB_{inlet}} \cdot \eta_{PB} \; [MWh_{th}] \qquad \textit{Eq. 7}$$

Lastly, the net energy is obtained subtracting the electricity required to operate the plant, in this case the pump is assumed at full load as well as the power block for the operation of the plant, and this consumption is assumed to be the most relevant of the whole plant, neglecting the tracking consumption of the heliostats and other auxiliary consumptions.

$$E_{el_{net}} = E_{el_{produced}} - E_{SF_{aux}} \; [MWh_{th}] \qquad \textit{Eq. 8}$$

Once we have the energy performance of the plant on a year, these values are exported and the efficiency is also calculated, because these are important parameters when considering the design of a plant as well as the economic costs, the following equations are used for calculating the yearly efficiency of the different components.

$$\eta_{opt_{annual}} = \frac{\sum_{i=1}^{8760} E_{Receiver_{absorbed}}}{\sum_{i=1}^{8760} E_{SF\_op}} \quad \text{Eq. 9}$$

$$\eta_{Receiver\ thermal_{annual}} = \frac{\sum_{i=1}^{8760} E_{HTF_{absorbed}}}{\sum_{i=1}^{8760} E_{Receiver_{absorbed}}} \quad \text{Eq. 10}$$

$$\eta_{Piping\ Thermal_{annual}} = \frac{\sum_{i=1}^{8760} E_{PB_{inlet}}}{\sum_{i=1}^{8760} E_{HTF_{absorbed}}} \quad \text{Eq. 11}$$

$$\eta_{PB_{annual}} = \frac{\sum_{i=1}^{8760} E_{el_{produced}}}{\sum_{i=1}^{8760} E_{PB_{inlet}}} \quad \text{Eq. 12}$$

$$\eta_{aux_{annual}} = \frac{\sum_{i=1}^{8760} E_{el_{net}}}{\sum_{i=1}^{8760} E_{el_{produced}}} \quad \text{Eq. 13}$$

$$\eta_{sun-to-el_{annual}} = \frac{\sum_{i=1}^{8760} E_{el_{net}}}{\sum_{i=1}^{8760} E_{SF}} \quad \text{Eq. 14}$$

One consideration is that the $\eta_{sun-to-el_{annual}}$ considers all the energy arriving at the solar field, while E_{SF_op} is only considering the useful energy which would be energy higher than the energy required to operate the plant. So, in the $\eta_{sun-to-el_{annual}}$ the operational losses are considered.

4. Single Tower Performance

This work started from Vast Solar Pilot plant, where the modular approach for Solar Towers was combined with Sodium as a HTF and a sCO_2 Power Block, so the analysis forward will consider the same HTF and PB but comparing a central tower and a billboard type receiver tower.

Solar Tower can be very complex due to their large number of variables that end up influencing the performance of the tower, so data was extracted from NREL in terms of operational and future CSP plants to have a starting point for the parametric analysis and reduce the time required for all the simulations.

Table 4-1 shows data extracted from SolarPaces with different CSP Solar Tower projects, this information was extracted to have an initial starting point for the different solar towers with different thermal powers, not all the data were found directly in [45] and some of the numbers needed to be extrapolated from similar towers with a correlation regarding heliostats total reflective area (Assuming a similar optical efficiency between similar towers).

Table 4-1: Different CSP solar tower projects worldwide with respective Thermal Power, Tower Height and Receiver Type [45]

Power Tower Projects	Receiver Thermal Power [MWth]	PB Power [MW]	Tower Height [m]	Receiver Type
Jemalong Solar Thermal Station	1.2	1.1	30	Billboard
Dahan Power Plant	8	1	118	Cavity
Julich Solar Tower	7.8	1.5	60	Cavity
Sundrop CSP	37	1.5	127	Cavity
Planta Solar 10 (PS10)	55	11	115	Cavity
Planta Solar 20 (PS20)	100	20	165	Cavity
Qinghai Gonghe CSP	262	50	171	Central
Khi Solar One	293	50	200	Central
SUPCON Delingha	276	50	200	Central
NOOR III	660	150	250	Central
Crescent Dunes Solar Energy	608	110	195.2	Central
Lumeng Haixi	308	50	188	Central
Shouhang Dunhuang Phase I	120	10	138	Central
Ashalim Plot B (Megalim)	534	121	240	Central
Gemasolar Thermosolar Plant	120	19.9	140	Central
Ivanpah Solar Electric (ISEGS)	455	131	140	Central
Atacama-1	700	110	243	Central
Sierra SunTower	19	5	55	Dual Cavity

Table 4-2 shows all the different towers simulated, we can see the three different cases, one being Molten Salts Central Tower, the second one Sodium Central Tower and lastly the Sodium South Oriented Field, all of these are simulated in SolarPILOT using parametric analysis looking for the best techno economical solution with a starting from real data extracted from Table 4-1.

Table 4-2: Different Solar Tower configuration with their respective thermal power for simulating.

Sodium Central	Sodium Polar
$500\ MWth$	$50\ MWth$
$250\ MWth$	$30\ MWth$
$150\ MWth$	$20\ MWth$
	$10\ MWth$
	$5\ MWth$
	$1.2\ MWth$

The design point conditions selected for the performance analysis are:

- Direct Normal Irradiation: 950 [W/m2].
- 20 of march.
- Autumnal Equinox (Southern Hemisphere).
- DELSOL3 Clear Day.

4.1. Solar Field and Layout

As for the Layout setup on SolarPILOT, the different thermal powers were considered in the Solar field design power and the Heliostat selection criteria was set to Power to Receiver in order to obtain the desired Thermal Output, after that the design field boundaries were set, as for the layout method it depended on the type of field we wanted, for surrounded fields the Radial Stagger method with DELSOL Empirical Fit was selected, while for the Polar Field the Cornfield method was chosen, this methods are displayed in Figure 4-1.

With the Radial Stagger method heliostats rows are placed alternatingly along iso-azimuthal lines at constant radii while the Cornfield uses a cartesian layout aligning the heliostat in straight lines. [46]

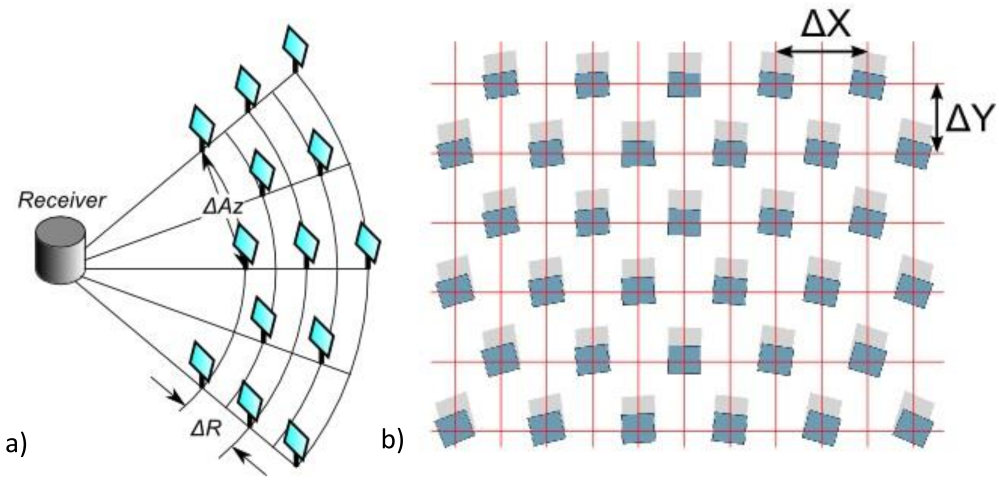

Figure 4-1: a) Radial Stagger Method, b) Cornfield Method [46].

While for the size of the Heliostats, three types where selected which depend on the thermal power onto the tower, the three different types are:

- Heliostat 1: Height $1.34\ [m]$, Width $2.68\ [m]$. Estimated from Jemalong Solar Plant.
- Heliostat 2: Height $2.38\ [m]$, Width $4.76\ [m]$. Twice each dimension from Heliostat 1.
- Heliostat 3: Height $11\ [m]$, Width $12\ [m]$. Estimated from Gemasolar.

Table 4-3: Heliostat type chosen for the different Thermal Powers.

Thermal Power $[\boldsymbol{MWth}]$	**Heliostat Type**
$\mathbf{500 - 250 - 150}$	3
$\mathbf{50 - 30 - 20}$	2
$\mathbf{10 - 5 - 1.2}$	1

The last aspect to consider is the costs related to the heliostat and to the site preparation, both were taken from NREL System Advisory Model (SAM) which is another software for different energy sources and with some reliable cost information, these costs are:

- Site Improvement Cost: $\$16/m^2$ [47]
- Heliostat Field Cost: $\$140/m^2$ [47]

4.2. Tower

Another main component of a CSP system is the Solar Tower, which gives height to the receiver, increasing this parameter usually increases the optical efficiency of the solar field but also increases the cost of the plant, so and optimization should be made, as a starting point for the tower height a similar solar tower already built is chosen, Table 4-4 shows the initial guess for the tower height of different towers.

Table 4-4: Initial guess for the tower height value for different thermal power into the receiver.

	Tower Height [m]:	
Thermal Power $[\boldsymbol{MWth}]$	Sodium Central	Sodium Polar
$\mathbf{500}$	190	–
$\mathbf{250}$	150	–
$\mathbf{150}$	140	–
$\mathbf{50}$	–	80
$\mathbf{30}$	–	70
$\mathbf{20}$	–	70
$\mathbf{10}$	–	50
$\mathbf{5}$	–	50
$\mathbf{1.2}$	–	27

CSP Towers have two common type of constructions, one being with steel and the other with reinforced concrete, the choice depends on the tower height where Falcone in 1986 estimated that steel towers are more cost effective with heights lower than $120\ [m]$, while higher towers are more cost effective with reinforced concrete. [48]

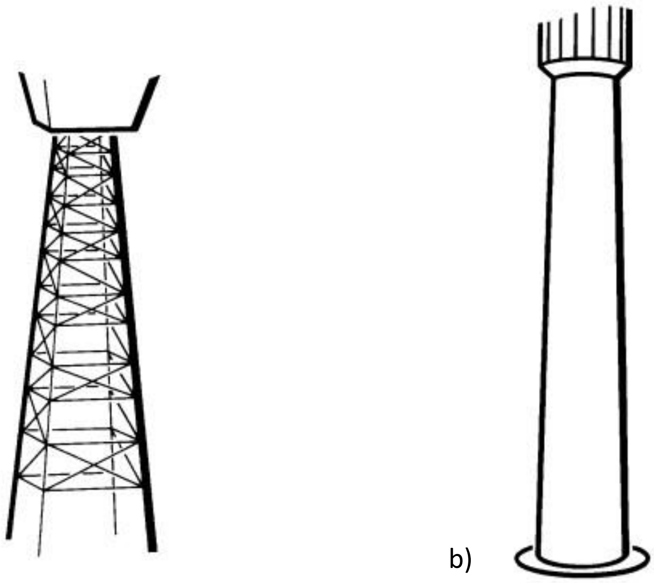

a) b)

Figure 4-2: a) Freestanding Steel Tower, b) Reinforced Concrete Tower. [48]

Figure 4-2 shows the different choices of towers, while for the costs of the two types of towers, Falcone estimated that they can be calculated from Eq. 15 & Eq. 16: [48]

$$THTB \geq 120\ [m]$$
$$CTOW\ [\$] = CTOW1 \times e^{CTOW2 \times THTB} \tag{Eq. 15}$$

$$THTB < 120\ [m]$$
$$CTOW\ [\$] = CTOW3 \times e^{XTOW \times THTB} \tag{Eq. 16}$$

Where $THTB$ is the actual tower height, and the default values considered were the following ones:

- $CTOW1 = 0.78232 \times 10^6\ [\$]$
- $CTOW2 = 0.0113\ [1/m]$
- $CTOW3 = 1.09025 \times 10^6\ [\$]$
- $XTOW = 0.00879\ [1/m]$

While in the cases of SolarPILOT and SAM they use the same equations as before for calculating the tower costs with more updated values than the ones from Falcone's Handbook, but those software's do not have a differentiation for small towers. Eq. 17 shows the equation employed within the SolarPILOT and SAM software's. [46] [47]

$$c_{Tower}\ [\$] = c_{Tower,fixed} \times e^{k \times h_{Tower}} \tag{Eq. 17}$$

With h_{Tower} being the Tower Height, k the cost scaling exponent and $c_{Tower,fixed}$ the fixed tower cost. The default values for these are:

- $c_{Tower,fixed} = 3 \times 10^6\ [\$]$

- $k = 0.0113\ [1/m]$

Since Eq. 17 does not consider the small towers, and it is good for big towers, it is used for the central receiver towers which have higher tower heights, while for the modular towers a correlation from [22] is used which comes from a study regarding modular systems.

$$c_{Tower}\ [M\$] = 1.50227 - 0.00879597 \cdot h_{Tower} + 0.000189709 \cdot h_{Tower}^2 \qquad \text{Eq. 18}$$

The cost correlation from Eq. 18 is valid for tower heights between 50 and 200 [m].

4.3. Heat Transfer Fluid

Different Heat Transfer Fluid (HTF) have been considered over the years for CSP applications, being Thermal Oils the most common for Parabolic Trough and Molten Salts for Solar Towers, while for this work which involves Solar Towers two fluids where chosen, the common Solar Salts and the solution implemented by Vast Solar which is Sodium.

Sodium has an advantage over molten salts since it has a wider operating temperature range as a fluid, being able to operate at higher temperatures than solar salts and enabling the option of using more efficient power block cycles such as a sCO_2 cycle which can achieve efficiencies of 50% while Rankine cycles operate at around 40%.

The operating range of the chosen fluids are:

$$Solar\ Salts\ @290℃ - 565℃$$

$$Sodium\ @550℃ - 760℃$$

So, for solar salts we have the common temperature range where they operate, having 565℃ as a safety choice to avoid the 600℃ stability limit, while for Sodium the choice of a higher temperature was selected to take advantage of this possibility and make use of better efficiency cycles, these values are taken from [49].

Table 4-5: Heat Transfer Fluid Properties. [50]

$\boldsymbol{Name}$	$\boldsymbol{Melting\ Point}$ [℃]	$\boldsymbol{Stability\ Limit}$ [℃]	$\boldsymbol{Viscosity}$ $[\boldsymbol{Pa \cdot s}]$	$\boldsymbol{Thermal\ Conductivity}$ $[\boldsymbol{W/mK}]$	$\boldsymbol{Heat\ Capcity}$ $[\boldsymbol{kJ/kgK}]$	$\boldsymbol{Cost}$ $[\$/\boldsymbol{kg}]$
$\boldsymbol{Solar\ salts}$	220	600	0.00326 @300℃	0.55 @300℃	1.1 @600℃	0.5
$\boldsymbol{Sodium}$	98	883	0.0016 @800℃	57.6 @800℃	1.26 @800℃	2

4.4. Receiver (Cylindrical or Flat Plate, dimensions, thermal losses)

The receivers are very important for the operation of the plant since here the rays focused by the heliostat are absorbed and transferred to the HTF for electricity generation or thermal storage, these also must be carefully though of since they operate at very high temperatures so the piping material must be carefully selected, there are two main types of receivers, the External Receiver, and the Cavity Receiver, these are shown in Figure 4-3.

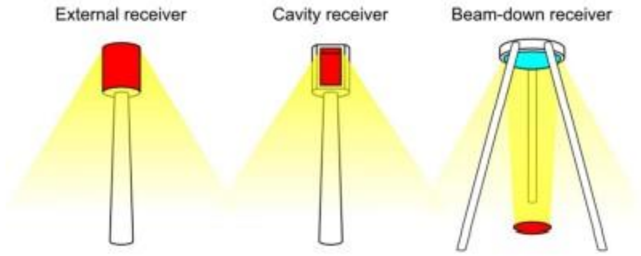

Figure 4-3: Different Type of Receivers for Solar Towers, where External and Cavity are more common. [51]

For this work the external receiver was considered for surrounded fields and a Billboard type receiver (which is like a cavity receiver) for the polar field cases, an example of the billboard type is the one employed by Vast Solar in its Jemalong plant which can be seen in Figure 4-4.

Figure 4-4: Jemalong Solar Thermal Station, Solar Receiver. [52]

For the initial guess of the receiver size, it was chosen from limiting the peak heat flux onto the receiver, having 1.2 $\left[\frac{MW}{m^2}\right]$ for Solar Salts and 2.5 $\left[\frac{MW}{m^2}\right]$ for Sodium receivers [53], this was made by varying the receiver dimensions in SolarPILOT using as aiming strategy the "Image Size Priority" and searching for the limit mentioned, the results from this are shown in Table 4-6, while the aspect ratio considered for later analysis ranged between 1 and 2 for external receivers which were found to be the usual values found in literature. For Billboard receivers a wider parametric analysis was made, and the range which was analyzed was between 0.5 and 2 for the aspect ratio, and also for this type of receiver an inclination was considered like the one from Vast Solar (Figure 4-4), an assumption of 22.5° was made, this inclination is for increasing the optical efficiency but without exaggerating as the higher the inclination the higher the mechanical stress.

Table 4-6: Initial guess for the receiver size, this is obtained by considering a high flux scenario and Aspect Ratio=1.

	Sodium Central		**Sodium Polar**	
Thermal Power	External Receiver		Billboard Receiver	
$[\boldsymbol{MWth}]$	Diameter [m]	Height [m]	Width [m]	Height [m]
$\mathbf{500}$	11	11	–	–
$\mathbf{250}$	9	9	–	–
$\mathbf{150}$	8	8	–	–
$\mathbf{50}$	–	–	5.5	5.5
$\mathbf{30}$	–	–	4	4
$\mathbf{20}$	–	–	3.3	3.3
$\mathbf{10}$	–	–	1.75	1.75
$\mathbf{5}$	–	–	1.5	1.5
$\mathbf{1.2}$	–	–	1.2	1.2

For the simulation, the design point thermal losses had to be added, for these two sources where used, for the central receiver system a study into a plant in South African [54] which had thermal losses information was taken because it had similar on design conditions as the ones used for the simulations, while for the billboard type receiver a correlation [55] was found for calculating the design point thermal losses, the results of these two sources are as follow:

Fluid	*Design Point Thermal Losses*	*Source*
$Solar\ Salts\ @290°C - 565°C$	$32.09\ [kW/m^2]$	[54]

Fluid	*Design Point Thermal Losses*	*Source*
$Sodium\ @550°C - 760°C$	$63.65\ [kW/m^2]$	[55]

The correlation mentioned above uses the radiative losses to compute the convective ones, while for the radiative losses an assumption is made that the temperature considered for radiation is the average temperature of the heat transfer fluid through the receiver plus 100 degrees, the equation for radiation losses and the correlation are shown below:

$$Q_{rad} = \varepsilon \cdot \sigma \cdot A_{rec} \cdot \left(T_{rec}^4 - T_{sky}^4\right) \quad \text{Eq. 19}$$

$$FC = a \cdot \ln(OR \cdot T_{rec}^4 \cdot 10^{-12}) + b$$

$$a = -4.611 \cdot 10^{-4}(V^2) + 5.517 \cdot 10^{-3}(V) - 1.071 \cdot 10^{-1}$$
$$b = -5.917 \cdot 10^{-4}(V^2) + 3.158 \cdot 10^{-2}(V) - 1.190 \cdot 10^{-1} \quad \text{Eq. 20}$$

$$Q_{total} = Q_{rad} \cdot \frac{1}{(1 - FC)} \quad \text{Eq. 21}$$

For the wind speed the velocity assumed was $2\ m/s$, while for the receiver the temperature the same assumption as the one made for the radiation losses is used. The OR is related to the type of receiver, which in case of the Billboard one it is equal to 1.

When we use Sodium at high temperatures the losses almost double, this is mainly due to the radiation losses which scale up with the temperature differences to the power of 4, these losses together with convection losses could be mitigated but not completely, with cavity receivers.

The use of Sodium as a HTF allows for a reduction on the receiver size due to the higher heat flux possible, having something more compact and economical, but increasing flux can have some issues on the material and increasing the temperature can also be a disadvantage since the radiative and convective losses will increase, for Solar Salts receiver the material for the receiver piping is considered to be the same as for Sodium at $750℃$ because most of the modern CSP plants are using Haynes 230 or Inconel 617 which have a good compatibility with Sodium at this operating temperature, Haynes 230 is usually considered due to its high performance at elevated temperatures [53], even though this material is much more expensive than SS316, as we can see in the costs associated to this different materials, which are:

Table 4-7: Costs related to different piping materials for the receivers.

$Material$	$Cost\ [\$/kg]$	$Source$
$Stainless\ Steel\ 316$	$2.5 - 5\ [\$/kg]$	[56]
$Haynes\ 230$	$40 - 80\ [\$/kg]$	[56]

As we can see the costs are 40 times more for Haynes 230, but this material allows for higher temperature without jeopardizing the mechanical reliability and longevity, and in the long term is preferred over the cheap SS316 steel.

The cost calculation of the receiver comes from SolarPILOT as well, which uses the following formula to estimate it:

$$C_{rec} = C_{rec,ref} \left(\frac{A_{rec}}{A_{rec,ref}} \right)^{k_{rec}} \qquad \text{Eq. 22}$$

With $C_{rec,ref}$ the receiver reference cost, $A_{rec,ref}$ the area of the receiver reference and k_{rec} the receiver cost scaling exponent, these are the values considered for the variables:

- $C_{rec,ref,surround} = 1.03 \times 10^8\ [\$]$; $C_{rec,ref,modular} = 2.2 \times 10^5\ [\$]$
- $A_{rec,ref,surround} = 1571\ [m^2]$; $A_{rec,ref,modular} = 2.25\ [m^2]$
- $k_{rec} = 0.7\ [-]$

These values are considered for molten salts receivers but are assume equal for Sodium.

One thing that should be noted is that there are still studies regarding Sodium for high temperature, where the main limits are in corrosion of the materials at high temperatures, deeper studies should go into the cyclic strain and corrosion of Haynes 230 and Inconel 617 at higher temperatures ($800℃$) which allow for even higher efficiency Brayton Cycles, while regarding as well the thermal losses of the receiver searching for a better receiver configuration which limits the radiative losses.

If Haynes 230 is shown to not work and more expensive materials are needed, the following correction factor is suggested for making a rough estimation into the costs of the new receiver, in order to make an estimation of how much this price would increase we are going to start from the Falcone handbook, where it says that 50% of the receiver cost can be attributed to the piping while the other 50% to the structure [48], so assuming that the structure remains more or less the same and only the piping changes, only 50% of the costs will increase with respect to the molten salts case, and the increase of that part of the receiver will come from the difference in price of the material used for Molten Salts compared to the one of Sodium, the price difference is:

$$\frac{p_{new,material}\left[\frac{\$}{kg}\right]}{p_{Common,CSP}\left[\frac{\$}{kg}\right]} = x$$

So, the increase in cost of the receiver will be scaled with the following correction factor:

$$f_{rec,corr} = x \times 0.5 + 0.5$$

In the end the Receiver cost calculation will be:

$$C_{rec} = f_{rec,corr} \times C_{rec,ref}\left(\frac{A_{rec}}{A_{rec,ref}}\right)^{k_{rec}} \qquad \textit{Eq. 23}$$

4.5. Parametric Analysis

After considering each component by itself, a parametric analysis is made to find the best compromise between efficiency and costs, changing the values of the receiver and the tower height starting from the initial guesses proposed and the limits imposed.

The parametric has two parts, one being the optimization of the plant by varying the design values and the second one, once its optimized, it is a parametric analysis of different sun positions which are possible for the location to draw an efficiency map for later yearly performance analysis.

4.5.1. Optimization (Best Design Point)

One important part of CSP engineering is CSP towers plants optimization, since they have many different design choices making it harder for finding an optimal solution, for PT its easier since the modules are more or less standardized limiting the design choices for the engineering of the plant, this is why most investments on CSP where focused on this technology rather than Solar Towers, but since Solar Towers can achieve better efficiencies than PT they should be explored and developed.

The aim of this part is to find the optimal solution, but what this means is for us not to focus only on the efficiency part of the equation but also on the economical one since the later will be the one influencing the development of any future projects, so the variable considered for the optimization is one given by SolarPILOT called Cost/Energy metric, which makes a rough calculation of the relationship between the total cost and the energy produced, looking for the lowest possible value while still maintaining the limitations given by each technology.

The parametric analysis is made by varying multiple receiver dimensions together with different tower heights at the same time, analyzing many different options, trying to minimize the possible error of leaving an optimum out of the analysis.

4.5.2. Performance (Efficiency Map)

While the second part of the parametric analysis, is simpler since its simulating different sun positions accordingly to the desired location, but without varying the design parameters, so it is a result rather than searching for something. In this work the location chosen is Antofagasta, Chile, where the sun angles are the following:

$$Solar\ Azimuth: \qquad \gamma_s = [-130°, 135°]$$

$$Solar\ Elevation: \qquad \alpha_s = [0°, 90°]$$

*These values were taken from SolarGIS.

5. Piping

In modular technologies piping will be considerable when we start having many towers one far from another, like parabolic through, so a deeper analysis must be made to ensure correct operation of the plant, since when we start having many towers pressure and thermal losses in the piping become more relevant as well as the costs related to the materials.

The layout proposed in this thesis consists of 4 quadrants (NW,NE,SW and SE), and the towers are distributed equally across this quadrants, and then for a quadrant a maximum number of towers is defined for each row, this is made in order to have a more simple model without differences between quadrants while the maximum number of towers is meant to ensure that the piping is better distributed because if we have a very big number of towers in one row, the last tower of that row will be very far away from the power block, loosing too much energy, a visual representation of the distribution is shown in Figure 5-1.

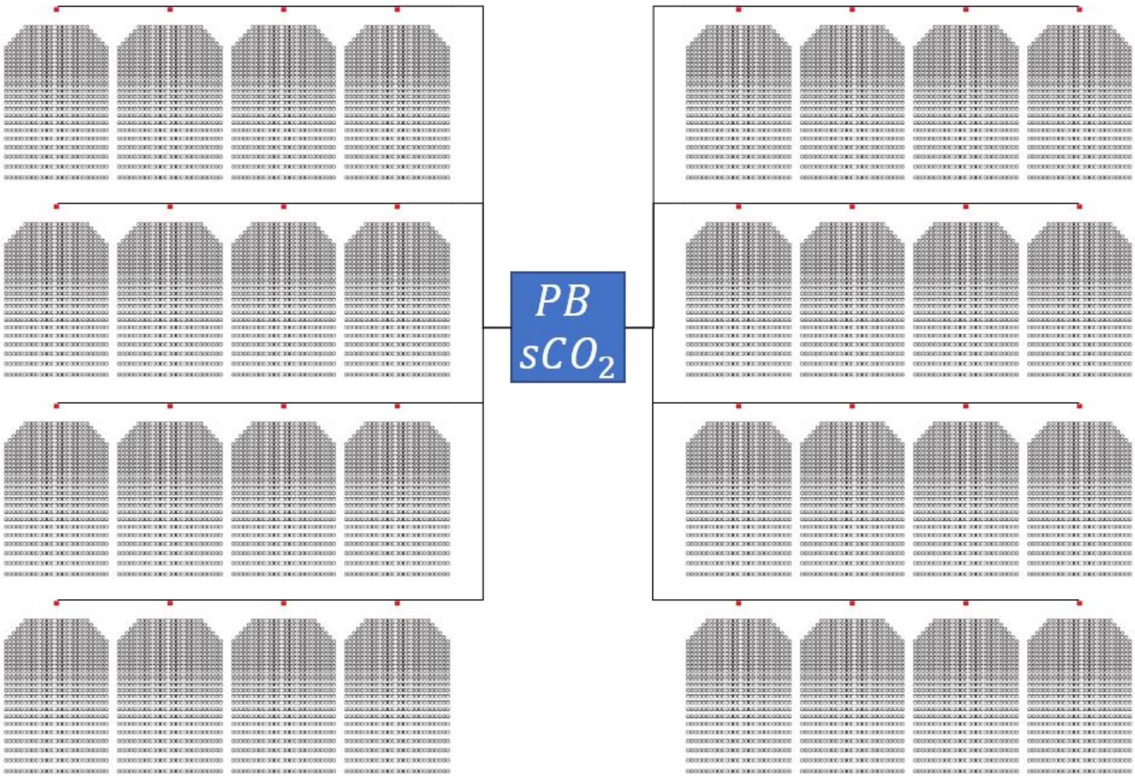

Figure 5-1: Schematic of a 32 Tower plant layout. The Tower and Solar Field are taken from Jemalong Plant in [53].

As we can see the flow into the power block is divided in four, which go to each quadrant, this is for sake of simplicity since there is a space in the middle which could be used but is not explored in the code and depending on the power block size it could be very small and unable to place more modules.

Since there is a symmetry in the field layout, the code developed only calculates one of the quadrants and then it is replicated to the other ones.

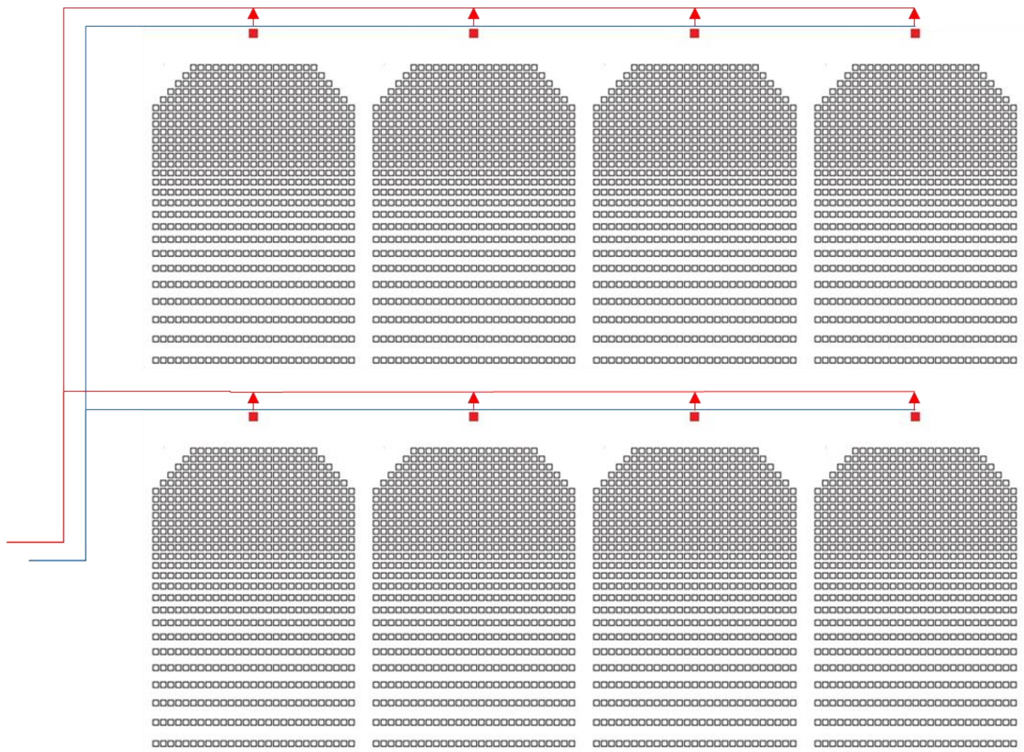

Figure 5-2: Schematic of one of the quadrants of the plant layout.

So the first approach in order to design the field layout is to set the target thermal power which we want to achieve and then set the maximum number of towers which can go into a row, with this information the layout will be set in order to achieve the target thermal adding as many towers as needed, calculating the total number of modules and the number of rows, for example, in the previous case we had 32 modules, with a maximum of 4 modules per row, so in total the plant had 8 rows, but only one of the quadrants is calculated since they are all symmetrical.

After having the layout, the performance and design characteristics must be calculated for this, two different models are used, one for the piping sizing and the temperature and heat losses through the pipe, and another one for the pressure losses of different components within the piping network, with these models the performance of the plant is calculated, and the characteristics of the piping are obtained.

5.1. Mechanical Requirements

Piping is an essential part of a CSP plant, it must be able to ensure the transport of high temperature HTF and deliver a reasonable lifetime, materials usually loose a big part of their strength at very high temperatures, Table 5-1 shows this trend and the values for design tensile strength at different temperatures for different materials involving receiver materials.

Table 5-1: Maximum Allowable Stresses for different alloys at different temperatures. [57]

$\boldsymbol{Candidate\ Alloy}$	$\boldsymbol{Design\ Tensile\ Strength}$ $[\boldsymbol{MPa}]$				
	$\boldsymbol{Temperature}$ [°C]				
	550	**600**	**650**	**700**	**750 − 760**
$SS316$	111	85	51	28	16
$SS304$	93	65	42	27	11
$Haynes$ 230	194	160	108	73	46
$Inconel$ 617	144	143	125	77	46
$Inconel$ 625	206	200	138	80	46

As we can see SS316 behaves badly at high temperatures losing most of its tensile strength at very high temperatures, while Haynes 230 and Inconel's have a much better strength at high temperatures, having almost the same as SS316 at 650°C, and almost 4 times the one at 750°C, making it a better choice for high temperature applications, while this is true, the cost related to Inconel and Haynes 230 is much higher than the more common SS316, so for this reason Haynes 230 is chosen for the receiver since it requires less material and operates at more harsh conditions than the piping, and for the piping system of the plant SS316 is chosen, a study into Sodium showed that it had good compatibility with ferritic and austenitic stainless steels up to its boiling temperature but special consideration regarding the diluted oxygen presence has to be made since it is the major factor regarding corrosion rates, so if this is kept below a certain level the corrosion effect can be avoided, with regards to SS316 good compatibility was found if the diluted oxygen levels where kept below a few ppm [58].

Table 5-1, is good as a first approach for choosing material, in this case SS316 is chosen for the piping and Haynes 230 is the one that will be used for the receiver, further study has to be made in the receiver design and materials if we would want to increase even more the temperature, but for the operating temperature range limited to 700°C the material is adequate, but special consideration into the design of this component should be made. A Study into sodium receiver designs showed than Inconel 617 and Haynes 230 where superior to other receiver materials, having a good thermal stability up until ~800°C making it suitable for high temperature applications [53], the property table of Haynes 230 is shown in Table 5-2, where we can see that at high temperatures it still keeps some of its strength, even at higher temperatures than the boiling point of Sodium, while this is true other issues such as creep-fatigue due to cyclic thermal stress has to be considered.

Table 5-2: Haynes® 230® Properties [59]

Test Temperature [°C]	0.2% Yield Strength $[MPa]$	Ultimate Tensile Strength $[MPa]$	Elongation [%]
21	417	837	47.3
538	294	690	51.7
649	291	666	56.9
760	311	538	59.5
871	236	308	74.2
982	123	169	54.1
1093	69	90	37

For the piping dimensions, the first step is to determine the inner diameter required for the correct flow of Sodium in the different sections, this value can be easily calculated with the following hydraulic formula:

$$D_{in,SS316} = \sqrt{\frac{4\dot{m}_{HTF}}{\pi \rho_{avg} v_{desired}}} \qquad \text{Eq. 24}$$

Where $D_{in,SS316}$ is the inner diameter, $\dot{m}_{HTF}$ is the Sodium mass flow through the pipe, ρ_{avg} the Sodium density at the average temperature of the section, and finally $v_{desired}$ is the imposed velocity for the fluid, one consideration regarding this value is that it should not exceed 6 $[m/s]$ because of possible corrosion and erosion problems [60].

After obtaining the inner diameter, the thickness of the SS316 piping must be calculated, this is obtained by considering the stresses in the pipe to provide good strength and a good durability, the following formula from [61] is used:

$$t = \frac{\left(p_{avg} - p_{amb}\right) \cdot D_{in,SS316}}{2 \cdot \frac{\sigma_{des}}{F_s} - 1.6 \cdot \left(p_{avg} - p_{amb}\right)} \qquad \text{Eq. 25}$$

Where t is the thickness, p_{avg} is the average pressure in the pipe and p_{amb} is the ambient pressure, σ_{des} is the design tensile strength taken from Table 5-1, F_s is the security factor which is considered to be 1.5.

This section is to ensure appropriate mechanical resistance and longevity because generation plants have high operational lifetime, and mechanical failures lead to maintenance and stopping the electricity production which in the end means earning less money and spending more.

5.2. Thermal Model

For the thermal model, MATLAB was used to develop a code for computing with an iterative procedure the thermal losses and temperatures of the different sections of the piping, which carries the HTF from the towers into the power block or thermal storage.

The thermal resistance model was employed for the calculation of temperatures and flows, these resistances are three, one for conduction through tube walls, one for convections (in and out) and radiation, these resistances are calculated with the following formulas:

$$R_{Conduction} = \frac{\ln \frac{R_{ext}}{R_{int}}}{2\pi k \Delta l} \quad \left[\frac{K}{W}\right] \qquad \text{Eq. 26}$$

$$R_{Convection} = \frac{1}{hA_s} \quad \left[\frac{K}{W}\right] \qquad \text{Eq. 27}$$

$$R_{Radiation} = \frac{1}{h_{rad}A_s} \ [MPa] \qquad \text{Eq. 28}$$

$$h_{rad} = \varepsilon\sigma\left(T_s^{\ 2} + T_{surr}^{\ 2}\right)(T_s + T_{surr})$$

Depending on whether it is the receiver or the piping the values will differ, so now a more detailed look at each component is made.

For the piping thermal model, the first big assumption is that we neglect the entrance region and assume a fully developed flow, this way we can use the correlation regarding that type of flow, and since the tube are very large the entrance region should be very limited in comparison to the fully developed part of the flow, so this assumption is correct.

Then the radial heat flow is determined by the equivalence network, Figure 5-3 shows a schematic of the heat flow and the different sources of losses with the corresponding geometric characteristics while Figure 5-4 shows the thermal resistance network for calculating the heat losses.

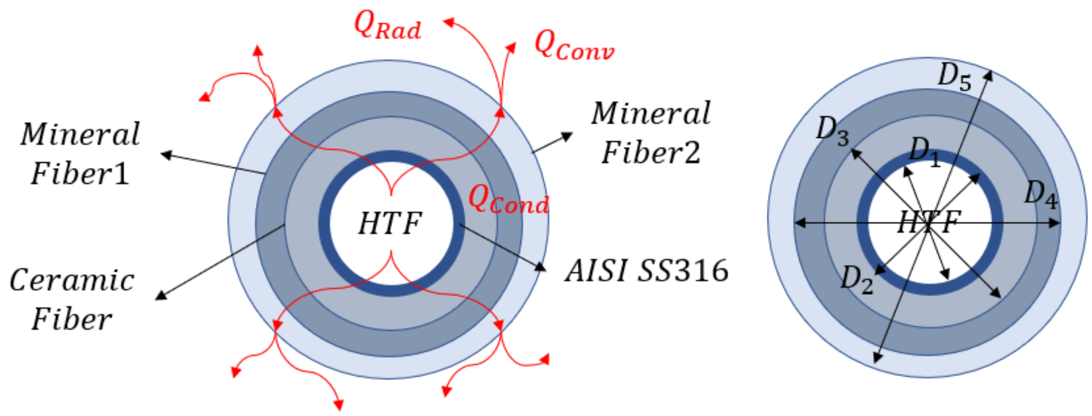

Figure 5-3: Thermal Model for the Piping Section.

As we saw in (Eq. 26,Eq. 27,Eq. 28) the resistances can be calculated but first some values must be assigned.

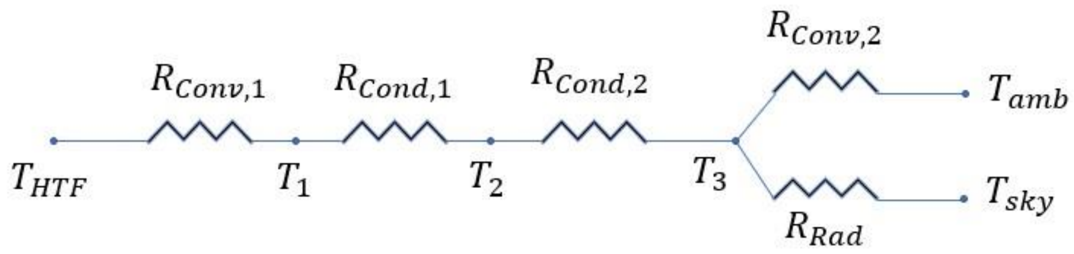

Figure 5-4: Thermal Resistance Model for the Piping Section.

<u>Internal Forced Convection:</u>

Starting with the internal convection we have the following correlation for determining the Nusselt number which is then uses for determining the heat transfer coefficient:

$$Nu_{in} = \frac{h_{in} \cdot D_{in}}{k} = 6.3 + 0.0167 \cdot Re^{0.85} \cdot Pr^{0.93} \quad \text{Eq. 29}$$

Where h is the internal heat transfer coefficient of Sodium, D_{in} the internal Diameter and k the thermal conductivity of Sodium at that temperature.

This Correlation is taken from Sleicher, C.A. & Rouse, M. W., which is specific for internal turbulent flow of Sodium. [20] [62].

$$h_{in} = \frac{Nu \cdot k}{D_{in}} \left[\frac{W}{m^2 K}\right] \quad \text{Eq. 30}$$

<u>Conduction:</u>

Then we move onto the conduction through the steel pipe and through the insulation material, the resistance formula is the one presented in Eq. 26, where we need the external diameter and the internal diameter of the 2 materials, for the steel pipe the internal and external diameter are already calculated with the mechanical requirements and the thermal conductivity of SS316 at @500℃ is 21.5 $[W/mK]$ [63], which extrapolated to @700℃ gives a final thermal conductivity value of 24.15 $[W/mK]$.

While for the insulation the material, first Microtherm® MPS was first selected because it offers good thermal properties for CSP applications [64], having a thermal conductivity of 0.029 $[W/mK]$ @600℃ which would be more than the average temperature of operation inside the insulation, but the cost associated to this insulation was too high so a different approach had to be done, a combination of three insulating materials was chosen to provide a better cost effective solution, the materials chosen where Ceramic Fiber and two different mineral fibers, which have different maximum operating temperatures, the thermophysical properties of the materials can be seen in Table 5-3:

Table 5-3: Thermophysical Properties of piping materials. [65]

$Material$	$k(T) = \alpha T^2 + \beta T + \gamma\ [W/mK]$			T_{max} [°C]
	α	β	γ	
$SS316L$ [63]	$2.86 \cdot 10^{-6}$	$1.09 \cdot 10^{-2}$	13.76	$-$
$Ceramic\ Fiber$ [66]	$1.88 \cdot 10^{-7}$	$2.75 \cdot 10^{-5}$	$3.75 \cdot 10^{-2}$	1100
$Mineral\ Fiber1$ [67]	$3.61 \cdot 10^{-7}$	$7.55 \cdot 10^{-5}$	$3.70 \cdot 10^{-2}$	640
$Mineral\ Fiber2$ [68]	$8.33 \cdot 10^{-7}$	$6.83 \cdot 10^{-5}$	$3.78 \cdot 10^{-2}$	350

One difference with the steel pipe is that the geometric characteristics are not known, so an iterative procedure is conducted searching for a maximum temperature on the outside diameter of the insulation which is set to 40°C because that is the temperature which is considered safe to handle without causing harm [69], and the other consideration was to use the layers of insulating material considering the maximum operating temperature allowed for each.

The resistance of the insulating material and steel are then calculated considering the operating temperatures and the conductivity at said temperature using the formula from Table 5-3 and the total conductive resistance is calculated with Eq. 31.

$$R_{Conduction} = R_{SS316} + \sum R_{Insulation} \qquad \text{Eq. 31}$$

Finally, we reach the outside of the piping and here we have two sources of losses, one regarding the convection losses and another regarding the radiative losses, a value proposed by Moretti [13] of $10\ [W/m^2K]$ is considered as a reference value for comparison, but due to the fact that the conditions are different this value is compared to the ones obtained with a different set of correlations.

So, starting with the convective losses, we have a combination of forced and natural convection, where the convective heat transfer of both combined can be calculated with:

$$h_{conv} = \left({h_{for}}^{a} + {h_{nat}}^{a}\right)^{1/a} \qquad \text{Eq. 32}$$

Where a is assumed as 3.2, which is a value used for cylindrical external type receivers [50], which of course is not the case, but the pipe still has a cylindrical shape and an asymmetric radiation profile, so it is a rough assumption, otherwise only forced convection could be assumed.

<u>External Natural Convection:</u>

For Natural Convection, the correlation of Churchill and Chu [70] is the one used, being the following one:

$$Nu_{nat} = \left(0.6 + \frac{0.387 \cdot Ra^{1/6}}{(1 + (0.559/Pr)^{9/16})^{8/27}}\right)^2 \qquad \text{Eq. 33}$$

$$Ra_{nat} = \frac{g\beta(T_s - T_{amb}){D_{coat}}^3}{\alpha\nu} \qquad \text{Eq. 34}$$

Where g is the gravity, β is the volumetric thermal expansion coefficient, α is the thermal diffusivity, ν kinematic viscosity, Ra is the Rayleigh number, T_s is the surface temperature and D_{coat} is the external diameter of the insulation.

This correlation is valid for:

$$10^5 < Ra_{nat} < 10^{12}$$

External Forced Convection:

For Forced Convection, the correlation proposed by Cengel [71] is used, which uses the following formula and coefficients:

$$Nu_{cyl} = 0.3 + \frac{0.62 Re^{1/2} Pr^{1/3}}{[1 + (0.4/Pr)^{2/3}]^{1/4}} \left[1 + \left(\frac{Re}{282000}\right)^{5/8}\right]^{4/5} \qquad \text{Eq. 35}$$

This correlation is valid for:

$$Re \cdot Pr > 0.2$$

After obtaining the Grashof number and the Reynolds number corresponding to air over a cylinder, the Richardson number is calculated, this number is a ratio between the Grashof number and the Reynolds number to the power of two, this is used for comparison of the relevant convection losses to know if forced or natural convection can be neglected. [72]

$$Ri = \frac{Gr}{Re^2} \gg 1 \; forced\ convection\ may\ be\ ignored$$

$$Ri = \frac{Gr}{Re^2} \approx 1 \; combined\ forced\ and\ free\ convection$$

$$Ri = \frac{Gr}{Re^2} \ll 1 \; free\ convection\ may\ be\ neglected$$

External Radiation:

Finally, the last loss to be considered is the radiative losses to the ambient, in the receiver radiative losses are the main source of thermal losses, this is because the emissivity of Pyromark 2500 at that temperature is considerable, while in this case the insulating material has a low emissivity value, so it is more likely to be lower than the convective losses in this case. A value for emissivity proposed by the Paul Scherrer Insitut of 0.1 is taken [73], with Eq. 28 the resistance of the radiation is calculated.

Thermal and Piping Model:

The thermal model will gather the properties from the fluid, such as pressure, temperature, type of fluid and it will combine those with the ones from the materials to compute the thermal losses and outlet temperature using the thermal resistance model showed and the considerations made.

After calculating all the different losses, the iterative procedure works until finding a solution where the outside temperature of the insulation is lower than the targeted one, this is done for different sections of the piping, calculating the inlet and outlet temperature of the fluid inside the pipe, this way the different temperatures along the whole plant are calculated, Figure 5-5 shows the different sections or discretization with which the losses are calculated.

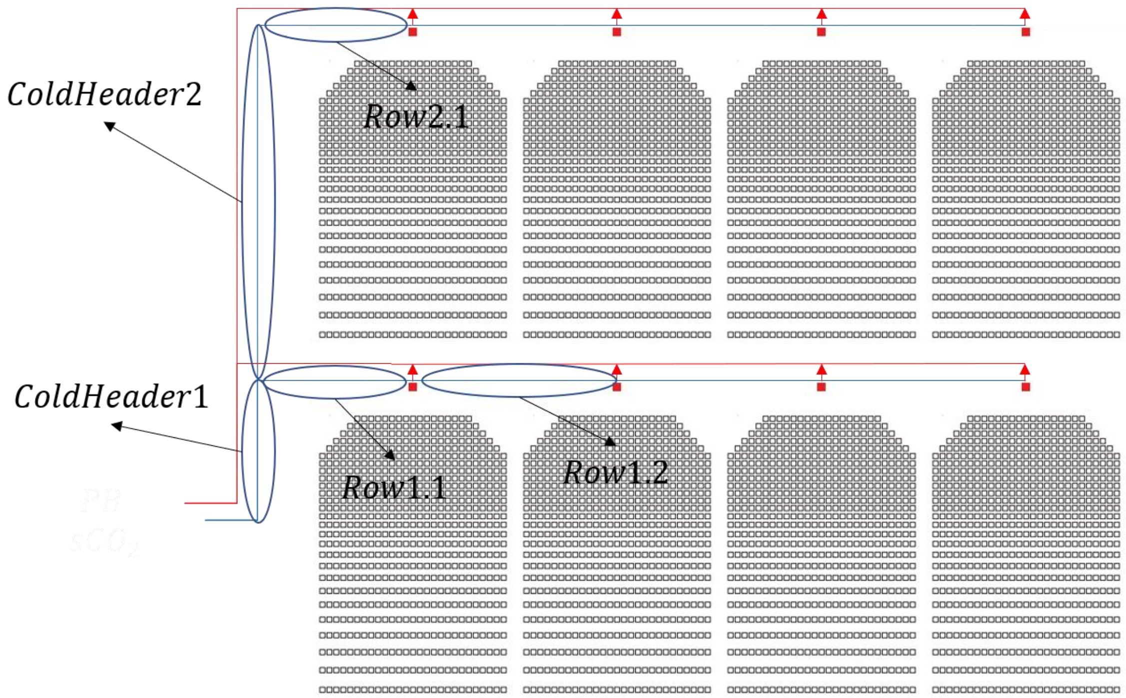

Figure 5-5: Discretization of piping through the plant.

One last consideration made for the plant is the use of expansion loops, which are bended tubes that absorb the thermal expansion of the piping, reducing the mechanical stress caused by the temperature thermal expansion of very hot tubes, Figure 2-15 shows the thermal expansion loops used at Vast Solar and Figure 5-6 shows a basic sketch of the expansion loop, which is basically a bended tube making a U shape.

This extra length is added to the total length for calculating with the thermal losses, while for the pressure losses it adds a K factor to the minor losses. The length chosen is $2W = 6[m]$ which corresponds to the one employed by Vast Solar plant the value is taken from Google Earth measuring tool.

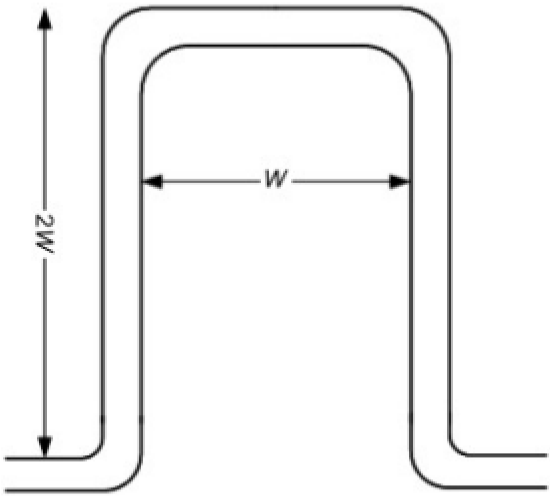

Figure 5-6: Sketch of a Thermal Expansion Loop. [74]

The code employed starts from the initial temperature exiting the Power Block $(550°C)$ and then "Follows" the fluid into the different rows and towers, calculating firstly the whole cold piping system, after having done this, it starts from the towers calculating the outlet temperature of the towers by means of the following formula:

$$T_{out} = \frac{Q_{HTF}}{c_p \cdot \dot{m}_f} + T_{in} \quad \text{Eq. 36}$$

Where Q_{HTF} is the thermal power absorbed by the heat transfer fluid, c_p is the heat capacity of Sodium at the average temperature between inlet and outlet, $\dot{m}_f$ is the mass flow of sodium through the receiver and T_{in} and T_{out} are the inlet and outlet temperature in the receiver, respectively.

After having calculated the outlet temperature of the receiver it starts from the last tower and "Follows" the fluid once more, when it reaches another tower a simple mixing equation is employed with the different temperatures from the towers:

$$T_{mix} = \frac{\dot{m}_{f_t} \cdot T_{hot_t} + \dot{m}_{f_g} \cdot T_{hot_g}}{\dot{m}_{f_t} + \dot{m}_{f_g}} \quad \text{Eq. 37}$$

Where T_{mix} and $\left(\dot{m}_{f_t} + \dot{m}_{f_g}\right)$ is the mixed temperature and mixed flow, while $\dot{m}_{f_t} \cdot T_{hot_t}$ corresponds to the tower flow and temperature and $\dot{m}_{f_g} \cdot T_{hot_g}$ to the ground flow and temperature, this equation comes from the energy equation and considers that all the flows have the same c_p which is a valid assumption considering that the flows have all similar temperatures.

Lastly the flows from the rows converge into the header, using the same mixing equation as before and reaching back the power block, obtaining the initial and final temperature as well as multiple temperatures across the plant.

5.3. Pressure Drop Model

Another relevant factor to consider are the pressure drops through the piping system, this is made to ensure the proper sizing of the pump and consequently the proper operation of the plant, because if we consider the pressure drop, we might find ourselves in the situation that the pressure is not enough to reach the top of the tower, and there we would have a big problem.

The two main sources of losses are named major and minor losses, the first one is due to the friction factor between the fluid and the pipe and covers the whole length of the piping system, while the second one is referred to "accessories" which in some way interfere with the flow of the fluid causing pressure drops the difference between both sources of losses is that one is global to the piping and the other are local.

As for the major losses they are determined by the Darcy friction factor, which can be calculated in two ways, the first one Eq. 38 consists of the Colebrook-White equation while the second one is the one proposed by Petukhov (1970) Eq. 39 and used in [75] which also consisted of a Sodium piping system for CSP applications. The difference between both is that one needs and iterative solver to achieve convergence while the second one is a straightforward calculation but for a limited range of application.

$$\frac{1}{\sqrt{f}} = -2\log\left(\frac{e}{3.7 \cdot D_h} + \frac{2.51}{Re\sqrt{f}}\right) \qquad \text{Eq. 38}$$

$$4 * 10^3 < Re$$

$$f = \frac{1}{(0.79 \cdot \ln Re - 1.64)^2} \qquad \text{Eq. 39}$$

$$3 * 10^3 < Re < 5 * 10^5$$

And once we have the friction factor the pressure drop can be easily calculated with the following formula:

$$p_{loss\,major} = f \cdot \frac{L}{D_{in}} \cdot \frac{\rho \cdot v^2}{2} \qquad \text{Eq. 40}$$

So as was told before the maximum speed of Sodium through the piping is 6 $[m/s]$ but by increasing the velocity the pressure drop also increases to the power of two, so in order choose a reasonable value and avoid high pressure drops and the possibility of high erosion and corrosion, a value of 3 $[m/s]$ is chosen as design point velocity of Sodium flow.

Meanwhile, for the minor losses they can be calculated with their specific loss coefficient with a similar formula as the one before:

$$p_{loss\,minor} = k \cdot \frac{\rho \cdot v^2}{2} \qquad \text{Eq. 41}$$

A list of common components employed in this piping system is shown in Table 5-4:

Table 5-4: Minor los coefficients for the common components in the piping system. [76]

TYPE OF COMPONENT OR FITTING	MINOR LOSS COEFFICIENT
FLANGED TEES, LINE FLOW	0.2
FLANGED TESS, BRANCHED FLOW	1
FLANGED REGULAR $90°$ ELBOWS	0.3

Those are simplified numbers for loss coefficients, for example for the $90°$ elbows, in the Book of Frank White the following formula is proposed:

$$K = 1.49 \cdot Re^{-0.145} \quad \text{Eq. 42}$$

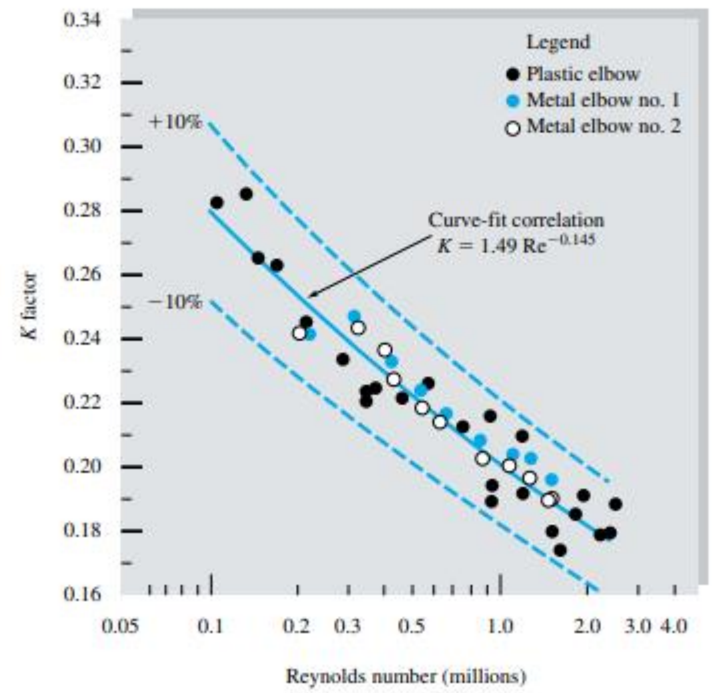

Figure 5-7: Loss Coefficients for $90°$ elbows. [77]

This value proposed by Frank White is lower than the one assumed, so for conservative reasons, the chosen value will continue to be the one from Table 5-4.

While for the Tees, one more consideration must be made, because these Tees are not common Tees because they have a change in diameter both to the branch flow and to the line flow, as seen in Figure 5-8, so two minor losses are present in these components, one regarding the line and branch flow and the other one regarding the contraction or expansion of the pipe.

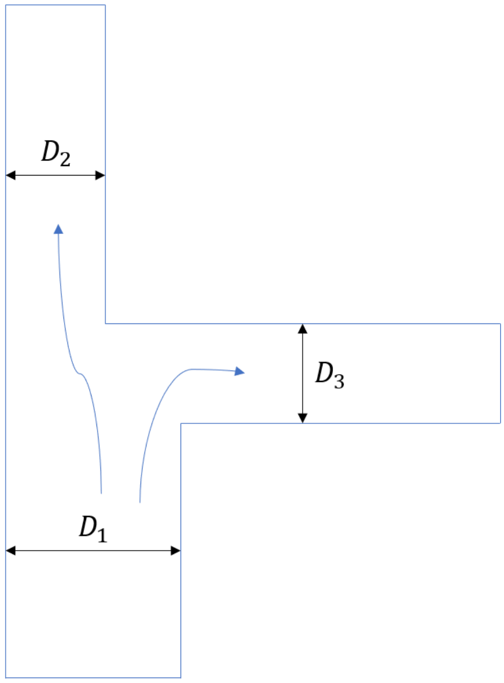

Figure 5-8: schematic of the Tees which can be found in the piping system.

For the cold piping we have a sudden contraction after the Tee, both for the flow going into the row and for the flow continuing through the header, the formula used for contraction loss coefficient is the one proposed by the Book in Fluid Mechanics of Frank White [77]:

$$K_{SC} = 0.42 \cdot \left(1 - \frac{d^2}{D^2}\right) \qquad \text{Eq. 43}$$

Eq. 43 hold true for values up to $d/D = 0.76$, after that value, the equation "merges" into the sudden expansion equation, the following formula for expansion loss coefficient is used:

$$K_{SE} = \left(1 - \frac{d^2}{D^2}\right) \qquad \text{Eq. 44}$$

Figure 5-9 shows the behavior of both equations, as well as the diameters employed for the calculation.

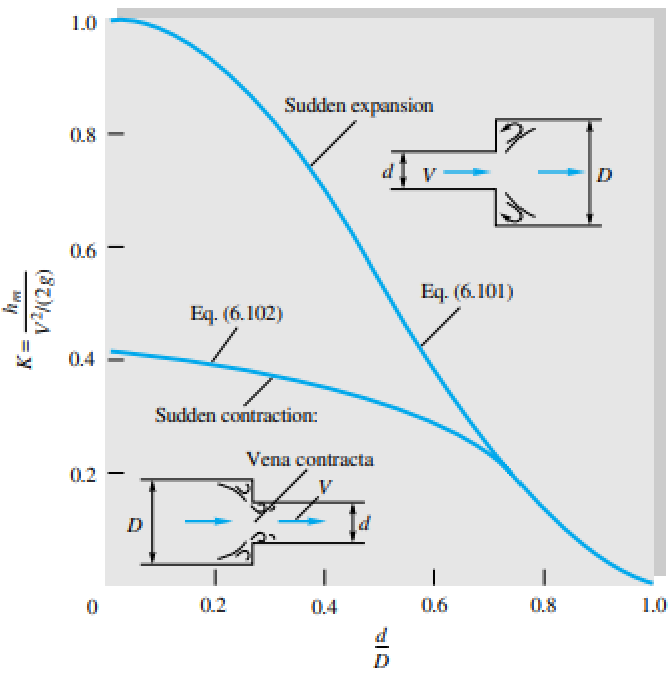

Figure 5-9: Sudden expansion and contraction losses. [77]

For the cold piping only dividing flows occur, while for the hot piping converging flows happen, which are not calculated with the same loss coefficient since they are different physical behaviors.

For the converging flows the following correlation taken from a CFD analysis work published in the international journal of energy and environmental engineering [78].

$$K_{com,st} = 8.919 \cdot \left(\frac{Q_{s,i}}{Q_{c,i}}\right)^{0.165} \cdot Re^{\left[0.169\left(\frac{Q_{s,i}}{Q_{c,i}}\right)-0.306\right]} \quad \text{Eq. 45}$$

$$K_{com,s} = \left[-88.64 \cdot \left(\frac{Q_{s,i}}{Q_{c,i}}\right)^2 + 1.954 \cdot \left(\frac{Q_{s,i}}{Q_{c,i}}\right) - 0.086\right] \cdot \ln(Re) + \left[908.8 \cdot \left(\frac{Q_{s,i}}{Q_{c,i}}\right)^2 + 13.381 \cdot \left(\frac{Q_{s,i}}{Q_{c,i}}\right) - 0.752\right] \quad \text{Eq. 46}$$

These correlations showed a maximum mean deviation of $\pm 6\%$. Figure 5-10 and Figure 5-11 show the trend of the data collected during the work, from which the correlations where developed.

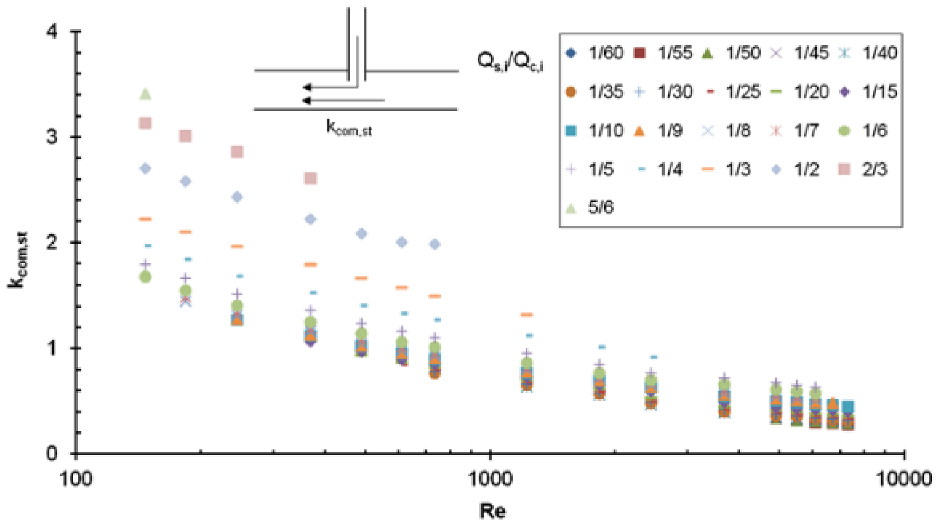

Figure 5-10: Variation of $k_{com,st}$ with Re and the ratio between the flows. [78]

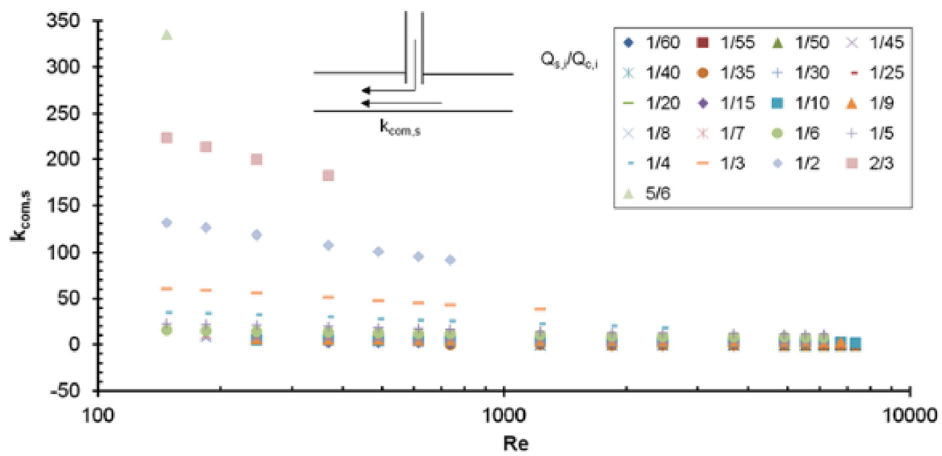

Figure 5-11: Variation of $k_{com,s}$ with Re and the ratio between the flows. [78]

After the convergence of flows a sudden expansion loss is considered using equation Eq. 44, because there is a difference in diameters before and after the Tee.

Finally, the total pressure drop is calculated considering both sources of losses:

$$p_{loss\ total} = p_{loss\ major} + \sum_i p_{loss\ minor,i} \tag{Eq. 47}$$

While for the pump requirements de geodetic step must be considered as well, so the pressure drop that the pump must overcome is:

$$p_{loss\ total} = p_{loss\ major} + \sum_i p_{loss\ minor,i} + H * g * \rho \tag{Eq. 48}$$

And the Pump requirements considering an isentropic efficiency of 85% [79] is:

$$W_{pump} = \frac{Q * \Delta p}{\eta_{is}} \tag{Eq. 49}$$

5.4. Piping Costs

One important consideration to be made is the piping costs when considering modular technologies, because having multiple towers requires more piping steel and insulation to allow for a proper operation of the plant.

The first consideration is made regarding the piping material costs, which would be the steel involved with the layers of insulation, costs regarding this material can be found in Table 5-5 which where extracted from a paper regarding piping losses, the amount of material needed is calculated with the thermal model and mechanical requirements of the plant's piping.

Table 5-5: Costs related to piping material. [65] ($/€ exchange rate of 1.2)

$Material$	$Cost$ $[\$/m^3]$
$SS316L$ [63]	57600
$Ceramic\ Fiber$ [66]	840
$Mineral\ Fiber$ [67]	132
$Mineral\ Fiber$ [68]	72

For other considerations regarding the piping, such as, labor, valves, supports, etc. an overview of the cost share of a parabolic trough plant in the piping section is looked at, assuming that the cost share would be similar to the layout proposed for modular towers due to some similarity regarding the layouts of both type of plants, the cost share is taken from a 322.5 $MWth$ PT plant, where the costs are generated using an excel file for ANDASOL1 Parabolic Trough, these costs are shown in Table 5-6, showing its corresponding value and share of total cost.

Table 5-6:Costs regarding a Parabolic Trough plant of 322.5 $MWth$.

Metallic	Collector field	Share
Pipe	$5,064,121	52.2%
Elbows	$148,697	1.5%
Valves	$574,554	5.9%
Reducers	$47,547	0.5%
Supports	$1,689,824	17.4%
Other	$2,184,000	22.5%

Total	$9,708,744	100%
Insulation		
Pipe	$2,290,036	76.6%
Elbows	$199,603	6.7%
Valves	$37,491	1.3%
Reducers	$26,811	0.9%
Supports	$0	0.0%
Other	$433,844	14.5%

Total	$2,987,785	100%

We use Table 5-6 to calculate the other components regarding the piping costs, but we are still missing the labor costs, which are embedded in the Pipe cost, so a similar approach is made to obtain these, starting from Table 5-7 where the pipe material costs and the labor are seen, and from that a factor is obtained to calculate the $(Labor + Material)$ cost of the pipe.

Table 5-7: Pipe Material and Labor Costs.

Description	Cost	Factor
cold header pipe material	**$601,221**	**-**
cold header pipe labor	**$1,375,656**	**2.2881**
hot header pipe material	**$683,774**	**-**
hot header pipe labor	**$1,550,729**	**2.2679**

Then the pipe material is calculated from:

$$c_{pipe} = c_{cold\ pipe\ material} \cdot (1 + 2.2881) + c_{hot\ pipe\ material} \cdot (1 + 2.2679) \quad \text{Eq. 50}$$

With this, the piping costs are calculated:

$$c_{piping} = \frac{c_{pipe}}{0.522} + \frac{c_{insulation}}{0.766} \quad \textit{Eq. 51}$$

This is a rough estimation into the other components of the piping, a further study should be employed in the cost section regarding labor and other components working with very hot piping and the layouts proposed.

5.5. Piping Models

In this part the simplified flow diagrams are shown and explained, to provide with a visual of the though process of the model. Starting from the plant layout, the model starts with the first section of header and calculates the temperature drops and the piping dimensions required both thermally and mechanically, and with this information the model continues to the first row and does the same calculation, and then to the towers, and when it finishes with one row it moves on to the next section of header and next row, and so on. The flow diagram associated to the thermal losses and piping dimensions of the plant is shown in Figure 5-12.

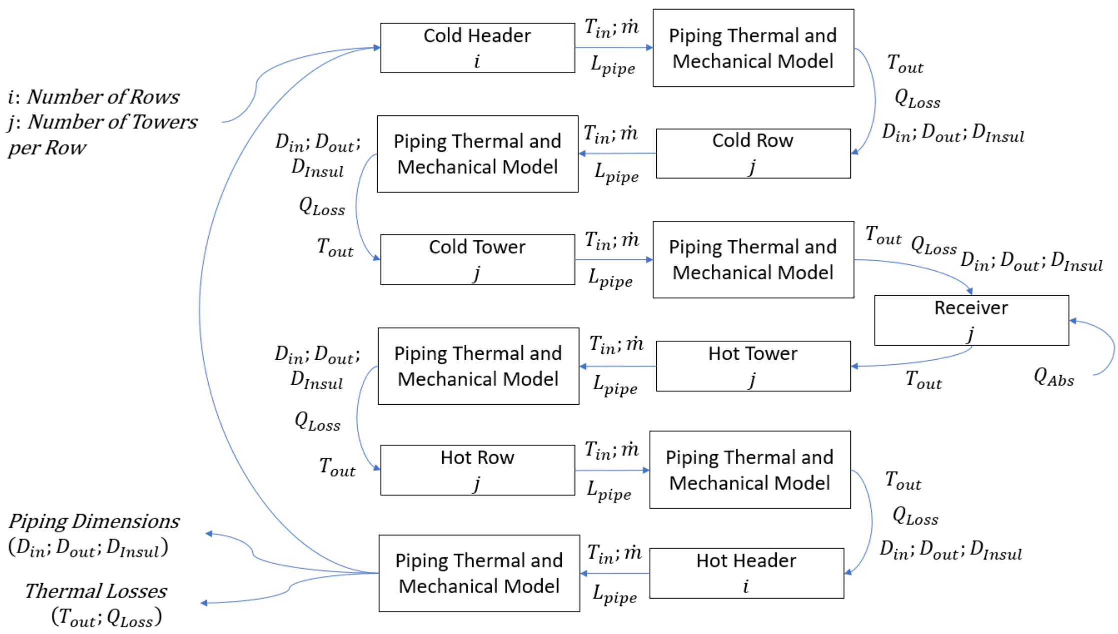

Figure 5-12: Simplified Flow Diagram for the Piping Model for the whole plant. Piping Dimensions and thermal losses.

When the model finishes the cold section of the piping it moves on to the hot one, starting from the last row, to pass from the cold section to the hot one the absorbed heat from the single tower performance is used, and with that input data the outlet temperature from the tower is obtained.

After that, the hot piping follows a similar procedure as the cold piping but instead of having diverging flows it has converging ones, so when there is converging flows, it calculates the temperature through an energy balance, with this being the main difference regarding the procedure.

For the pressure drop the same loop as before is used, but instead of calculating the piping dimensions and thermal losses it calculates the pressure drops using as input the piping dimensions and all sources of local pressure drops which are present in that specific section of piping, the flow diagram associated to the pressure drop can be seen in Figure 5-13.

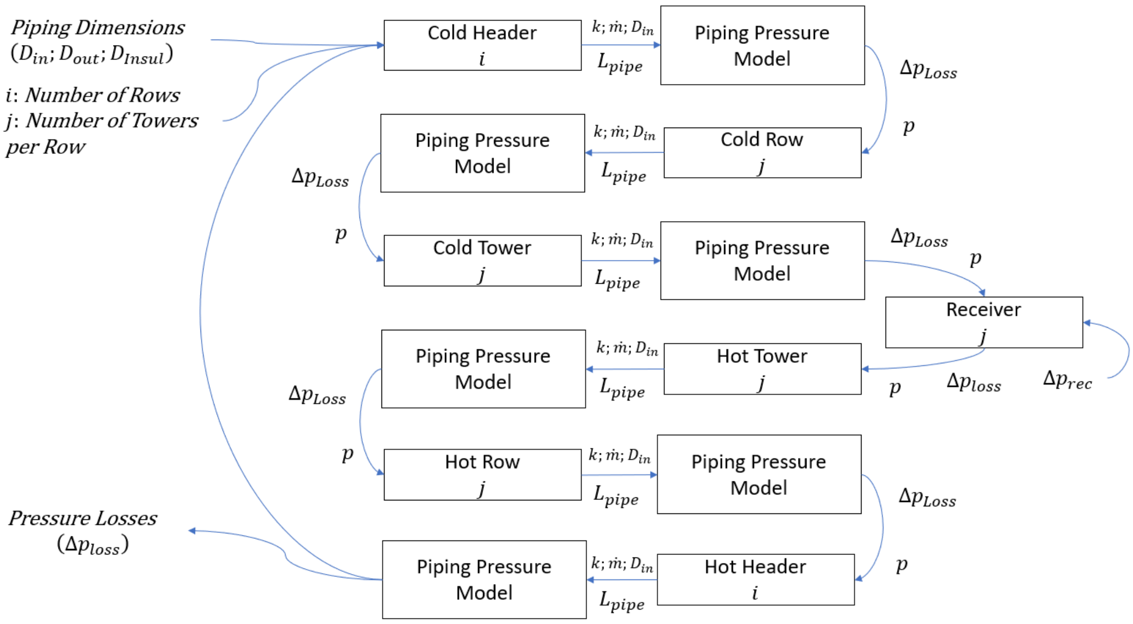

Figure 5-13: Simplified Flow Diagram for the Piping Model for the whole plant. Piping Pressure losses.

The specific simplified flow diagram of the thermal model is shown in Figure 5-14, where for the input, the ambient conditions, the material properties of the pipe and the heat transfer fluid conditions are given, and with this information the internal convection, the conduction and the external convection are calculated to obtain the thermal losses, these are done by means of an iterative procedure until the temperature guess is equal to the calculated temperature, which means that a solution to the equation was found.

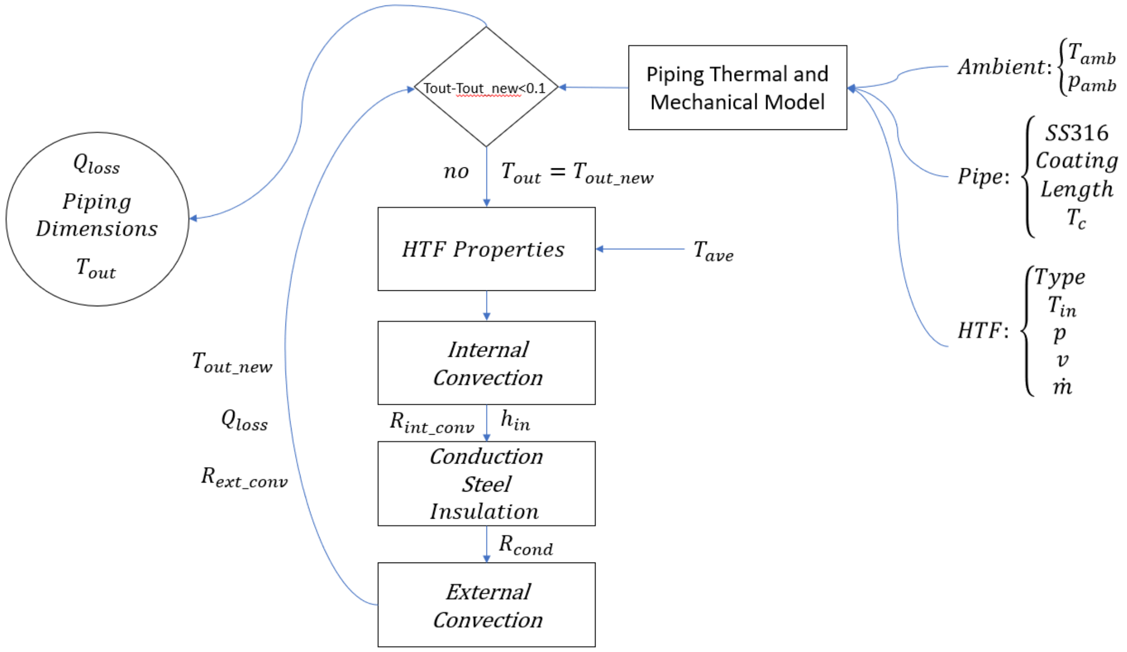

Figure 5-14: Simplified Thermal and Mechanical model. For calculating the thermal losses and piping dimensions.

A further explaining of the conduction model is made, where the flow diagram is shown in Figure 5-15, the model starts with the Ceramic Fiber, which is the first layer of insulating material, and it starts an iterative procedure searching for a temperature which is lower than the maximum allowed by the next insulating layer with some safety margin considered, the same is done with the first layer of mineral fiber which has a higher operating temperature than the second one, while for the last layer of insulating material the iterative procedure continues until reaching the safety limit of pipe coating temperature for human touching.

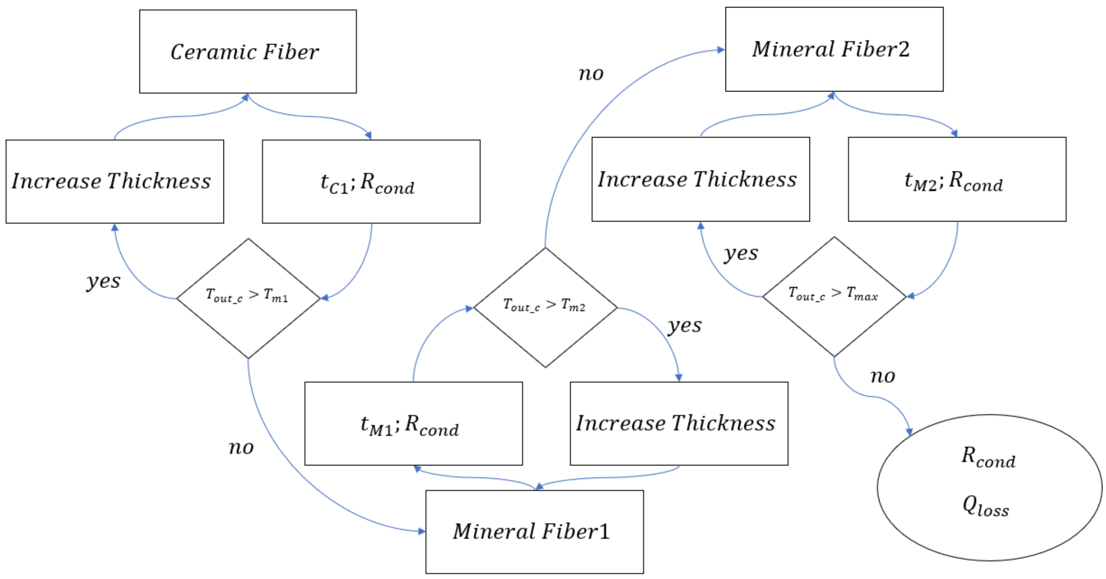

Figure 5-15: Simplified Conduction Model for three layers of insulation.

6. Plant Simulations

In this section, the last components are considered together with the design consideration for the plant, these components are the Power Block and the thermal energy storage, for simplification both components where not designed but the efficiencies and costs associated where estimated from previous works done to these components.

While for the plant, in this section the last considerations are made regarding the plant working conditions and cost estimations. With this, the plant investment and performance are estimated together with the of design performance and LCOE which are later used for the analysis and comparison of the resulting plants.

6.1. Power Block

Starting with the power block, a Supercritical CO_2 cycle is used, specifically a Recompression with Main Compression Intercooling (RMCI) cycle was used, performance regarding this cycle came from a paper regarding these types of cycles [49], this cycle was chosen due to it being superior in terms of performance when compared to the Recompression Cycle and the Partial Cooling Cycle, and the aim of using Supercritical CO_2 is to achieve a better cycle efficiency than the common Rankine cycle employed in CSP towers. A schematic from the cycle selected is shown in Figure 6-1.

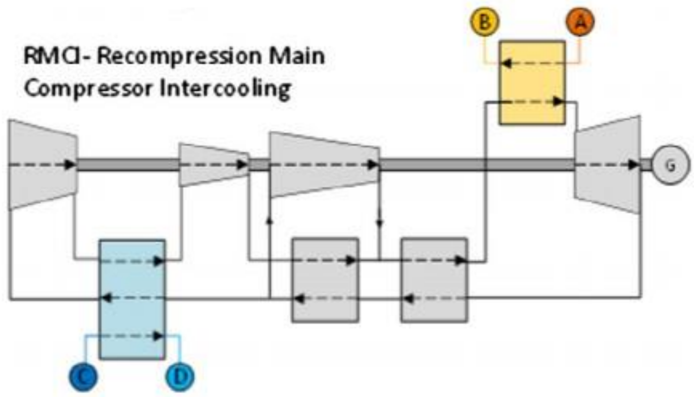

Figure 6-1: Schematic of a Recompression Main Compressor Intercooling sCO2 cycle. [49]

In this type of cycle, the sCO_2 exits the gas turbine at a high temperature and passes through two regenerators, one called High Temperature Regenerator (HTR) while the second one is the Low Temperature Regenerator (LTR), when the sCO_2 exits the second regenerator its flow is divided in two, where one part goes to a compressor and back into the HTR and the other is cooled to the Main Intercooled compressor [50], all of the parameters regarding the design of this plant are taken from the previous work mentioned.

While for the performance of the selected cycle (RMCI), it has a 50% cycle efficiency at a temperature of around 800 °C and an efficiency of 44% for a temperature of around 625 °C, the temperatures mentioned are the Turbine Inlet Temperature (TIT) and not the Temperature arriving from the Solar Field, a pitch point of $\Delta 15°C$ is considered at the heat exchanger between the Sodium and the sCO_2, the performance can be looked at graphically in Figure 6-2, where the three cycles are shown.

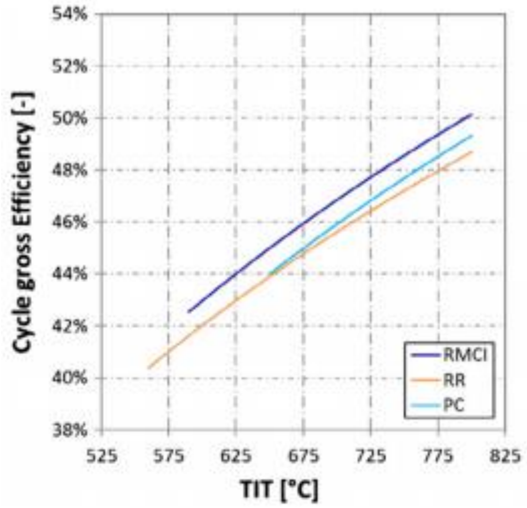

Figure 6-2: Performance of RMCI, RR and PC sCO_2 cycles, Efficiency vs Turbine Inlet Temperature. [49]

As we can see the RMCI cycle outperforms the other cycles for the whole range of temperatures considered, that is why it is considered for this work. Using excel the following formula is taken to compute the efficiency at different temperatures, since depending on the layout and module, in this model the temperatures reaching the PB depend on the layout and modules so the performance of the power cycle will be computed in design conditions with the temperature reaching the PB and the TIT achieved.

The cost associated to the Power Cycle was taken from a multi-tower study [22] which considers that at higher power ratings the specific cost of the turbine is lower, Eq. 52 shows the equation employed for the cost calculation:

$$c_{sCO2\ cycle} = 9650 \cdot P_{eGT}^{0.7}\ [\$] \qquad \textit{Eq. 52}$$

The equation is a function of the electric power output of the turbine P_{eGT} which is in kW, and the cost is in USD. This equation has a $\pm 10\%$ accuracy for powers ranging from 1 to 500 MWe.

6.2. Thermal Energy Storage

The biggest added value of CSP technology is the capability of producing electricity whenever they want, in this way they can produce even when the sun is not shining or when other renewables do not have their energy source active, somewhat stabilizing the generation of electricity and stop depending on the irregularity of other sources.

Also, having a TES allows for a more constant operation of the power block because it can supply the shortage of energy from the solar field and take out the excess when there is one, allowing for a full load condition at the power block and better turbine efficiency, this component of CSP does not only improve the operating conditions but it also allows to operate the plant at better hours (economically) where the price of electricity is higher, selling the same energy but at a higher value.

An in-depth analysis of this component is not made, but a two-tank sodium storage is considered from [80], where a $\$/kWh_{th}$ is obtained, the operating temperature of that work was 700°C and 390°C for the hot and cold temperature respectively, while this work operates at 750°C and 550°C so making a simple assumption that the cost is proportional to the embodied energy and that the embodied energy is proportional to the ΔT the cost of the respective thermal storage is obtained with:

$$c_{Sodium\ TES} = \left(43.43 \cdot \frac{\Delta T_{ref}}{\Delta T_{actual}}\right) \cdot SC\ [\$] \qquad \textit{Eq. 53}$$

43.43 is the $\$/kWh_{th}$ obtained by the reference two-tank sodium storage and ΔT_{ref} is its temperature difference, while ΔT_{actual} is the actual temperature difference of the plant and SC is the storage capacity.

The Storage capacity will depend on two factors, the amount of storage hours required and the power block efficiency and rated power.

There are other types of storage technologies like for example a single tank thermocline where a reduction in costs is seen from removing one tank from the equation, there are others like the graphite storage technology as well, but for sake of simplicity the two-tank sodium storage was chosen, further study should be employed on the best type of storage for sodium and high temperature applications.

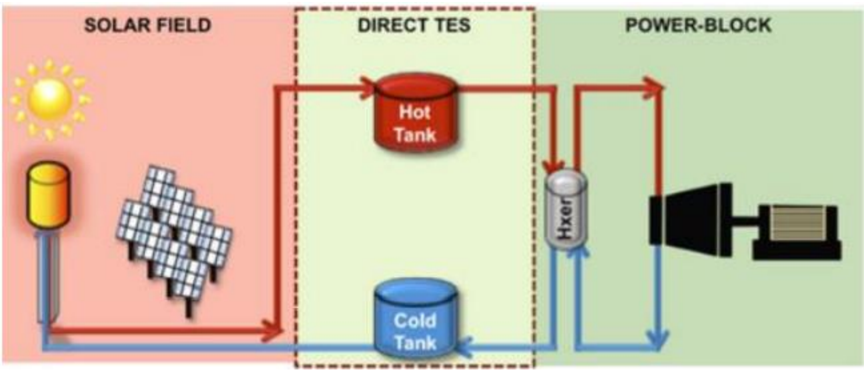

Figure 6-3: Simple schematic of a two-tank direct thermal storage system for CSP tower plants. [50]

6.3. Receiver Thermal Model

This design point thermal loss is for the simulations with SolarPILOT, afterwards the losses at design point are considered the same for off design conditions, meaning variable incident radiation hitting the receiver, assuming that the receiver operates at similar conditions, like same inlet and outlet temperatures through the receiver at off design operation, this assumption is somewhat strong because the internal convection and the temperature distribution through the receiver will change when we operate at “Part Load” changing the losses, but this effect should be somewhat limited and won’t have a big effect as long as the operating temperatures are not changed.

6.4. Plant Cost

This section shows a summary from all the costs assumed for the simulations and the financial considerations regarding the power plant, with this the initial capital investment, the operational expenses and the LCOE are obtained.

Solar Field:

$$c_{Solar\ Field} = (16 + 140) \cdot A_{SF}\ [\$] \qquad \textit{Eq. 54}$$

Tower:

$$c_{Tower} = 1.50227 - 0.00879597 \cdot h_{Tower} + 0.000189709 \cdot h_{Tower}^2 [M\$] \qquad \textit{Eq. 55}$$

$$c_{Tower}\ [\$] = 3 \times 10^6 \times e^{0.0113 \times h_{Tower}} \qquad \textit{Eq. 56}$$

Receiver:

$$C_{rec} = C_{rec,ref} \left(\frac{A_{rec}}{A_{rec,ref}}\right)^{0.7} \qquad \textit{Eq. 57}$$

- $C_{rec,ref,surround} = 1.03 \times 10^8\ [\$]$; $C_{rec,ref,modular} = 2.2 \times 10^5\ [\$]$
- $A_{rec,ref,surround} = 1571\ [m^2]$; $A_{rec,ref,modular} = 2.25\ [m^2]$

Power Block:

$$c_{sCO2\ cycle} = 9650 \cdot P_{eGT}^{0.7}\ [\$] \qquad \textit{Eq. 58}$$

Thermal Energy Storage:

$$c_{Sodium\ TES} = \left(43.43 \cdot \frac{\Delta T_{ref}}{\Delta T_{actual}}\right) \cdot SC\ [\$] \qquad \textit{Eq. 59}$$

Heat Transfer Fluid:

$$c_{Sodium} = 2 \cdot m_{kg\ of\ sodium}\ [\$] \qquad \textit{Eq. 60}$$

Piping:

$$c_{pipe\ material} = (57600) \cdot m^3_{SS316} + (840) \cdot m^3_{ceramic} + (132) \cdot m^3_{Mineral1} + (72) \cdot m^3_{Mineral2}\ [\$] \qquad \text{Eq. 61}$$

$$c_{pipe} = c_{cold\ pipe\ material} \cdot (1 + 2.2881) + c_{hot\ pipe\ material} \cdot (1 + 2.2679)\ [\$] \qquad \text{Eq. 62}$$

$$c_{piping} = \frac{c_{pipe}}{0.522} + \frac{c_{insulation}}{0.766}\ [\$] \qquad \text{Eq. 63}$$

Lastly for contingency a 7% of the sum of all the costs shown above is considered. With this the Total Plant Installed Costs is obtained. 25% of the installed costs is assumed for the indirect costs.

One special consideration is made regarding the towers, in which they will experience economies of scale due to the learning curve that would be applied if multiple towers of the same characteristics are made, taking into consideration that the learning rate for CSP is that every time that the capacity is doubled the costs are reduced by 20% [81], the same idea will be applied for the costs of the towers where every time we double the amount of towers the costs per tower will reduce in 10%, with this in consideration the cost of multiple towers will be:

$$c_{MT} = c_{ST} \cdot x^{0.848}_{Towers}\ [\$] \qquad \textit{Eq. 64}$$

Where c_{ST} is the single tower investment cost, and c_{MT} is the total cost of the multiple towers, being x the number of towers.

For the rest of the components no economies of scale are applied.

<u>LCOE Calculation:</u>

LCOE is commonly used for evaluation of the economical and energy of power generation systems, for the evaluation of this, the following equation from [82] is used:

$$LCOE = \frac{I_0 + \sum_{yr=1}^{N_{yr}} \frac{O\&M_{yr}}{(1+r_d)^{yr}}}{\sum_{yr=1}^{N_{yr}} \frac{Q_{yr,e}}{(1+r_d)^{yr}}}\ [\$/kWh] \qquad \textit{Eq. 65}$$

Where the following considerations where made:

- Plant lifetime 30 years [75].
- Discount rate of 6% [83].
- $O\&M_{yr}$ is assumed equal to 1.5% of the total plant investment cost. [22]

I_0 is the total investment of the plant (CAPEX) at $yr = 0$, $O\&M_{yr}$ is the operation and maintenance cost of the plant and lastly $Q_{yr,e}$ is the electricity generated throughout the year.

7. Results and Discussion

This section will showcase the results obtained while also making an analysis of those results, this is very important for the analysis of benefits and disadvantages of modular technologies compared to single tower CSP, while also obtaining results from a state-of-the-art CSP, which uses Sodium at high temperatures and Supercritical CO_2 cycles to improve the performance of CSP towers.

The first step of this process is to make a validation of the code and assumptions employed, and later a in depth analysis of multiple data and results from the different layouts and plants proposed.

7.1. Validation and Analysis of Vast Solar Module

For the validation of the code the single tower performance of one of vast modules is used, for the SolarPILOT simulation the heliostats distribution from Figure 7-1 is used, an inclination was assumed of 22.5° for the receiver in order to improve the optical efficiency of the plant.

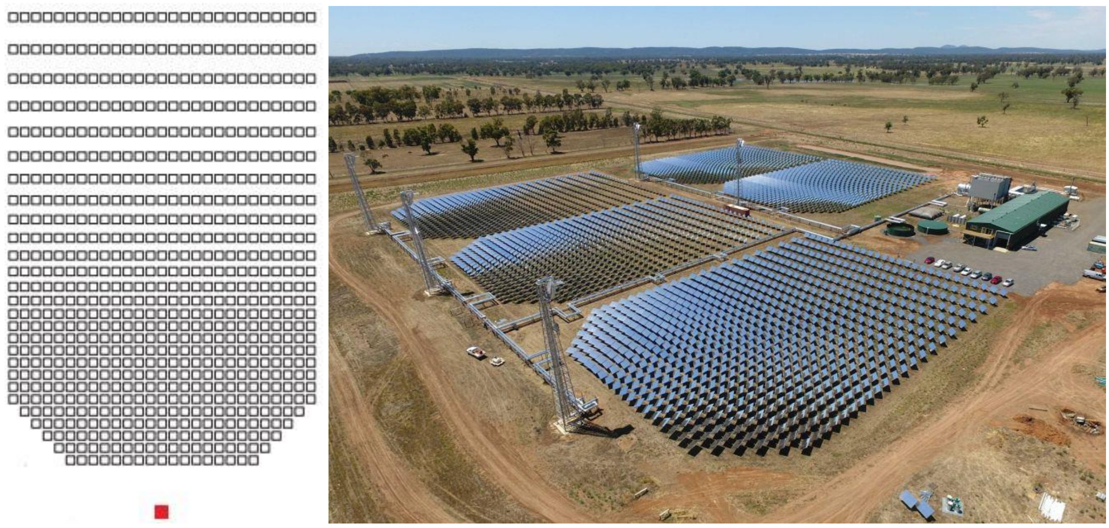

Figure 7-1: (left): Heliostats placement for SolarPILOT simulation, taken from [51]. (right): Aerial view of Jemalong Pilot Plant, taken from [84].

The results from the single tower simulation were done with SolarPILOT, taking as place the north of Chile, Antofagasta, where the biggest CSP in south America was built, the performance simulation was done at the autumnal equinox, obtaining the results shown in Table 7-1.

Table 7-1: Results from SolarPILOT simulation for the Vast Solar Module, performance on Antofagasta at the autumnal equinox.

	Units	Value	Mean	Minimum	Maximum	Std. dev
Simulated heliostat area	m^2	2447.7				
Simulated heliostat count	-	699				
Power incident on field	kW	2325.3				
Power absorbed by the receiver	kW	1496				
Power absorbed by HTF	kW	1352.8				
Cloudiness efficiency	%	100	100	100	100	0
Shading efficiency	%	100	100	100	100	0
Cosine efficiency	%	92.94	92.94	86.76	99.98	3.3234
Reflection efficiency	%	90.25	90.25	90.25	90.25	0
Blocking efficiency	%	94	94	79.91	100	5.0707
Attenuation efficiency	%	98.66	98.66	98.11	99.02	0.2398
Image intercept efficiency	%	87.98	87.83	75.44	100	6.9829
Absorption efficiency	%	94				
Solar field optical efficiency	%	68.44		54.85	88.89	8.3209
Optical efficiency incl. receiver	%	64.33		51.56	83.56	7.8217
Annualized heliostat efficiency	%	0		0	0	0
Incident flux	kW/m2	707.31		249.2	891.23	144.3879

The power absorbed by the heat transfer fluid is $1.4\ MWth$, while the one specified by Vast Solar was $1.2\ MWth$ per module, having a $+15\%$ increase/error with respect to the one predicted, this can be due to many factors, one mainly being the location chosen for the simulation and the inclination of the receiver, or another reason could be with the assumptions taken by Vast Solar.

To further check if the error comes from location or bad assumptions, an analysis was made into the receiver thermal efficiency and the annual optical efficiency, comparing them to previous studies regarding this module. For the annual optical efficiency, a value of 58.8% was obtained, while for a previous study made a value of 56.5% was assumed [74], so the optical efficiency difference could be due to the location simulation and the inclination provided to the receiver, it should be noted that the value from the previous study was assumed and not calculated. In the case of thermal efficiency, 85.5% was obtained from this study while for the previous study a value close to 90% [74] was obtained, which also makes sense since the operating conditions of that simulation where at lower temperatures compared to our simulation.

It is very likely that it would be difficult to achieve the exact same results as Vast Solar, since probably a more detailed study onto the sun rays was made at the location, which would be more accurate than the values from SolarPILOT database, and the day and time at which the simulation was made influences heavily the results, but since the results are not farfetched, the simulation is assumed to be realistic.

While for the modular plant the physical dimensions of the single plant have to be taken into account, the horizontal and vertical distance are obtained from the heliostat field, the results are $70\ [m]$ and $110\ [m]$ which where corroborated with google earth measuring the dimensions of a single module from the Jemalong plant.

The physical dimensions and the single tower performance are used as inputs for the modular plant simulation, but for this plant and to have some sort of validation, different parameters where investigated.

The first and second parameter changed where the fluid velocity and the coating temperature, for both cases a simple plant consisting of four modules was simulated while changing the parameters.

Firstly, the fluid velocity was investigated, ranging from $1\ [m/s]$ up to $6\ [m/s]$ which as mentioned before is a safety limit for sodium flow through steel pipes (avoiding corrosion issues), the results obtained are shown in Table 7-2.

Table 7-2: Results of the piping performance from changing the fluid velocity through the piping.

VELOCITY $[\boldsymbol{m/s}]$	**PRESSURE DROP** $[\boldsymbol{MPa}]$	**PUMP POWER** $[\boldsymbol{kW}]$	**THERMAL LOSS** $[\boldsymbol{MWth}]$	**PIPING THERMAL EFFICIENCY** [%]	**AUX EFFICIENCY** [%]
1	0.24	7.38	0.28	94.83%	99.24%
2	0.35	10.52	0.25	95.43%	98.93%
3	0.55	16.78	0.23	95.72%	98.30%
4	0.88	26.69	0.22	95.91%	97.30%
5	1.34	40.70	0.21	96.05%	95.89%
6	1.95	59.16	0.21	96.15%	94.03%

Since pressure drops are proportional to the square of the velocity, increasing the velocity would increase the pressure drop and the pumping power, which is proportional to the pressure drop, finally the auxiliary efficiency considers the electric power consumed by the operation of the plant, which is lost, so having a higher pump consumption will affect this efficiency as well. All the factors mentioned above follow the logic behind fluid mechanics, for a comparison the pressure drop calculated by a study regarding the Jemalong plant was of 611kPa [74], which falls in between a fluid velocity of $3 - 4\ [m/s]$, and the simulation conditions were similar with some difference which would influence this difference.

While for the thermal performance an opposite trend is shown, where the higher velocity has a better thermal efficiency, so a careful consideration must be made regarding the fluid velocity due to the pump consumption and thermal losses, the thermal losses do not only affect a direct loss of heat but also influence the performance of the power block where the HTF arrives at a lower temperature to it, and as we saw before the performance of the sCO_2 depends on the inlet temperature at the turbine which is also influenced by the temperature of the HTF, where a constant $\Delta T = 15°C$ is assumed. Figure 7-2 shows the temperature of the HTF arriving at the power block, while Figure 7-3 shows the effect of the fluid velocity on the performance of the piping and the plant.

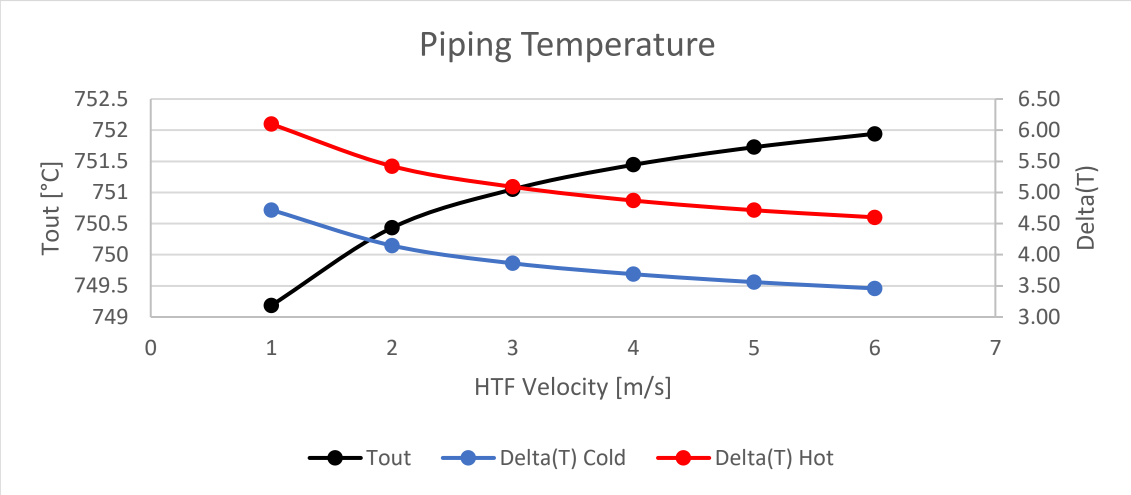

Figure 7-2: HTF temperature arriving at the power block and the temperature drop from the cold and hot piping when varying the fluid velocity through the pipe.

As we can see, the thermal losses affect directly the temperature of the fluid, as was expected, where at $1\ [m/s]$ a total temperature drop of more than 10℃ is perceived, which is a very high value, although all have the same condition of coating temperature, the loss of low flow velocity is higher because a bigger inlet diameter is required to achieve the amount of mass flow needed, and having a bigger diameter means having a bigger area which is in contact with the environment, resulting in a higher thermal loss and more insulating material needed.

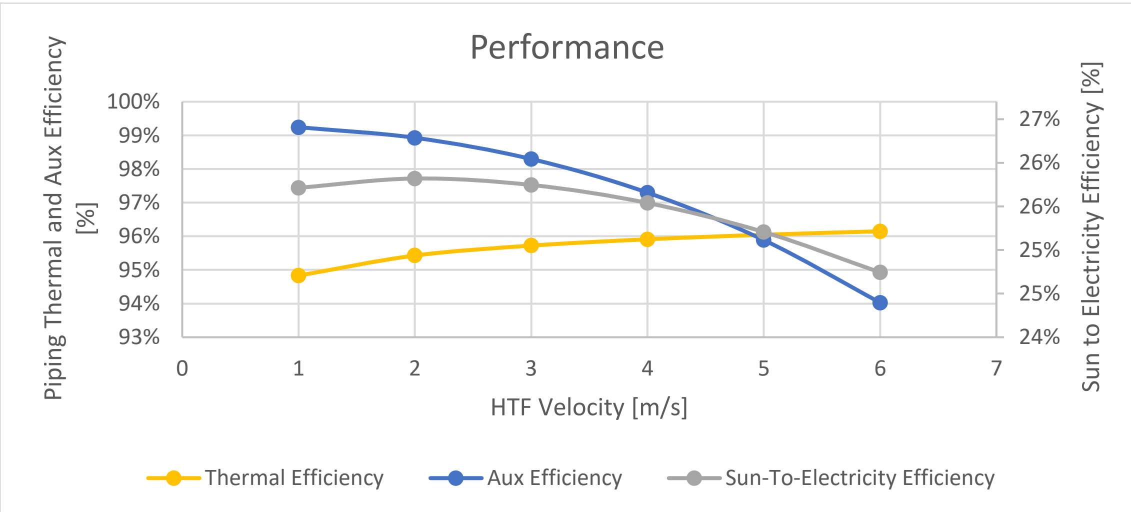

Figure 7-3: Piping performance and overall performance of the plant when varying the fluid velocity through the pipe.

While for the performance there is a maximum which is around $2-3\ [m/s]$ of fluid velocity, this is the overall performance, the sun-to-electricity efficiency of the plant which is a relevant factor to consider. Another consideration is that the thermal loss does not vary as much as the auxiliary efficiency, so the pump consumption has a higher effect on the overall efficiency than the thermal losses through the piping.

Secondly, the coating temperature was varied, similar to the fluid velocity a safety factor was considered to not overcome $60℃$ which is the temperature at which the damage done to a human who touches it becomes severe [68], while for the lower limit a value of $30℃$ was used, ambient temperature was $25℃$ for the simulations, this was chosen due to ambient temperature limit, lowering that value could heavily increase the piping material required and could even become physically impossible to achieve, the results from this parametric analysis are the following:

Table 7-3: Results of the piping performance from changing the coating temperature allowed.

SURFACE TEMPERATURE [℃]	**PRESSURE DROP** $[\boldsymbol{MPa}]$	**PUMP POWER** $[\boldsymbol{kW}]$	**THERMAL LOSS** $[\boldsymbol{MWth}]$	**PIPING THERMAL EFFICIENCY** [%]	**AUX EFFICIENCY** [%]
30	0.55	16.77	0.16	97.04%	98.33%
35	0.55	16.77	0.20	96.30%	98.31%
40	0.55	16.78	0.23	95.72%	98.30%
45	0.55	16.78	0.26	95.22%	98.29%
50	0.55	16.78	0.28	94.76%	98.28%
55	0.55	16.78	0.31	94.33%	98.27%
60	0.55	16.79	0.33	93.92%	98.26%

The velocity selected for the parametric analysis of the coating temperature was $3[m/s]$ and it was kept constant for the different temperatures, as expected the pressure drop remains constant at the same value as the one investigated in the previous analysis, the pump power has some small difference which comes from the density of the fluid at the different temperatures arriving the power block.

While for the thermal performance it is expected to have higher losses when having a higher coating temperature, which is exactly the case shown in Table 7-3, where the highest thermal loss comes from the coating temperature of $60℃$, having a thermal efficiency of $\sim 94\%$ which is very low. Having a better thermal efficiency improves the overall performance but also comes at a higher price, having the need of more piping material to achieve the desired temperature.

Like for the previous case, the temperature of the HTF arriving the power block is shown in Figure 7-4, and the performance of the plant is shown in Figure 7-5, as expected the best performance is shown in the case with the lowest coating temperature, which minimizes the thermal losses while keeping the same auxiliary efficiency, but unfortunately performance is not the only parameter which matters when deciding in what to invest, the economic aspects must be taken into account and finally the LCOE is a good parameter to evaluate the best choice, later the economic aspects of these simulations is shown.

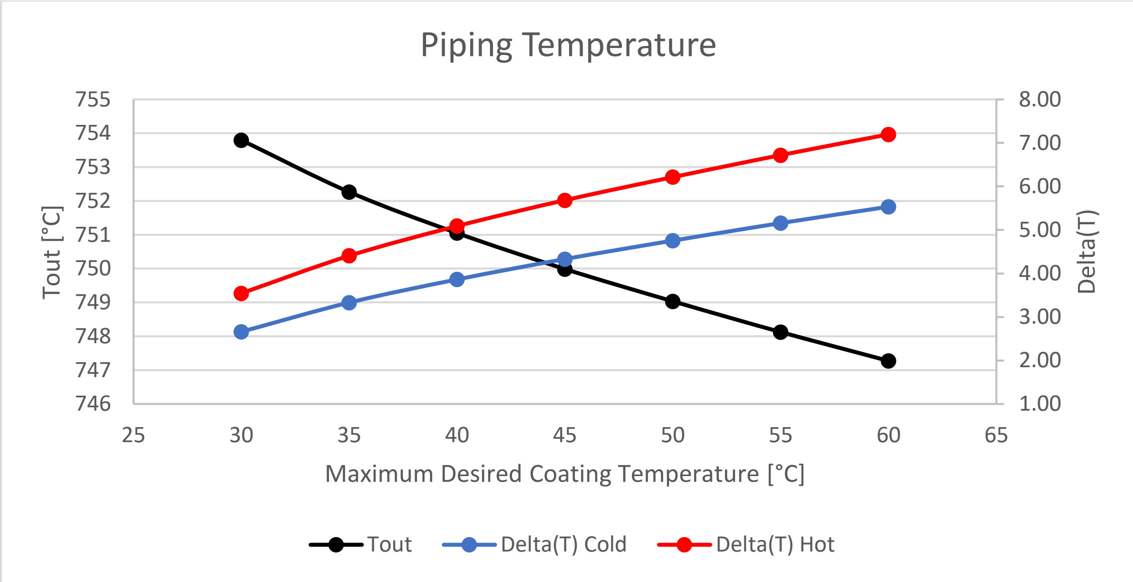

Figure 7-4: HTF temperature arriving at the power block and the temperature drop from the cold and hot piping when varying the allowed coating temperature.

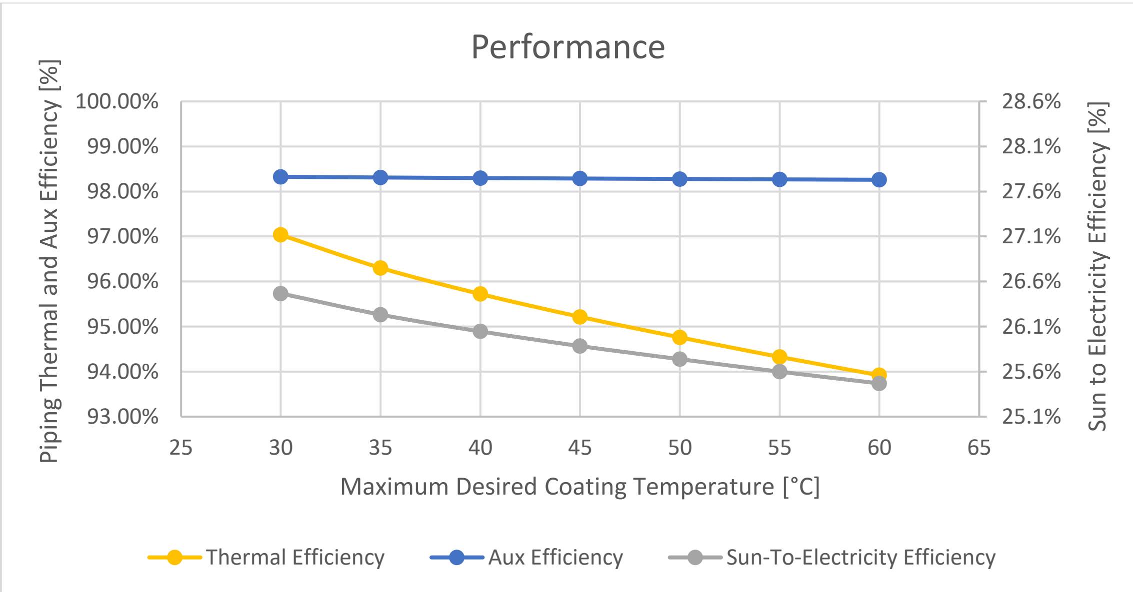

Figure 7-5: Piping performance and overall performance of the plant when varying the coating temperature allowed.

The last parametric analysis made was to vary the number of rows of a plant, to see the effect on a big plant, and how the piping efficiency and costs vary with the number of rows, for this a 120 modules plant was chosen, varying the number of rows, having 120, 60, 40, 24, 20, 12, 8 and 4 rows for the plants simulated, the performance of the different simulated plants are:

Table 7-4: Results of the piping performance from changing the number of rows for the plant layout.

# OF ROWS	PRESSURE DROP $[MPa]$	PUMP POWER $[kW]$	THERMAL LOSS $[MWth]$	THERMAL EFFICIENCY [%]	AUX EFFICIENCY [%]
120	3.80	3459.54	14.84	90.85%	87.58%
60	2.17	1979.34	10.13	93.75%	93.15%
40	1.73	1573.84	8.77	94.59%	94.60%
24	1.50	1363.50	7.89	95.13%	95.36%
20	1.48	1350.48	7.73	95.23%	95.41%
12	1.60	1456.72	7.60	95.32%	95.05%
8	1.85	1681.43	7.75	95.22%	94.28%
4	2.62	2384.62	8.53	94.74%	91.84%

This parametric analysis is not as straightforward as the two from before, since the thermal and auxiliary efficiency have a maximum point in between the parametric analysis, so there is an optimum layout which maximizes the plant performance, the extreme cases which would be one column of towers and one row of towers have the worst efficiencies, both in terms of pumping and thermal losses, but having one column is definitely the worst case since it covers larger distances than all the other cases.

A good reference for thermal performance is the temperature reaching the power block, which can be visualized in Figure 7-6, where comparing with the results above the best thermal performance is the same as the highest temperature, which makes sense, since the thermal energy is related to the temperature of the fluid.

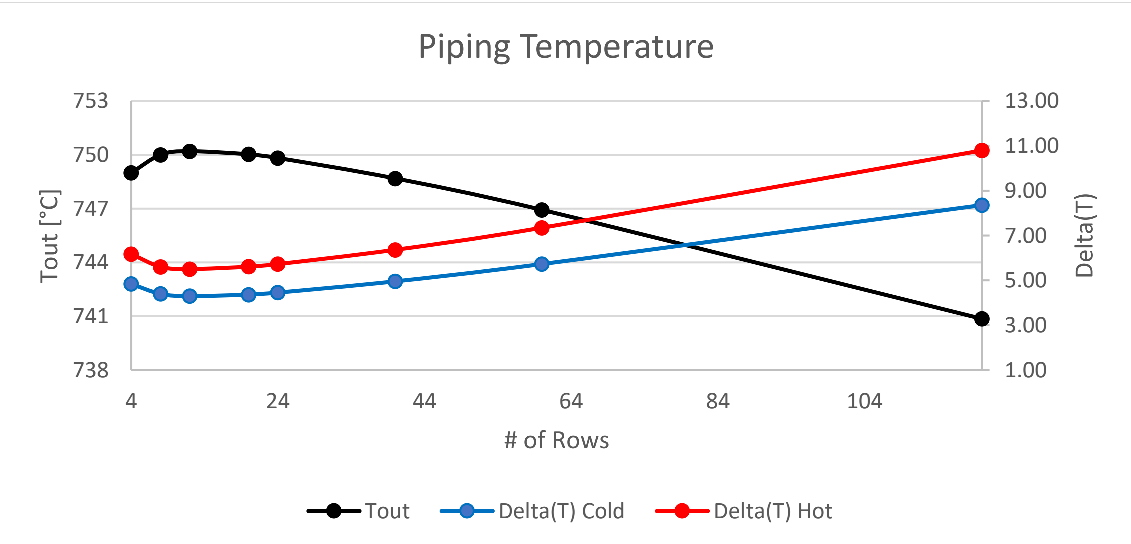

Figure 7-6: HTF temperature arriving at the power block and the temperature drop from the cold and hot piping when varying the number of rows for the plant layout.

When the plant starts to have a high number of rows the thermal performance drops drastically, which can be seen from the results and the temperature reaching the power block, reaching in the worst-case scenario at around ~ 741℃ which compared with the best-case scenario of ~ 750℃ it is a ~ 9℃ loss through the piping, this loss affects the cycle performance and the plant efficiency, it affect directly and indirectly, directly from the thermal loss, and indirectly by having a worst exergy and worsening the sCO_2 cycle, that even though it is very low the effect, it is still something which could be avoided by changing the layout.

For the overall performance of the plant there is a clear maximum around the same point of the best thermal efficiency, this is illustrated in Figure 7-7, where the overall efficiency is highly affected by the auxiliary efficiency, while the thermal efficiency seems to vary less.

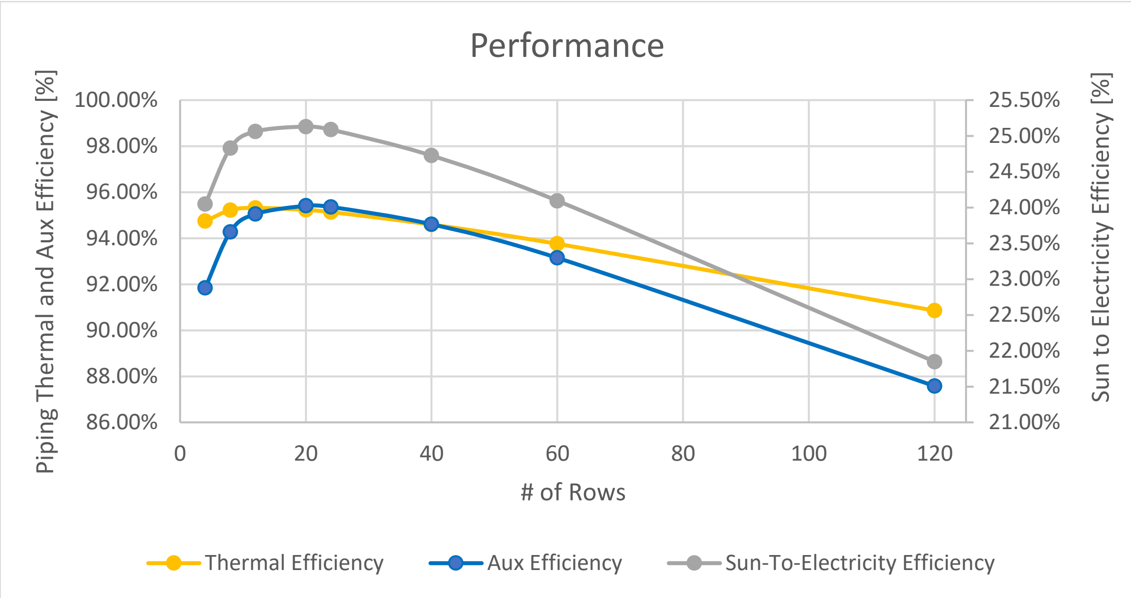

Figure 7-7: Piping performance and overall performance of the plant when varying row numbers for the plant.

Finally, the Vast Solar plant was recreated with the code, simulating two different layouts, and combining them to reach the recreated vast solar plant, the results from these two simulations are shown in Table 7-5 and Table 7-6, where the power and the efficiencies are summarized respectively.

Table 7-5: Summary of power results from the two layouts simulated for the recreation of vast solar.

Thermal Target $[MWth]$	$n_{modules}$	n_{rows}	**Power Field** $[MW]$	**Power Receiver** $[MWth]$			**Thermal Power Left** $[MWth]$	**PB Power** $[MWe]$	**Net Power** $[MWe]$
				Inc	Abs	HTF			
10.816	8	4	18.60	12.72	11.96	10.82	10.52	2.31	2.28
5.408	4	4	9.30	6.36	5.98	5.41	5.25	1.16	1.14

Table 7-6: Summary of the efficiencies from the two layouts simulated for the recreation of vast solar.

Thermal Target $[MWth]$	$n_{modules}$	n_{rows}	$\eta_{optical}$	$\eta_{absorptance}$	$\eta_{receiver}$	η_{Piping}	η_{PB}	$\eta_{sun-to-el}$
10.816	8	4	68.40%	94.02%	90.42%	95.75%	33.00%	18.37%
5.408	4	4	68.40%	94.02%	90.42%	95.93%	33.00%	18.41%

Then the simulation involving 8 modules is “divided” by two to obtain 4 modules, with 2 modules per row, and then the 4-module plant was “divided” by four to obtain the last remaining module, combining these 5 modules the Vast Solar plant was recreated, Figure 7-8 shows the layout simulated with the temperatures at different sections, this is not the same as vast solar pilot plant but very similar to it, the results from the simulation for the recreated plant are:

Table 7-7: Power results from recreated vast solar plant.

Thermal Target $[MWth]$	$n_{modules}$	n_{rows}	**Power Field** $[MW]$	**Power Receiver** $[MWth]$			**Thermal Power Left** $[MWth]$	**PB Power** $[MWe]$	**Net Power** $[MWe]$
				Inc	Abs	HTF			
6.76	5	3	11.63	7.95	7.48	6.76	6.57	1.10	1.08

Table 7-8: Efficiency from the recreated vast solar plant.

Thermal Target $[MWth]$	$n_{modules}$	n_{rows}	$\eta_{optical}$	$\eta_{absorptance}$	$\eta_{receiver}$	η_{Piping}	η_{PB}	$\eta_{sun-to-el}$
6.76	5	3	68.40%	94.02%	90.42%	95.32%	33.00%	18.29%

The power block efficiency of 33% was assumed for the small-scale Rankine cycle [74], this bad efficiency is due to scale of the plant, for large scale Rankine cycles efficiencies can rise to 40%. In this case the power block efficiency is really limiting the sun-to-electricity efficiency, having only 18.29% which when compared to the previous cases studied with the same module but a higher temperature and sCO_2, the sun-to-electricity efficiency was around $\sim 25 - 26\%$, this is a 36.6% improvement in overall efficiency.

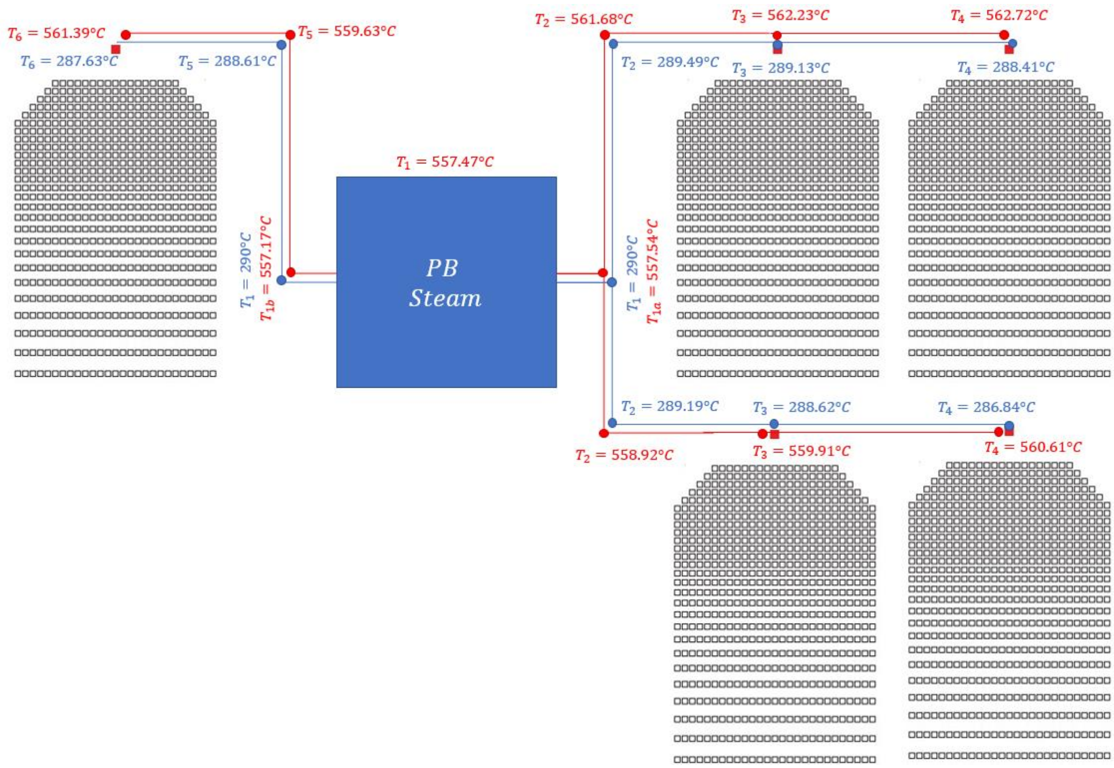

Figure 7-8: Recreation of Jemalong plant using the MATLAB code created for the piping, showing the temperature distribution through the piping.

One thing to notice is that the temperature drop for the same section from the left side is higher than the one on the right side, this is due to the higher mass flow through the pipe when having two modules instead of only one, the actual Jemalong plant takes advantage of this and the mass flow for the two towers at the top side go together with the remaining tower, so the temperature drop should be lower for the real plant.

For the case of these simulations different cost correlations where used, because there were some studies into this plant and modules with some economic considerations, and the cost correlations mentioned before do not apply for small towers like the ones from vast solar.

For these simulations, the following considerations where taken, the heliostat specific cost was assumed at $(200\ [\$/m^2])$ and the heliostat field was assumed to be 36% of the total investment of the module, then for the receiver a 5% of that investment cost is attributed to a reference receiver which would be the low-cost receiver of $1m^2$, that receiver is scaled up to the material cost and size, then adding that to the total investment cost [74], finally the tower cost is assumed at 10% of this new total investment, these calculations are shown below on [Cost of Vast Solar Components].

Using those values the share of costs for the vast solar plant is shown in Figure 7-9, while the total cost of the plant rose to \$6.780.266.

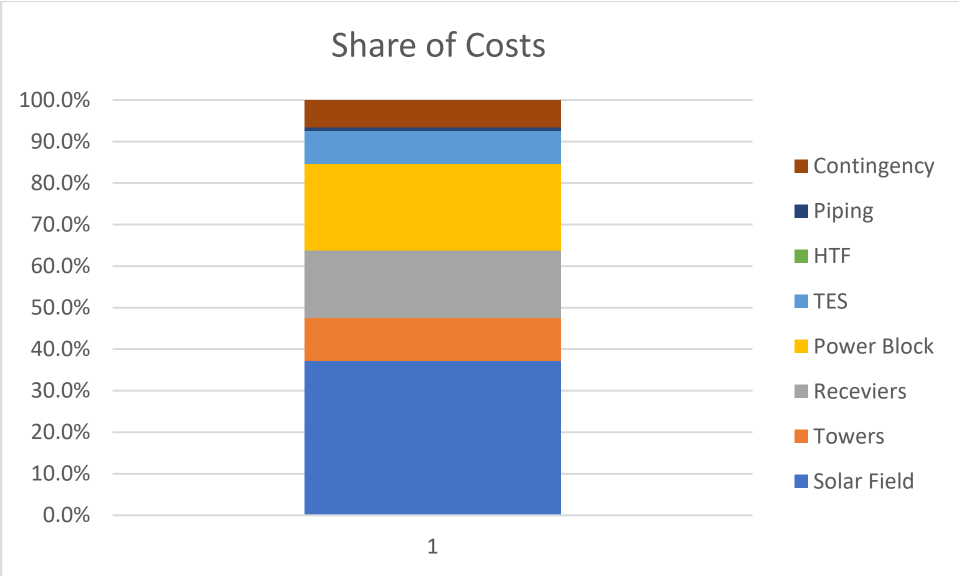

Figure 7-9: Cost share for the recreated vast solar plant.

The piping costs for the recreation where very low due to the lower operating temperatures, so less insulating material was needed and the steel properties are better so less steel is required, resulting in a low piping cost for that small plant.

A huge part of the costs goes to the power block, because of the small size the specific costs of the turbine are very high, resulting in a higher share of costs, while for the tower a 10% of the costs was assumed, this was taken from Irena which stated a 5% of the costs for the tower, but due to the small scale a higher percentage was assumed.

7.2. Single Tower Results

On the Appendix more detailed results from the single towers are shown, showing the parametric analysis range and step employed, and the best choices for each parametric analysis, also the results from the best choice of the single tower are shown, the layout, performance results, flux distribution and efficiency map of the whole set of angles for which it will operate.

It is very important to optimize the layout of the single towers, in order to optimize the multi-tower/modular-tower arrangement, because there is no point in doing a modular plant with bad performing modules, that is why a parametric analysis was made for each single tower searching for the best in terms of performance and cost-efficiency.

The following sections will show the results from the different configurations and solar nominal power, and then a summary of the results is shown for comparison.

7.2.1. Sodium Central Receiver

Central receivers are widely used for high thermal powers on towers, since having an equator facing field with a very high thermal target at the receiver would mean having heliostats very far away where the attenuation losses overcome the cosine gains from this type of field, the surround field or central field allows for more closely packed heliostats, reducing the optical losses from far away heliostats.

For the purpose of this work, three central towers where studied, one of 150 $MWth$, the second one $250MWth$ and the last one $500MWth$. The performance of these plants is further studied in this section.

While for the design choices, the best choice was selected in terms of energy and cost related to the plant, the results for the best choices are shown in Table 7-9, where we see that higher thermal power require higher towers and bigger fields, the higher tower is to provide with a better optical efficiency while the bigger field is due to the higher number of sunrays which have to be reflected to the receiver.

Table 7-9: Design choices for the Sodium Central Towers considered.

	$\mathbf{150MWth}$	$\mathbf{250MWth}$	$\mathbf{500MWth}$
$\boldsymbol{Tower\ Height}\ [\boldsymbol{m}]$	142	166	197.5
$\boldsymbol{Receiver\ Height}\ [\boldsymbol{m}]$	8	9.9	14.2
$\boldsymbol{Receiver\ Diameter}\ [\boldsymbol{m}]$	6.4	7.92	8.67
$\boldsymbol{Receiver\ A.R.}\ [-]$	1.25	1.25	1.6
$\boldsymbol{Horizontal\ distance}\ [\boldsymbol{m}]$	1108	1491	2518
$\boldsymbol{Vertical\ distance}\ [\boldsymbol{m}]$	1105	1478	2501

These choices showed that aiming for higher flux at the receiver achieved better cost/energy metrics, the reason behind this is that aiming for higher fluxes allows for smaller receivers and lower thermal losses, even though smaller receivers also have lower optical efficiencies, but the economic aspect together with the thermal one overcame the optical loss, for the three towers the peak incident flux recorded at equinox was around $\sim 2100 \div 2200\ [kW/m^2]$, this is one big advantage of sodium which allows high fluxes at the receiver, reducing the investment cost related to that component.

The performance results at the autumnal equinox are show in Table 7-10, the results were provided by SolarPILOT with the exception of the costs which considered the ones proposed for this work.

One important aspect to notice is the optical efficiency of the three plants, when comparing the smaller ones the optical efficiency does reduce when increasing the thermal target but on a small scale, from 66.56% to 64.24%, but when we increase the thermal target up to $500MWth$ the optical efficiency greatly reduces to 55.46%, this is caused by three factors, the cosine, attenuation and the image intercept efficiency, which are the most influenced efficiencies when increasing or reducing the solar field size.

Table 7-10: Performance at the autumnal equinox for the selected towers.

	Units	**150MWth**	**250MWth**	**500MWth**
Total plant cost	$M\$$	\$53.55	\$88.37	\$186.92
Simulated heliostat area	m^2	265555	453774	1028289
Simulated heliostat count	–	2074	3544	8031
Power incident on field	kW	252277	431085	976875
Power absorbed by the receiver	kW	157851	260299	509223
Power absorbed by HTF	kW	147613	244620	484605
Cloudiness efficiency	%	100	100	100
Shading efficiency	%	100	100	100
Cosine efficiency	%	83.84	82.52	80.02
Reflection efficiency	%	90.25	90.25	90.25
Blocking efficiency	%	99.11	98.84	98.61
Attenuation efficiency	%	95.59	94.6	92.33
Image intercept efficiency	%	92.85	92.26	84.35
Absorption efficiency	%	94	94	94
Solar field optical efficiency	%	66.56	64.24	55.46
Optical efficiency incl. receiver	%	62.57	60.38	52.13
Incident flux	$kW/m2$	1044	1124.2	1400.6

One last aspect to consider is the thermal efficiency of the receiver, for this work the thermal efficiency will include the reflectivity, convective and radiative losses at the receiver, with this in consideration the thermal losses are, 87.91%, 88.33% and 89.45% for the $150MWth$, $250MWth$ and $500MWth$ respectively, the thermal efficiency is correlated with the average incident flux, the higher this value is, the higher the thermal efficiency will be, there are other physical factors which influence this like the operating temperature, but for similar conditions those two seem to be correlated.

The final consideration regarding these results is the overall efficiency of the receiver and heliostats, which is a very important indicator of performance of the single tower, and it will greatly influence the overall plant efficiency, for this the product between the thermal efficiency and the optical efficiency is made, the values are, 58.51%, 56.75% and 49.61% for the $150MWth$, $250MWth$ and $500MWth$ respectively, for the biggest tower more than half of the energy is lost before even going into the piping and power block.

7.2.2. Sodium Polar Field

Equator facing fields or polar fields are mostly used for small thermal targets, the benefit from this type of field comes from the better optical efficiency, mainly due to the cosine efficiency, the reason behind this only being used for small fields is that the cosine benefit is lost from worst attenuation and image intercept efficiencies, which become more relevant in bigger fields and a surround field is better suited for those cases.

One way of having the improvement of the cosine efficiency for large thermal targets is the use of modular systems, which is the focus of this work, for this multiple polar fields are studied, the design choices for these fields are shown in Table 7-11, these values come from a parametric analysis in which the best cost efficient layout was chosen.

Table 7-11: Design choices for the Sodium Polar Field Towers considered.

	$\boldsymbol{5MWth}$	$\boldsymbol{10MWth}$	$\boldsymbol{20MWth}$	$\boldsymbol{30MWth}$	$\boldsymbol{50MWth}$
$\boldsymbol{Tower\ Height\ [m]}$	50	56	70	78	99
$\boldsymbol{Receiver\ Height\ [m]}$	3.55	2.35	4.1	4.9	6.4
$\boldsymbol{Receiver\ Diameter\ [m]}$	1.78	4.7	4.69	5.6	7.31
$\boldsymbol{Receiver\ A.R.\ [-]}$	2	0.5	0.875	0.875	0.875
$\boldsymbol{Horizontal\ distance\ [m]}$	190	333	455	607	791
$\boldsymbol{Vertical\ distance\ [m]}$	188	252	391	513	669

In this case the horizontal and vertical distance are relevant information, because those will influence the piping length required for modular plants, for the smallest plant the vertical and horizontal distance are very similar, while for the largest plant the horizontal distance becomes greater than the vertical distance.

The performance results at the autumnal equinox are show in Table 7-12, similar to before, the performance was provided by SolarPILOT and the costs by the correlations seen in this work.

One important information is that the costs do not increase proportionally to the thermal target, increasing the thermal target reduced the specific cost of the single tower and field, this is true due to cost reductions achieved by bigger layouts, for example the $50MWth$ costs around ~ 6 times the cost of the $5MWth$, that is why it is very important to consider cost reductions of modular technologies as well.

While for the performance of the plant, the optical efficiency behaves in the same way as the central towers, the larger the field the lower the efficiency, where the $5MWth$ tower has a 71.54% optical efficiency while the $50MWth$ has 65.22%, about 5% less than the small field.

But on the thermal efficiency, the larger field has a better thermal efficiency than the small field, which could be inferred from the average incident flux at the receivers, where the trend seems to be that larger fields have higher incident flux, this could be because of the reduction in optical efficiency and the higher investment cost were investing more on improving the thermal efficiency becomes more appealing in the cost-efficient analysis to improve the overall efficiency of the tower.

Table 7-12: Performance at the autumnal equinox for the selected towers.

	Units	$5MWth$	$10MWth$	$20MWth$	$30MWth$	$50MWth$
Total plant cost	$M\$$	\$3.08	\$4.74	\$7.92	\$11.37	\$18.22
Simulated heliostat area	m^2	8649.4	17947	35427	54891	91816
Simulated heliostat count	−	2483	5152	2863	4436	7420
Power incident on field	kW	8217	17049	33656	52147	87225
Power absorbed by the receiver	kW	5526	10855	21224	31965	53475
Power absorbed by HTF	kW	5123.8	10152	20000	30219	50497
Cloudiness efficiency	%	100	100	100	100	100
Shading efficiency	%	100	100	100	100	100
Cosine efficiency	%	92.5	90.61	89.99	89.15	89.06
Reflection efficiency	%	90.25	90.25	90.25	90.25	90.25
Blocking efficiency	%	99.94	99.87	99.74	99.69	99.78
Attenuation efficiency	%	98.14	97.77	97.17	96.63	95.9
Image intercept efficiency	%	87.38	84.83	85.24	84.14	84.8
Absorption efficiency	%	94	94	94	94	94
Solar field optical efficiency	%	71.54	67.73	67.09	65.21	65.22
Optical efficiency incl. receiver	%	67.25	63.67	63.06	61.3	61.31
Incident flux	$kW/m2$	930.32	1045.6	1174.2	1239.3	1216

The optical efficiency shown is at autumnal equinox, while the maximum efficiency of the year can reach higher values, for example the $5MWth$ reaches a maximum optical efficiency of 74% and the $30MWth$ layout reaches 69.1% both improving around 4% their performance at the best point, this comes to show that the performance of the plant simulated at a given time is not the biggest reference when designing a plant, but a yearly simulation must be made.

Another important parameter to measure, would be the influence of the location on the efficiency of the modular technologies, because more centralized countries do not have the issue of cosine efficiencies in their plants, so further study could be made regarding the scope of modular technologies.

7.2.3. Comparison between fields

Small polar fields are the best performing fields of the simulated ones, having a better optical efficiency due to the closely packed heliostats, but once the polar field starts increasing the optical efficiency lowers and at a certain point it becomes better to have a surround field, this can be seen from the previous results where the last two polar fields show a lower efficiency than the $150MWth$ surround field for the day and time simulated at least.

The cosine efficiency is better for polar fields and this is the source of the improved optical efficiency, having between $92 \div 89\%$ of cosine efficiency for the simulated towers with the equator facing field, while the surround fields have between $83 \div 80\%$, but on the other side the surround fields showed better image intercept efficiencies, so there is a tradeoff, which for small fields is convenient but for larger fields it is not.

The optical and thermal efficiencies of all the simulated plants is shown in Table 7-13 for comparison, the overall efficiency ($\eta_{Optical} \cdot \eta_{Thermal}$) is also computed and shown.

Table 7-13: Efficiencies of the different layouts simulated and thermal targets.

	$\boldsymbol{\eta_{Optical}}$	$\boldsymbol{\eta_{Thermal}}$	$\boldsymbol{\eta_{Opt} \cdot \eta_{The}}$
$\mathbf{5}\boldsymbol{MWth}$	71.54%	87.16%	62.36%
$\mathbf{10}\boldsymbol{MWth}$	67.73%	87.92%	59.55%
$\mathbf{20}\boldsymbol{MWth}$	67.09%	88.57%	59.42%
$\mathbf{30}\boldsymbol{MWth}$	65.21%	88.87%	57.95%
$\mathbf{50}\boldsymbol{MWth}$	65.22%	88.77%	57.89%
$\mathbf{150}\boldsymbol{MWth}$	66.56%	87.91%	58.51%
$\mathbf{250}\boldsymbol{MWth}$	64.24%	88.33%	56.75%
$\mathbf{500}\boldsymbol{MWth}$	55.46%	89.45%	49.61%

The three smaller polar fields show a better performance than the surround fields, while the bigger polar fields show a worse performance than the $150MWth$ surround field, the difference in thermal efficiencies does not seem to be as relevant as the optical ones. The smallest field shows a great improved over the other towers simulated, having an overall efficiency of 62.36% which is around $\sim 3\%$ better than the second-best performing tower, of course this improvement is for the single field, for a plant with multiple modules the piping losses are relevant, and the real improvement must be measured on the plant design and annual simulation.

While the best performing tower is the smallest one, the specific cost ($\$/kWth$) of that tower is also the highest one, reaching ~ 600 [$\$/kWth$], while the surround field towers are at ~ 360 [$\$/kWth$], the trend of the specific cost can be seen in Figure 7-10, where it seems to have a minimum and then rise up again, this increase in specific cost must be related to the bad performance of the biggest tower simulated.

Figure 7-11 and Figure 7-12, show the trends of the design parameters for the simulated towers, where the tower height seems to increase faster for smaller fields than bigger fields, while the receiver area shows more of a proportionality between the thermal power and receiver area.

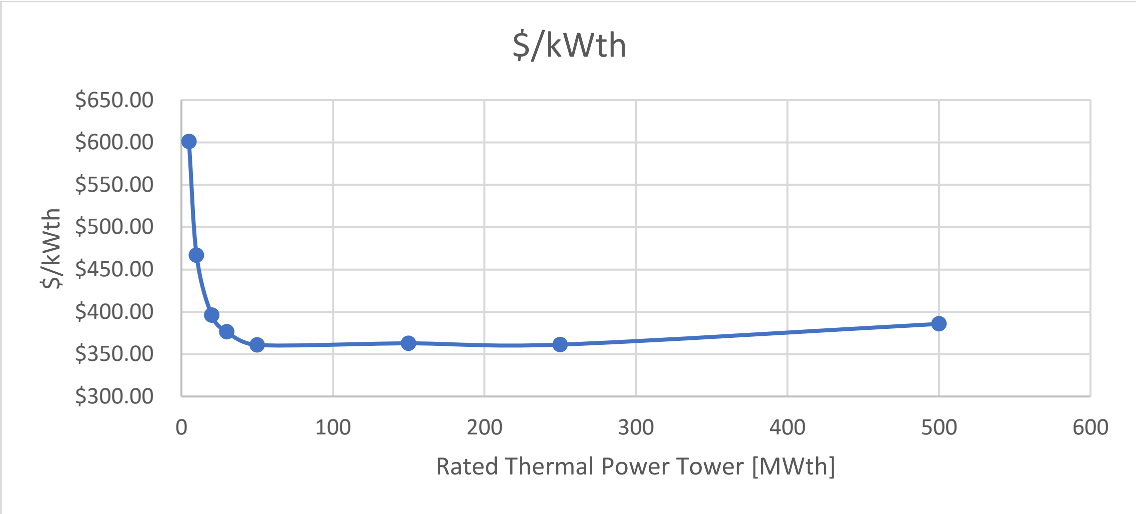

Figure 7-10: Specific cost of the simulated towers.

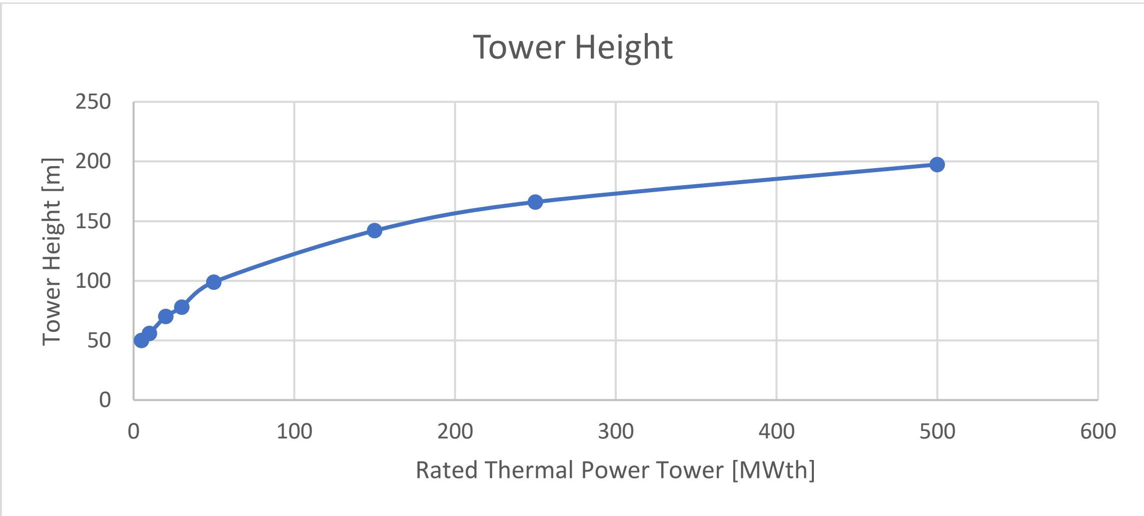

Figure 7-11: Tower height trend of the simulated towers.

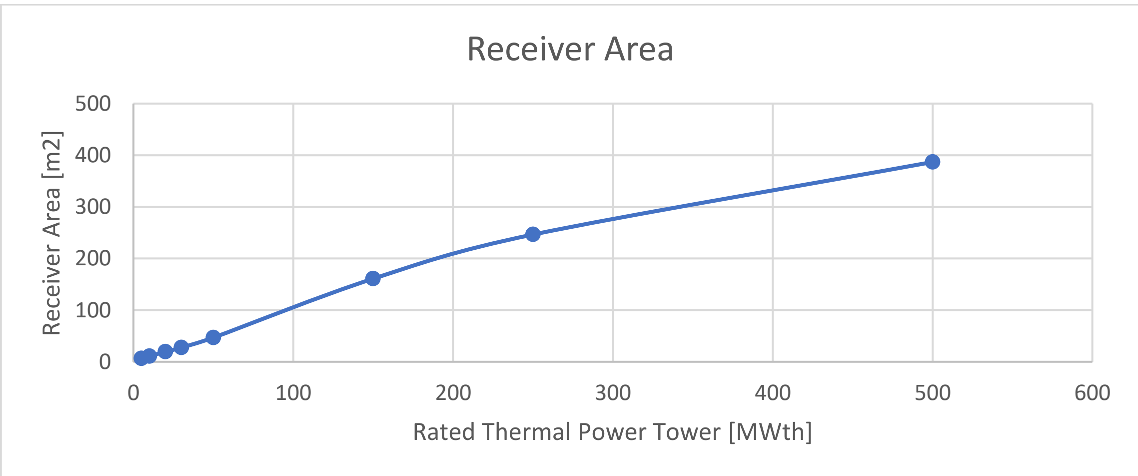

Figure 7-12: Receiver area trend of the simulated towers.

7.3. Plant On-Design Performance

The plant on design performance is made with the piping model described in previous chapters, this is made for the modular towers, while for the central towers the same model is used with some changes on the piping dimensions, like the horizontal and vertical distance, which for modular technologies is important, but for central towers the power block is usually located near the tower, so less piping is required, and no consideration is made regarding the plant layout dimensions.

For this section, the performance of the plants on design are analyzed and compared, from both the energy point of view and the economic one, together with some other design details extracted from the code.

Starting from the piping design, the stainless-steel thickness and the total insulating thickness are obtained for the different modules and for the different amount of those modules in the plant layout, only the header of the piping is shown, Figure 7-13 and Figure 7-14 show the steel thickness required by the different modules and layouts, while Figure 7-15 and Figure 7-16 show the insulating thickness required.

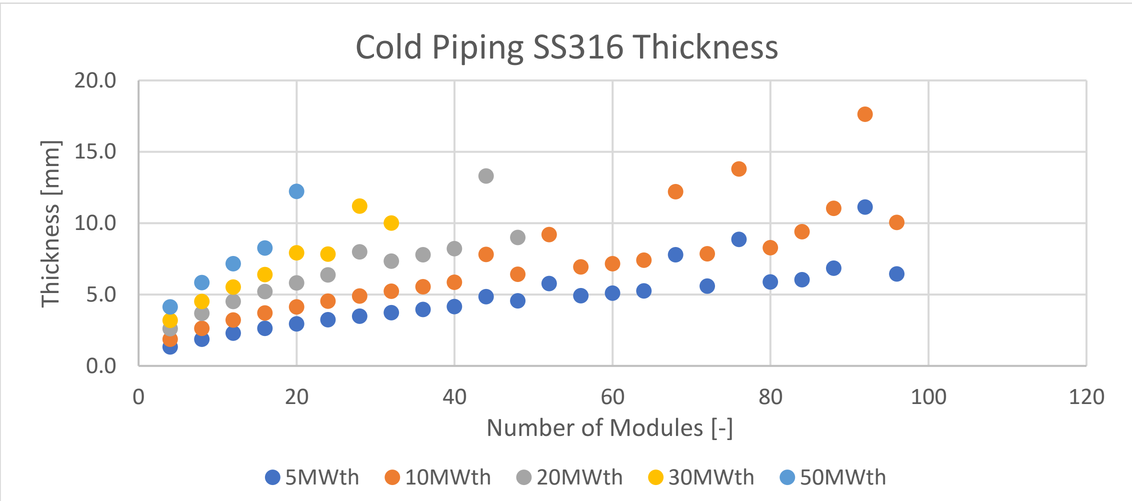

Figure 7-13: Stainless-Steel thickness for the cold piping header of the different modules and layouts.

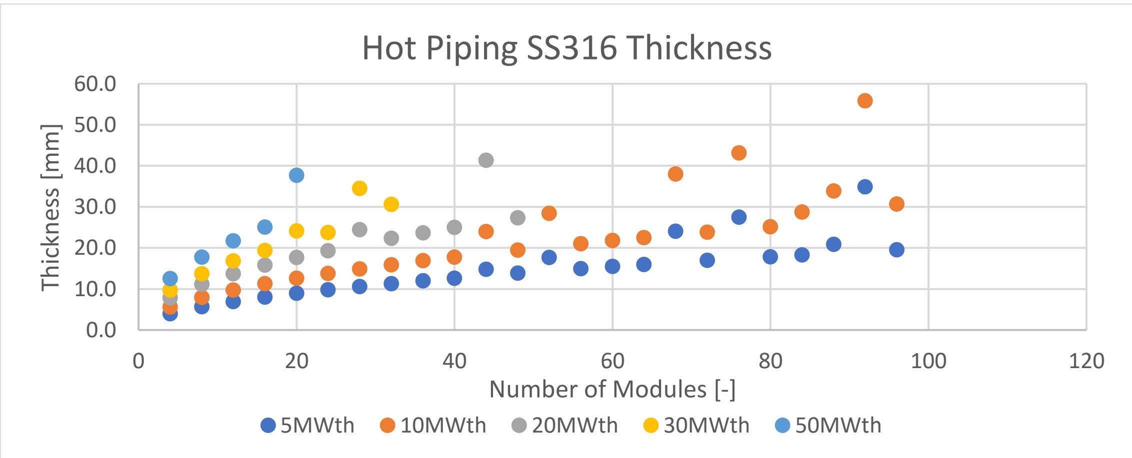

Figure 7-14: Stainless-Steel thickness for the hot piping header of the different modules and layouts.

The values provided by the graphs above are very useful for the design of the rest steel pipe required by the rest of the plants, since it shows the thickness required by an x number of modules up ahead, this makes future designing of plants simpler and easier, making it possible to standardize the piping for manufacturing, reducing the costs of piping.

It makes sense that the $50MWth$ requires more thickness at the same number of modules than the other ones, since it has more sodium flowing through the pipe at the same speed, requiring a bigger inlet diameter, in consequence of that, the steel pipe must be thicker for mechanical reasons from the pressure.

But if we compare for example 8 modules from the $5MWth$ it has the same dimensions than the $10MWth$ with 4 modules, because they both have almost the same flow going through the header.

For the insulating material, the same logic applies.

While when comparing the hot pipe with the cold pipe we notice big differences in terms of dimensions, for the case of steel it is due to the deteriorated mechanical properties of steel at high temperature, but for the insulating material it is to provide with the safety and efficiency considerations.

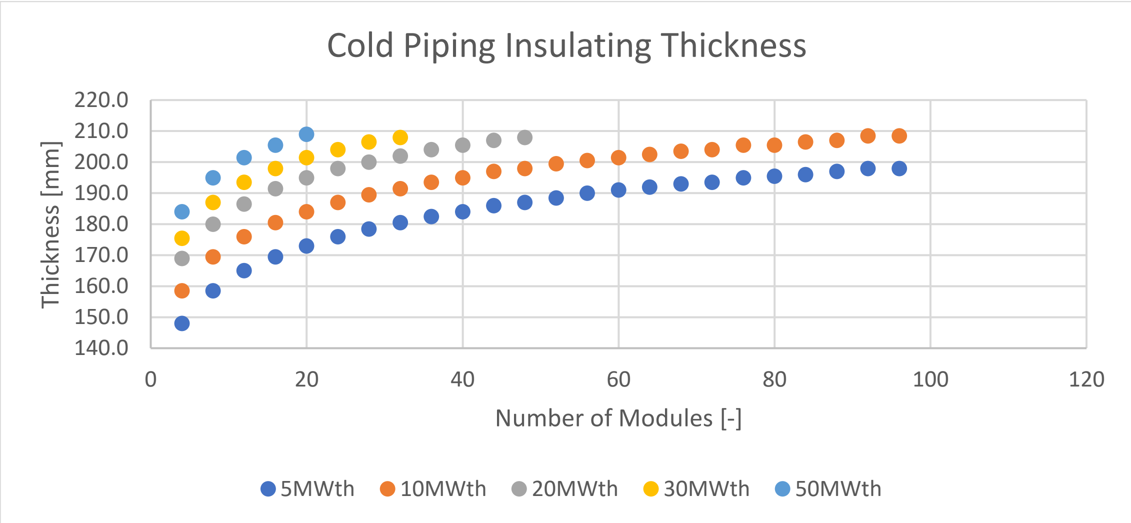

Figure 7-15: Insulating thickness for the cold piping header of the different modules and layouts.

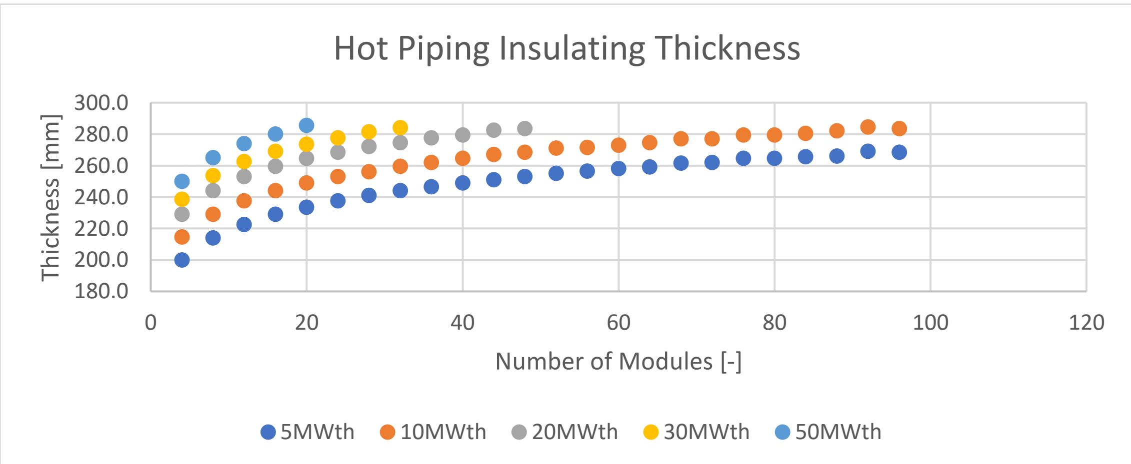

Figure 7-16: Insulating thickness for the hot piping header of the different modules and layouts.

Since the code developed operated with symmetrical layouts, some thermal targets show bad performance, and fall out of the "trends", for example for 28 modules the modules will go 7 to each quadrant, but then there are only two options for the code, to have one single row with 7 modules or to have one single column with 7 modules, and no in between is available, so the code selects the best performance between those, but that best performance is not really the best possible solution for that, evidence from this type of solutions can be seen in the steel thickness graph, where there are some data which fall out of the trend, this is because that solution operates at higher pressure due to the higher pressure drops from an suboptimal solution.

One key aspect from the modular systems is the piping, from the design aspects which were seen above, to the performance and cost of this component. Starting from the performance the Figure 7-17 shows the piping efficiency for the different layouts and modules, this efficiency considers both the thermal losses as the pump consumption.

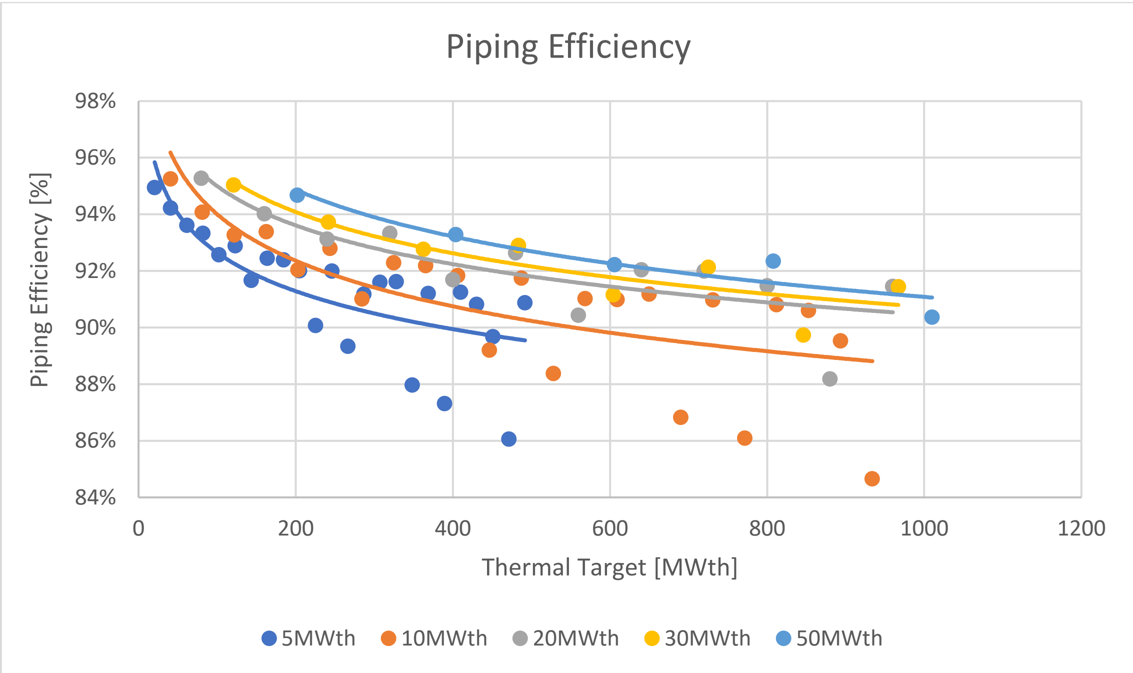

Figure 7-17: Piping Efficiency, considering the thermal loss and the pump consumption for the different modules and layouts.

The common trend seems to be that the small modules have worst performance for similar thermal targets, which makes sense because they require more modules which means longer piping, higher pressure drops and more thermal losses, in the piping efficiency graph it becomes clearer the suboptimal layouts, which have much worst performance than the other layouts and do not follow the same trend. For example, for the $5MWth$ module, the piping efficiency when targeting $471\ MWth$ is $\sim 86\%$ but if we target $492\ MWth$ the piping efficiency becomes $\sim 91\%$ which should not make sense since we are requiring a bigger number of modules.

One consequence from the thermal losses within the piping efficiency is the temperature drop through the piping, this is an important factor to consider mainly due to the power block design and operating temperatures, the temperature drops are shown in Figure 7-18 and Figure 7-19.

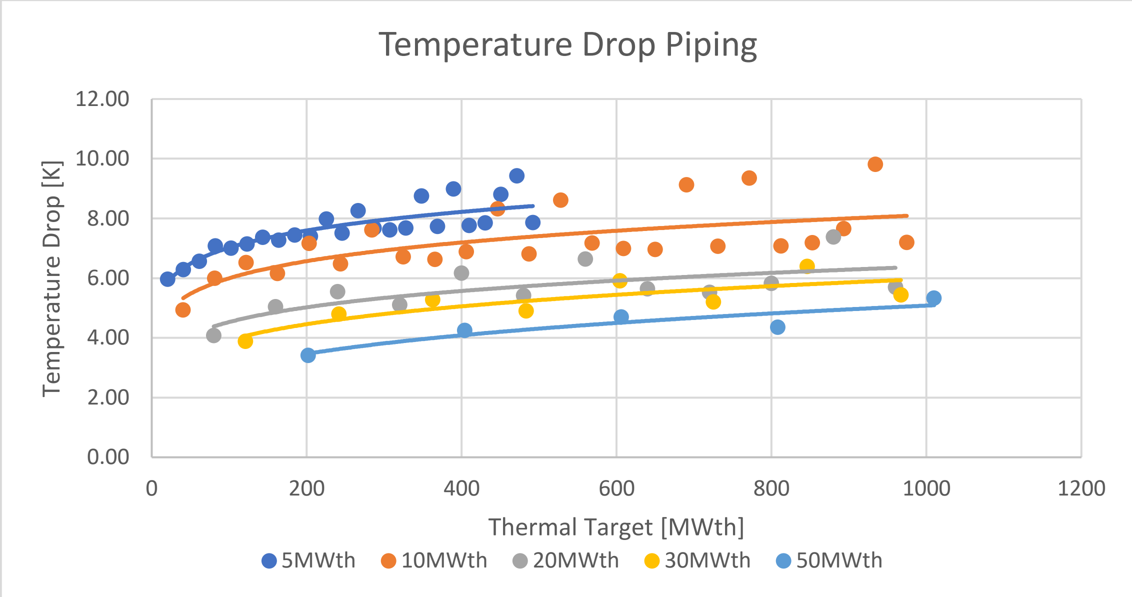

Figure 7-18: Temperature drop through the hot and cold piping for the different thermal targets.

As expected, the temperature drop is higher for the small size modules which have more modules for the given thermal targets, the lowers temperature drop is for the $50MWth$ field with four modules ($\sim 3.5[K]$), while for the small field the highest temperature drop recorded was much higher ($\sim 10[K]$) of course that value corresponds to a suboptimal layout, but for optimized layouts it is still much higher ($\sim 7.5[K]$) for similar thermal targets.

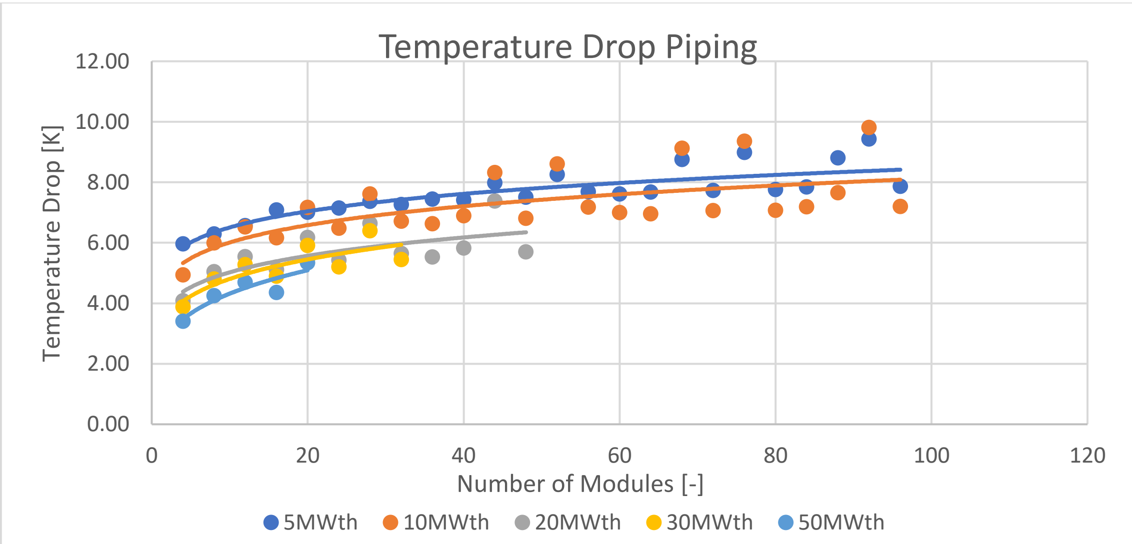

Figure 7-19: Temperature drop through the hot and cold piping for the different number of modules.

If we compare the temperature drop but with the number of modules, the behavior is very similar, the small field for the same number of modules still has the highest temperature drop, even though the bigger pipe required by the bigger fields has higher thermal losses, this means that the increase in thermal power is higher than the increase in thermal losses, proportionally speaking, so higher thermal powers tend to have better thermal piping efficiencies.

The second component in the piping efficiency is the pump consumption, which is characterized by the auxiliary efficiency showed in Figure 7-20 and Figure 7-21.

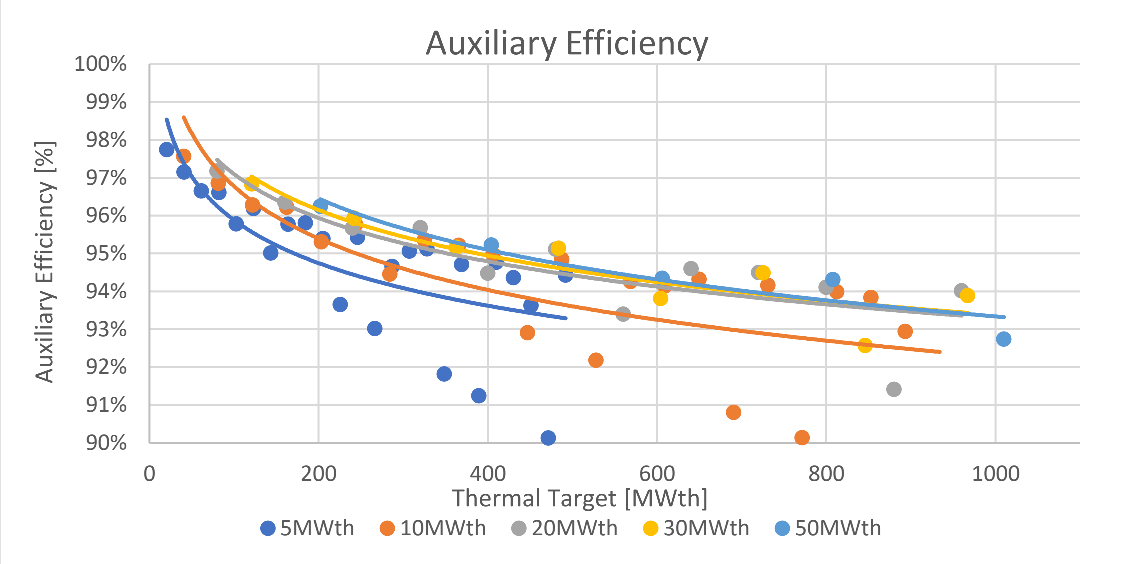

Figure 7-20: Auxiliary Efficiency, considering the pump consumption for the different thermal targets.

Similar to the thermal efficiency, the auxiliary efficiency for similar thermal targets is better for bigger modules, the reason behind this is that the are higher pressure drops when using more modules and consequently the higher the pump capacity required to overcome those pressure drops. For example, comparing the $5MWth$, $10MWth$ and $20MWth$ aiming for a thermal target $\sim 164MWth$ the pump consumptions are $1.27MW$, $1.14MW$ and $1.09MW$ respectively.

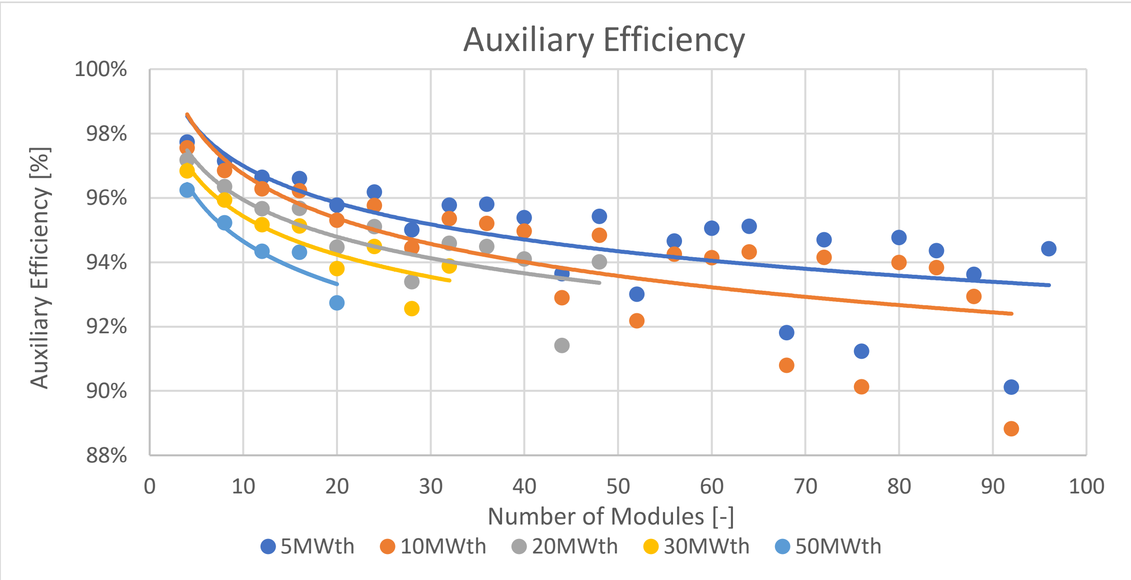

Figure 7-21: Auxiliary Efficiency, considering the pump consumption for the different number of modules.

When comparing the auxiliary efficiency with the same number of modules it makes sense that the behavior is opposite, because the smaller modules require less piping and have lower pressure drops on a per module basis, while the bigger modules require longer pipes and have higher pressure drops.

After seeing the piping performance for the different modules, the overall plant performance should be looked at, for this the sun-to-electricity efficiency is used, which is a key indicator for CSP plants, the results for this efficiency are shown in Figure 7-22.

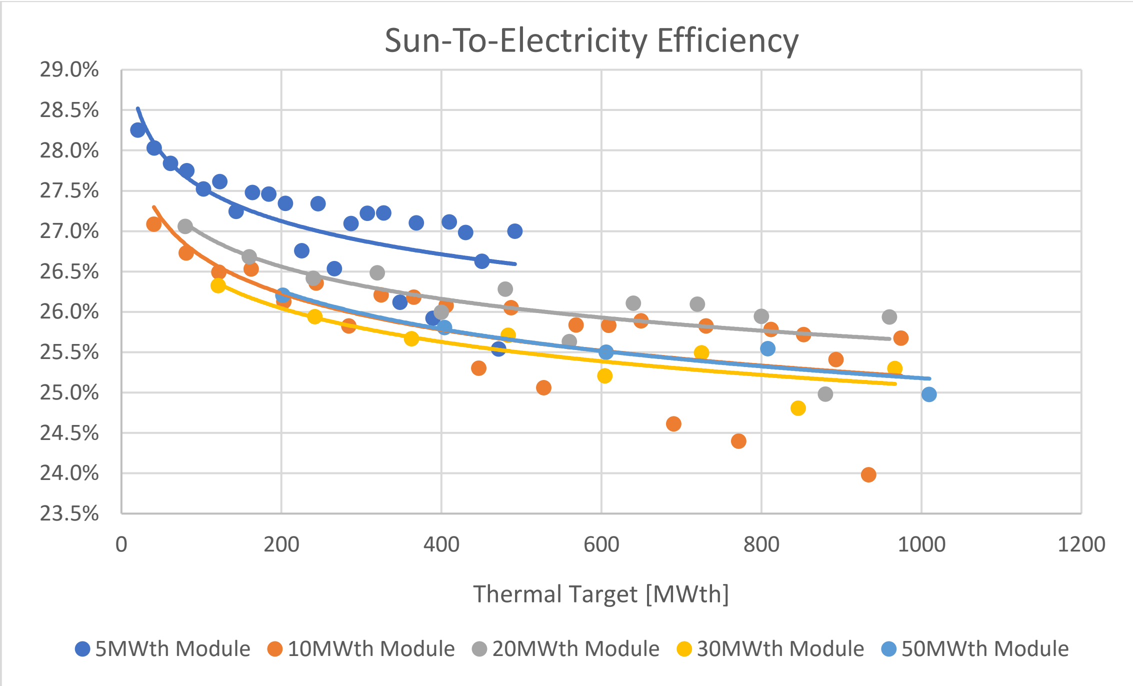

Figure 7-22: Sun-To-Electricity Efficiency at design point of the thermal targets, considering the 5 modules and their layouts.

Unlike the previous results from the piping performance, the overall plant performance has better results for the smallest module ($5MWth$), the great optical efficiency from this module overcomes the losses from the piping performance, reaching values of $\sim 28.5\%$ sun-to-electricity efficiency which is a very high value for CSP plants, and this module performs better for almost all the thermal targets simulated, with the exception of the suboptimal layouts, for the highest thermal target simulated for this module the overall efficiency reached $\sim 27\%$ which is similar to the highest values achieved by the 10 and 20 $MWth$ modules, showing that the optical efficiency plays a key role on the plant performance, overcoming the downsides of the piping performance.

The trend for the overall performance is not as simple as the previous trends, since the $20MWth$ performs better than the smaller $10MWth$ module, and the same happens with the $50MWth$ which performs like the $10MWth$ module and better than the $30MWth$ one, there are multiple factors which make this possible, as we saw the bigger modules have better piping efficiency, and the performance from the $10MWth$ module is close to the one of $20MWth$ making the bigger module better suited for the thermal target set, the same happens for the remaining two modules.

The second key important aspect other than performance is the cost associated to the plants, we can have the best efficient cycle or plant but if the costs are too high no one will invest on it, so an analysis on the cost of the modular technologies is made, starting from the cost share for the different layouts, which can be seen in Figure 7-23 for the different layouts and modules studied.

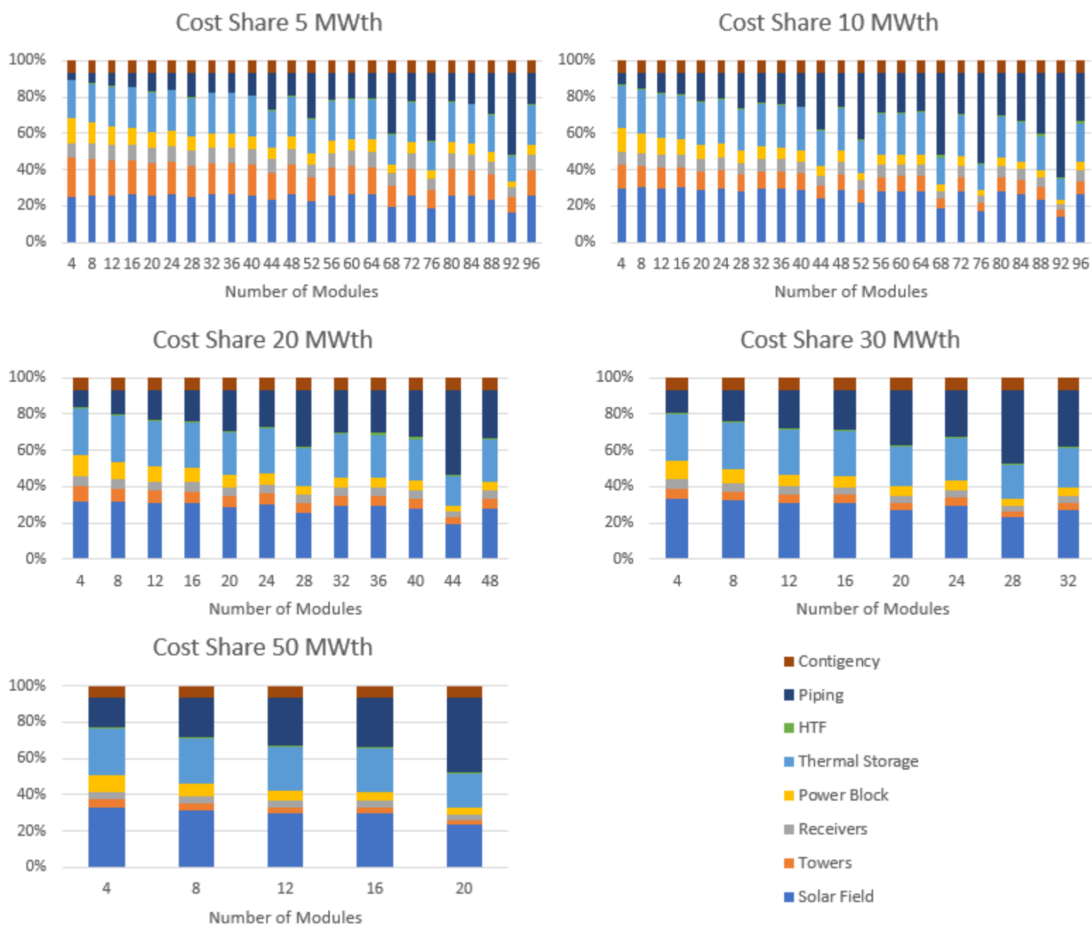

Figure 7-23: Cost share for the different sizes and number of modules.

The cost share for the different layouts within one type of modules changes, this has to do with cost reductions of certain components and increases in costs of other components. Starting from the cost reduction, two components benefit from this, the towers, and the power block, were the tower reduced its costs with a mass production while the power block reduces with the turbine size, this effect can be seen for all the modules, the power block (yellow) and the towers (orange) decrease their cost share of the total costs incurred on the plant layout.

The second effect on the cost share is the increase in cost of piping (dark blue), which taking away the suboptimal cases it still has an increasing trend, for example for the $5MWth$ module the piping share starts at 4% and reaches 17% for the biggest layout. Another increasing trend is with the module size by comparing the same number of modules the bigger ones show higher piping cost share than the smaller ones, a $4x50MWth$ layout has a 16% cost share associated to the piping, which is similar to the biggest $5MWth$ layout simulated.

The suboptimal layouts show a very bad cost share with regards to piping, these layouts can reach more than half of the costs of the plant, remarking how important it is to choose optimal layouts and discard the suboptimal ones, for real applications, suboptimal layouts would be changed to unsymmetrical layouts which will show better performance than the ones simulated here.

After analyzing the results from the modular technologies, a comparison is made with the surround fields in terms of performance and costs, for the performance, the best performing layouts are compared and then for a better comparison, similar thermal targets are compared, the results from this comparisons are shown in Table 7-14 and Table 7-15.

Table 7-14: Best performing layouts for the different modules and surround fields simulated.

$\boldsymbol{layout}$	$\eta_{Sun-To-Electricity}$
$\boldsymbol{4x5MWth}$	28.3%
$\boldsymbol{4x10MWth}$	27.1%
$\boldsymbol{4x20MWth}$	27.1%
$\boldsymbol{4x30MWth}$	26.3%
$\boldsymbol{4x50MWth}$	26.2%
$\boldsymbol{1x150MWth}$	27.0%
$\boldsymbol{1x250MWth}$	26.0%
$\boldsymbol{1x500MWth}$	22.6%

As expected, the modular technologies perform better than the surround field ones, with the exception of the $150MWth$ surround field which performs similar to the modular technologies and even better than the bigger modular fields, the best performing is the $5MWth$ module, of course a $1x5MWth$ will have a better performance due to the less piping required but low rated thermal powers will have trouble finding power block solutions and if they find one the specific cost of the turbine will be very high.

Table 7-15: Comparison between different layouts with similar thermal targets.

$\boldsymbol{Thermal\,Target}$	$\boldsymbol{layout}$	$\eta_{Sun-To-Electricity}$
480	$\boldsymbol{96x5MWth}$	27.0%
480	$\boldsymbol{48x10MWth}$	26.1%
480	$\boldsymbol{24x20MWth}$	26.3%
600	$\boldsymbol{20x30MWth}$	25.2%
600	$\boldsymbol{12x50MWth}$	25.5%
600	$\boldsymbol{4x150MWth}$	26.3%
250	$\boldsymbol{1x250MWth}$	26.0%
500	$\boldsymbol{1x500MWth}$	22.6%

When comparing the different modules but with similar thermal targets the $5MWth$ is still the best performing one between the modular technologies and even reaches a similar efficiency to the $1x150MWth$ mentioned above but for a thermal target of $480MWth$ which is a little more than 3 times the $150MWth$ tower, this comes to show than modular technologies can perform better at high thermal targets, at least at design conditions.

As we mentioned before the performance is one key indicator for a CSP plant, but there is another important aspect, the economical one, so the previous cases mentioned above will be compared in terms of total and specific costs.

The results from the total and specific costs are shown in Table 7-16 where the total costs are shown, and the specific costs related to the net power are also shown.

Table 7-16: Total and specific costs for the selected layouts.

$Single\ Field$	$layout$	$Total\ Cost$ [$]	$Specific\ Cost$ [$/kWe]
$5MWth\ module$	$4x5MWth$	$ 22,303,817	$ 6,004
	$96x5MWth$	$ 510,574,698	$ 5,993
$10MWth\ module$	$4x10MWth$	$ 38,643,994	$ 5,230
	$48x10MWth$	$ 476,323,026	$ 5,585
$20MWth\ module$	$4x20MWth$	$ 70,298,728	$ 4,824
	$24x20MWth$	$ 448,580,414	$ 5,282
$30MWth\ module$	$4x30MWth$	$ 105,408,998	$ 4,799
	$20x30MWth$	$ 637,400,706	$ 6,061
$50MWth\ module$	$4x50MWth$	$ 176,533,740	$ 4,826
	$12x50MWth$	$ 589,241,152	$ 5,519
$150MWth\ module$	$1x150MWth$	$ 133,327,171	$ 4,895
	$4x150MWth$	$ 651,938,001	$ 6,137
$250MWth\ module$	$1x250MWth$	$ 209,530,139	$ 4,667
$500MWth\ module$	$1x500MWth$	$ 404,980,203	$ 4,587

One key takeaway from this table is that the best performing layouts discussed above are not necessarily the best in terms of costs as seen in the specific costs, in this case the best specific cost is for the worst performing layout, the $500MWth$ one, this makes sense because of the cost reduction that comes with big layouts and in show why in reality CSP tower plants usually aim for very big fields, they are prioritizing the economical aspect over the efficiency one.

The same happens for modular technologies, for similar thermal targets the bigger modules have an economical advantage over the small ones and aiming for multiple towers seems to have a bad effect on the economical aspect, this has to do with the piping costs incurred in multiple towers and probably the field layout of the modules is optimized for a single module and no for multiple ones. For example, the vast solar module aims for a lower horizontal distance increasing the vertical one, this is not necessarily optimal for the single module but allows for less piping in multiple tower plants.

For the plants mentioned above all of them have the same solar multiple and storage hours to have a fair comparison between them, the values are the ones mentioned in previous chapters.

7.4. Plant Annual Performance

As has been mentioned before, the design point is only one day of the whole year, which does not necessarily reflect the real performance that the plant will have, it is good for the designing of the plant, but it is very important that the performance is evaluated on a yearly basis as well.

For this the annual simulation is performed with data taken from SAM (System Advisory Model) and the efficiency map taken from SolarPILOT, the simulation is carried on an hourly basis with weather and radiation data as well as the sun position at that hour, the results from the simulated plants are analyzed in this section.

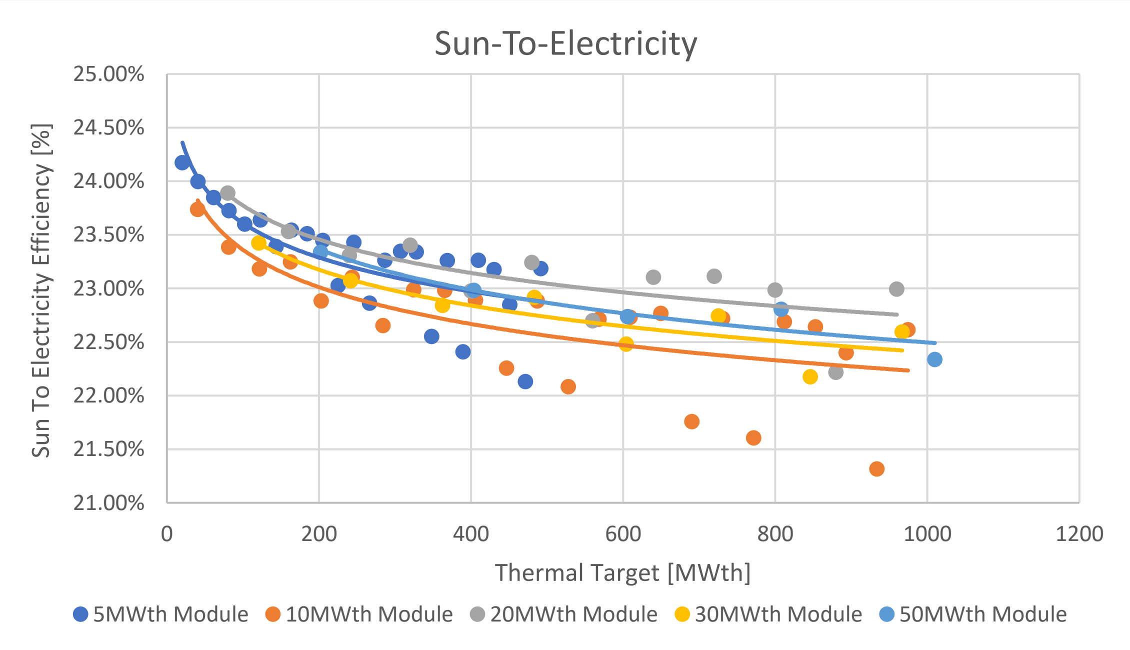

Figure 7-24: Annual performance of the modular layouts with respect to the thermal target.

The results shown above do not consider the defocusing of heliostats on an annual simulation, so the real annual sun to electricity efficiency will be lower than the ones shown above.

One difference that can be seen with respect to the design performance is that the difference in performance is not the same, at design conditions the $5MWth$ performed better than all the other ones and now, the $20MWth$ has a better performance than the smallest module performance, the reason behind this is the receiver thermal efficiency and the piping efficiency, which perform better than the small module, the small module still has better performance than the others at smaller thermal targets.

The reason behind this worsening of performance of the small module with respect to the $20MWth$ one is due to the high number of modules required to achieve similar thermal targets, having more modules requires more pumping power (pressure drop) and higher energy incoming to the receiver to operate (thermal losses) which in the end make the module perform worse.

If we were to see the performance but with respect to the number of modules of the plant a similar trend to the one seen in the design point would be seen. It is the off-design performance of the multiple modules and piping which have a bad effect on multiple modules.

The thermal efficiency at the receiver and the thermal losses of the piping play key roles on the overall performance because these losses limit the operating windows of sunlight as well as energy losses during operation of the plant.

For the economic aspect of the plants, one key indicator is the LCOE as was mentioned earlier on this work, this allows for a standardized indicator of costs and energy output of different energy systems, the LCOE for the modular technologies can be seen in Figure 7-25.

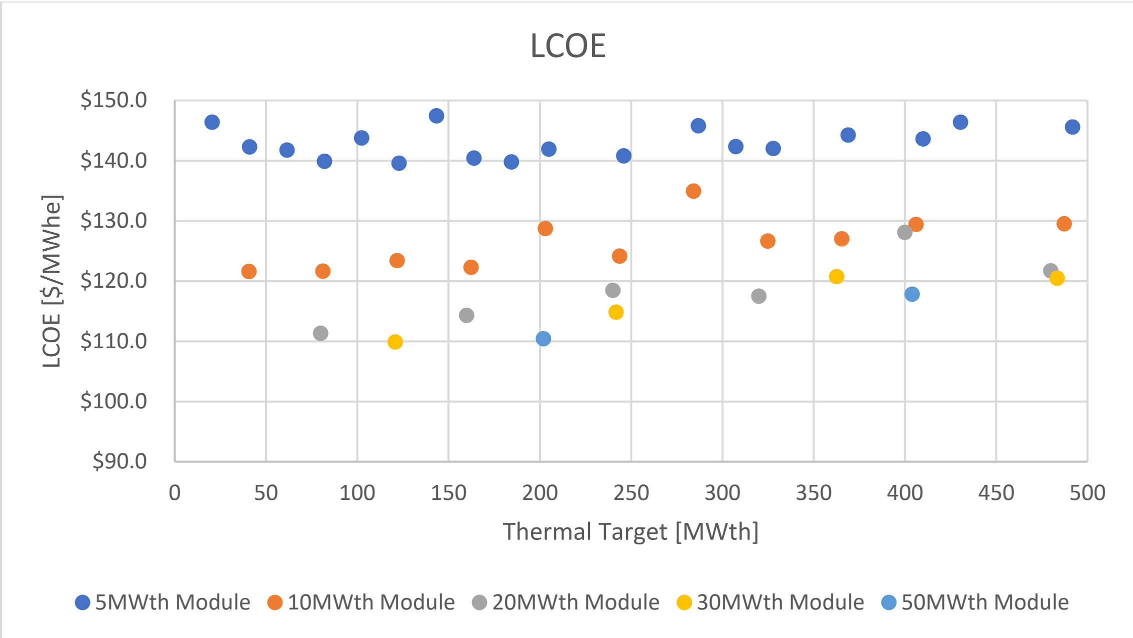

Figure 7-25: Levelized Cost of Electricity for different modules and layouts for different thermal targets.

The trend between modules is that bigger modules reach lower LCOE values for similar thermal targets, but smaller modules have a wider range of applications to meet demand requirements, for the smallest module ($5MWth$) there seems to be a decreasing and then increasing trend while for the bigger modules there is only an increasing trend this is because for the smallest module the cost reduction from increasing the modules in terms of tower and power block compensate the increase in costs of the piping, while for the other modules the increase in costs of piping is superior to the decrease in costs of tower and power block.

The lowest LCOE recorded was 109.9 $[\$/MWhe]$ for the $4x30MWth$ plant, which is a very low value but the north of Chile is known for having very good sun conditions for PV or CSP plants, one study regarding the potential for CSP in Chile showed that a minimum LCOE of 76 $[\$/MWhe]$ could be achieved in Copiapó [85]. So, the values obtained fall in line with current values of LCOE.

Lastly, the modular technologies are compared in terms of performance and LCOE with the central receiver systems simulated, the same layouts as the ones compared for the design point conditions are considered, the results are shown in Table 7-17.

Table 7-17: Performance and LCOE for the different layouts compared.

$Single\ Field$	$layout$	$\eta_{Sun-To-Electricity}$ [%]	$LCOE$ [$\$/MWhe$]
$5MWth\ module$	$4x5MWth$	24.17%	$ 146.35
	$96x5MWth$	23.18%	$ 145.55
$10MWth\ module$	$4x10MWth$	23.74%	$ 121.57
	$48x10MWth$	22.89%	$ 129.52
$20MWth\ module$	$4x20MWth$	23.89%	$ 111.32
	$24x20MWth$	23.24%	$ 121.69
$30MWth\ module$	$4x30MWth$	23.42%	$ 109.87
	$20x30MWth$	22.48%	$ 138.45
$50MWth\ module$	$4x50MWth$	23.34%	$ 110.42
	$12x50MWth$	22.74%	$ 126.09
$150MWth\ module$	$1x150MWth$	24.15%	$ 111.44
	$4x150MWth$	23.41%	$ 140.57
$250MWth\ module$	$1x250MWth$	23.63%	$ 104.74
$500MWth\ module$	$1x500MWth$	20.82%	$ 101.39

For the annual performance of the modular technologies, the smallest field has the best performance for a small layout but when scaling up to 96 modules the performance is no longer attractive when comparing for example with the $4x150MWth$ which has a higher thermal output and a higher overall efficiency.

In terms of performance the $1x150MWth$ has almost the same performance as the best modular layout but at the same time it benefits from the cost scaling of building bigger having an LCOE of 111.44 [$\$/MWhe$] instead of the high LCOE value of the smallest modular system.

Even though the $150MWth$ tower performs better than the modular ones, the LCOE value from the $4x30MWth$ and the $4x50MWth$ have lower values which could be achieved by the cost scaling associated to multitower systems making modular technologies competitive for a certain range of application.

For very big thermal targets the bigger single tower is preferred over the modular systems, even though the performance is the worst of them all, the costs from building a very big field and tower scale down the specific costs associated to the project and reach the lowest LCOE value of all the systems, increasing the number of modules for the multi tower approaches seem to increase the LCOE instead of decreasing it.

When trying to simulate a multitower with surround fields, the LCOE rose very much, making this type of layout very suboptimal solutions for multitower, the $150MWth$ with four modules increased its LCOE by about $\sim 26\%$, while building a bigger tower and receiver reduced the LCOE.

8. Conclusions and Future Work

One issue regarding renewable technologies is their dispatchability, and now that these sources of energy are emerging that issue must be addressed, multiple approaches into this are being assessed, with research going into batteries, hydrogen, and other sources of storage as well as CSP.

To address these challenges faced by renewable technologies, CSP poses a good solution, having very good dispatchability, one main issue of CSP over the years is its LCOE which is too high when compared to Wind and PV which are becoming very common for power plants, so a solution regarding the issues of CSP is necessary.

The aim of this work is to study the implementation of a multitower instead of the common big tower approach, which is commonly taken, the multitower approach is made together with the innovative solutions of Sodium and sCO_2 cycles which also impose a cost reduction and improved performance in CSP plants.

Starting from the literature review, multiple approaches to multitower were found but the most promising was the implementation by Vast Solar of a modular system which showed good performance and future projections, so this type of multi-tower and HTF approach was followed, implementing different modules sizes and layouts.

While for the power block a sCO_2 cycle was pursued because it allows to take advantage of the higher temperature of Sodium fluid having a higher efficiency cycle than the Rankine cycle commonly employed, since the aim was to increase the efficiency cycle a RMCI cycle was employed which showed the best performance.

For the single tower simulations, a parametric analysis was made to each different thermal target, for the optimization a cost/energy metric was used, for the parameters analyzed the tower height and receiver dimensions where studied, for the receiver the height was varied, and the width/diameter was varied accordingly to different aspect ratios which showed the best performance for CSP plants.

From the single tower analysis, it showed that for equator facing fields increasing the thermal power made the optical efficiency worse, and that at very high thermal powers the optical efficiency was better for a surrounded field, a $50MWth$ equator field showed similar optical efficiency values than the $150MWth$ surrounded field, so increasing the thermal power of equator facing field above $50MWth$ was not pursued and instead the surrounded fields where simulated.

Also from the optimization of the single towers, the surrounded fields showed higher peak heat fluxes ($\sim 2000\ [W/m2]$) for the optimal cost/energy metric, while the billboard receivers had lower than $1500\ [W/m2]$ peak heat flux, and the reason behind aiming for higher heat fluxes is to reduce the thermal losses from the high temperature operation of the receiver, but for billboard receivers aiming for higher fluxes than the ones obtained had the downside of reducing the optical efficiency from the field.

For the operating temperature of the plant the values where $550°C$ for the cold side and $760°C$ for the hot side of the piping, which were in line with the operating conditions of the power block chosen, and the higher temperature was set to achieve a greater power block efficiency but not to overdue the thermal stress on the piping, allowing for operation with steel pipes instead of Haynes 230 or Inconel which have much higher costs, the temperature difference between the Sodium and the PB was set to $15°C$ which was in line with literature on sCO_2 cycles.

During the literature review and the analysis it emerged that the most critical aspect of Sodium and high temperature operations was the temperature and the corrosivity of Sodium through the pipes, for the piping itself there where studies confirming that it was possible to use with high temperature but careful consideration regarding the oxygen concentration in Sodium had to be done, while for the receiver the operation was more critical due to much higher maximum temperatures reported which required better material at the receiver, there were some studies which showed that Haynes 230 was able to sustain the temperatures but no real life studies have shown the damage on the long run of this type of applications.

For the designing and on design performance analysis, the Modular technologies showed a very good efficiency and the smallest module simulated had the best performance for the different thermal targets due to its superior optical efficiency 71% even though the piping efficiency for that module at high thermal targets was worst than the others, but in terms of specific costs it showed that the costs where higher than the other modules and the central receiver towers, the cost correlations found in literature take into consideration the scaling of components for bigger fields making the specific costs lower for the bigger modules.

But, for the annual simulation the good performance shown by the smallest module had a falling and performed worse than other modules for similar thermal target and worse than the central receiver towers simulated, so not necessarily the best efficient module will have the best annual efficiency in a multi-tower approach and that the field layout of one module has a strong influence in the plant design and performance.

Finally for the economic aspects of modular technologies it was found that for a range of thermal targets $(120 \div 200\ MWth)$ the modular approach had a better LCOE than the surround field $(150MWth)$ but for larger thermal targets a single surround field showed a better LCOE even though the overall performance of the plant was worse.

Future Work:

Further development regarding the piping material compatibility with high temperature sodium must be made to ensure the longevity that it requires, as well as for receiver designs which are more critical than the plant piping.

While for the plant simulation, the different components should be studied in-depth and modeled together with the piping for a more complete detailed study, from the solar field up to the power block, and special consideration should be made when designing the single towers to obtain the best layout for a multitower plant and not a single tower one.

A more detailed cost study should be made involving the different components and design choices, as well as cost correlations for the future cost reduction that would come from making a standardize module. A cost correlation for smaller towers $(< 50[m])$ should be made for the implementation of small-scale towers with very high efficiencies.

An improved annual simulation considering the storage and defocusing needed during the yearly performance.

References

[1] V. Belessiotis e E. Papanicolaou, “3.03 History of Solar Energy,” Elsevier Ltd, Athens, Greece, 2012.

[2] M. Students, "2009 Product Engineering Processes," [Online]. Available: http://web.mit.edu/2.009/www/experiments/deathray/10_Mythbusters.html. [Accessed 01 03 2021].

[3] Wikipedia, "Nuclear Fusion - Wikipedia," [Online]. Available: https://en.wikipedia.org/wiki/Nuclear_fusion. [Accessed 01 03 2021].

[4] N. Sönnichsen, “Statista,” 04 02 2021. [Online]. Available: https://www.statista.com/statistics/280704/world-power-consumption/#:~:text=The%20world%27s%20electricity%20consumption%20amounted,seeing%20a%20more%20pronounced%20growth.. [Acesso em 01 03 2021].

[5] N. Hartmann, “Hidrógeno Verde - Oportunidad para Chile,” em *Desarrollo de una propuesta de estrategia para impulsar el mercado en Chile*.

[6] G. Manzolini, "Solar Energy," in *Solar and Biomass Course at Politecnico Di Milano*, 2019.

[7] "Global Solar Atlas," [Online]. Available: https://globalsolaratlas.info/download/world. [Accessed 13 February 2021].

[8] Z. Wang, “Solar Resource and Site Selection,” em *Design of Solar Thermal Power Plants*, 2019.

[9] V. Energy, “Vaisala Energy,” [Online]. Available: https://www.3tier.com/en/support/solar-prospecting-tools/what-global-horizontal-irradiance-solar-prospecting/. [Acesso em 01 03 2021].

[10] REN21, “REN21,” [Online]. Available: https://www.ren21.net/gsr-2020/chapters/chapter_03/chapter_03/. [Acesso em 02 03 2021].

[11] L. Aichmayer, “Solar Receiver Design and Verification for Small Scale Polygeneration Unit,” KTH School of Industrial Engineering and Management, Graz, 2011.

[12] “SolarPACES,” 12 June 2018. [Online]. Available: https://www.solarpaces.org/how-csp-works/. [Acesso em 02 March 2021].

[13] L. Moretti, “Thermodynamic optimization and annual performance characterization of concentrated solar power plants employing advanced supercritical CO2 Brayton cycle configurations,” Politecnico di Milano, Milan, 2014.

[14] Contour Global plc, “Contour Global,” [Online]. Available: https://www.contourglobal.com/asset/concentrated-solar-power-spain. [Acesso em 02 March 2021].

[15] S. Qazi, "Chapter 7 - Solar Thermal Electricity and Solar Insolation," in *Standalone Photovoltaic (PV) Systems for Disaster Relief and Remote Areas*, 2017, pp. 203-237.

[16] M. Fedkin, "John A. Dutton E-Education Institute," Penn State University, [Online]. Available: https://www.e-education.psu.edu/eme812/node/648. [Accessed 03 03 2021].

[17] K. Lovegrove and W. Stein, "9 - Parabolic dish concentrating solar power (CSP) systems," in *Concentrating Solar Power Technology*, Woodhead Publishing Series in Energy, 2012, pp. 284-322.

[18] C. Wood and K. Drewes, "Vast Solar: improving performance and reducing cost and risk using high temperature modular arrays and sodium heat transfer fluid," 2019.

[19] cmineracdt, “Construcción Minera & Energía,” [Online]. Available: https://www.construccionminera.cl/complejo-solar-cerro-dominador/#.YD-YBk7itPY. [Acesso em 03 03 2021].

[20] T. Conroy, M. N. Collins, J. Fisher and R. Grimes, "Thermohydraulic analysis of single phase heat transfer fluids in CSP solar receivers," Elsevier, 2018.

[21] A. G. Fernández, J. Gomez-Vidal, E. Oró, A. Kruizenga, A. Solé and L. F. Cabeza, "Mainstreaming commercial CSP systems: A technology review," ELSEVIER, 2019.

[22] F. Zaversky, I. Les, M. Sánchez, B. Valentin, J.-F. Brau, F. Siros, J. McGuire and F. Berard, "Techno-Economic Optimization and Benchmarking of a Solar-Only Powered Combined Cycle with High-Temperature TES Upstream the Gas Turbine," in *Green Energy and Enviroment*, IntechOpen, 2019.

[23] P. Schramek and D. R. Mills, "Multi-tower solar array," ELSEVIER, 2002.

[24] A. Danielli, Y. Yatir and O. Mor, "Improving the optical efficiency of a concentrated solar power field using a concatenated micro-tower configuration," ELSEVIER, 2011.

[25] F. Arbes, W. Landman, G. Weinrebe, M. Wöhrbach, D. Gebreiter, J. M. Estebaranz, D. Pereira and A. Jurado, "Multi Tower Systems and Simulation Tools," AIP Conference Proceedings, 2019.

[26] Z. A. Hussaini, P. King and C. Sansom, "Numerical Simulation and Design of Multi-Tower Concentrated Solar Power Fields," MDPI, 2020.

[27] Irena, “IRENA Renewable Cost Database,” [Online].

[28] A. Solar, "AORA Africa Overview," *The Tulip,* 2015.

[29] "Helios CSP," 15 January 2016. [Online]. Available: http://helioscsp.com/micro-csp-concentrated-solar-power/. [Accessed 13 February 2021].

[30] J. Nelson, N. G. Johnson, P. Doron and E. B. Stechel, "Thermodynamic modeling of solarized microturbine for combined heat and power applications," 2018.

[31] A. Giostri, M. Binotti, C. Sterpos and G. Lozza, "Small scale solar tower coupled with micro gas turbine," ELSEVIER, 2020.

[32] Solastor, "Solastor," [Online]. Available: https://solastor.com.au/the-solar-system/how-it-works/. [Accessed 23 02 2021].

[33] L. E. S. P. Limited, "Lake Cargelligo Solar Thermal Project - Advanced Electricity Storage Technologies Program," 2011.

[34] A. Lehmann and S. Hollis, "High efficiency passive adjustment toroidal heliostat collector for solar receiver with graphite energy storage," ScienceDirect, 2014.

[35] I. Todorovic, "Balkan Green Energy News," Cyprus, 17 02 2020. [Online]. Available: https://balkangreenenergynews.com/cyprus-passes-eur-60-2-million-guarantee-for-concentrated-solar-power-project/. [Accessed 23 02 2021].

[36] CSP Focus, "Sierra SunTower - CSP Focus," [Online]. Available: http://www.cspfocus.cn/en/study/detail_190.htm. [Accessed 05 April 2021].

[37] S. Schell, "Design and evaluation of esolar's heliostat fields," ScienceDirect, Pasadena, 2011.

[38] C. Tyner and D. Wasyluk, "eSolar's modular, scalable molten salt power tower reference plant design," ScienceDirect, 2014.

[39] J. E. Pacheco, C. Moursund, D. Rogers and D. Wasyluk, "Conceptual Design of a 100 MWe Modular Molten Salt Tower Plant".

[40] S. Polimeni, M. Binotti, L. Moretti and G. Manzolini, "Comparison of sodium and KCl-MgCl2 as heat transfer fluids in CSP solar tower with sCO2 power cycles," 2018.

[41] "Jemalong Solar Station Pilot 1.1 MWe," Vast Solar, [Online]. Available: https://vastsolar.com/portfolio-items/jemalong-solar-station-pilot-1-1mwe/. [Accessed 13 February 2021].

[42] Defectors, "Ground breaking dispatchable clean energy development to bring jobs and power to mount isa," Vast Solar, 23 July 2020. [Online]. Available: https://vastsolar.com/2020/07/23/ground-breaking-dispatchable-clean-energy-development-to-bring-jobs-and-power-to-mount-isa/. [Accessed 13 February 2021].

[43] N. E. S. Writer, "NS Energy," 21 July 2020. [Online]. Available: https://www.nsenergybusiness.com/news/vast-solar-project-west-queensland-australia/#. [Accessed 13 February 2021].

[44] NREL, "Solar Power tower Integrated Layout and Optimization Tool," NREL, [Online]. Available: https://www.nrel.gov/csp/solarpilot.html.

[45] SolarPaces, "Solar Paces," [Online]. Available: https://solarpaces.nrel.gov/by-technology/power-tower.

[46] M. J. Wagner, "SolarPILOT User's Manual".

[47] N. R. E. Laboratory, “System Advisor Model Version 2020.11.29 (SAM 2020.11.29) User Documentation”.

[48] P. K. Falcone, "A handbook for solar central receiver design," 1986.

[49] M. Binotti, M. Astolfi, S. Campanari, G. Manzolini and P. Silva, "Preliminary Assessment of sCO2 Cycles for Power Generation in CSP Solar Tower Plants," ELSEVIER, 2017.

[50] A. Marabelli, "Study of advanced solar tower plant using sodium as heat transfer fluid and sCO2 power cycle: technological limits and components design," Politecnico Di Milano, 2019.

[51] L. A. Weinstein, J. Loomis, B. Bhatia, D. M. Bierman, E. N. Wang and G. Chen, "Concentrating Solar Power," ACS Publications, 2015.

[52] M. Cagnoli, A. de la Calle, J. Pye, L. Savoldi and R. Zanino, "A CFD-supported dynamic system-level model of a sodium-cooled billboar-type receiver for central tower CSP applications," ELSEVIER, 2019.

[53] T. Conroy, M. N. Collins and R. Grimes, "Sodium receiver designs for integration with high temperature power cycles," ELSEVIER, 2019.

[54] O. de Meyer, F. Dinter and S. Govender, "Thermal Resistance Model For CSP Central Receivers," AIP Publishing, 2016.

[55] J. Kim, J.-S. Kim and W. Stein, "Simplified heat loss model for central tower solar receiver," ELSEVIER, 2015.

[56] M. d. l. R. Rodríguez Sánchez, "On the design of solar external receivers," Universidad Carlos III de Madrid, 2015.

[57] M. Sarvghad, T. Steinberg and S. Delkasar, "Materials compatibility for the next generation of Concentrated Solar Power plants," *Energy Storage Materials,* September 2018.

[58] J. Pacio and T. Wetzel, "Assessment of liquid metal technology status and research paths for their use as efficient heat transfer fluids in solar central receiver systems," ELSEVIER, 2013.

[59] Haynes® 230®, "Haynes® 230® Brochure".

[60] C. A. Asselineau, W. Logie, J. Pye e J. Coventry, “Limits of the cylindrical absorber design for a sodium receiver,” AIP Conf. Proc., 2018.

[61] B. Kelly and D. Kearney, "Parabolic Trough Solar System Piping Model," NREL, 2006.

[62] N. Boerema, G. Morrison, R. Taylor and G. Rosengarten, "High temperature solar thermal central-receiver billboard design," ELSEVIER, 2013.

[63] North American Stainless, "Flat Product Stainless Steel Grade Sheet 316".

[64] Promat, "Promat HPI in Concentrated Solar Thermal Power".

[65] A. M. Bonanos, M. C. Georgiou, K. G. Stokos and C. N. Papanicolas, "Engneering aspects and thermal performance of molten salt transfer lines in solar power applications," ELSEVIER, 2019.

[66] UNIFRAX, "Insulfrax S Blanket - Product Information Sheet".

[67] ROCKWOOL, “ProRox WM 950ES - Technical Insulation”.

[68] PAROC, "PAROC Pro Mat 50 AluCoat - Product Datasheet".

[69] Johns Manville A Berkshire Hathaway Company, "Too hot to handle?," [Online]. Available: https://www.jm.com/en/blog/2015/february/too-hot-to-handle/#:~:text=ASTM%20C1055%20(Standard%20Guide%20for,without%20sustaining%20irreversible%20burn%20damage.. [Accessed 06 May 2021].

[70] S. W. Churchill and H. H. Chu, "Correlating equations for laminar and turbulent free convection from a vertical plate," *Internation Journal of Heat and Mass Transfer,* vol. 18, no. 11, pp. 1323-1329, 1975.

[71] Y. A. çengel, "External Forced Convection," in *Heat and Mass Transfer*, Mc Graw Hill, pp. 395-450.

[72] Wikipedia, "Grashof Number - Wikipedia," Wikipedia, 09 February 2021. [Online]. Available: https://en.wikipedia.org/wiki/Grashof_number. [Accessed 28 March 2021].

[73] W. Leung, "Heat Removal System & System Analysis," 2005.

[74] I. Sutton, "Plant Design and Operations (Second Edition)," ScienceDirect, 2017.

[75] T. Conroy, M. N. Collins, J. Fisher and R. Grimes, "Levelized cost of electricity evaluation of liquid sodium receiver designs through a thermal performance, mechanical reliability, and pressure drop analysis," ELSEVIER, 2018.

[76] P. R. Vasava, "Fluid Flow in T-Junction of Pipes," 2007.

[77] F. White, Fluid Mechanics, McGrawHill.

[78] A. Waheed Badar, R. Buchholz, Y. Lou and F. Ziegler, "CFD based analysis of flow distribution in a coaxial vacuum tube solar collector with laminar flow conditions," *Internation Journal of Energy and Enviromental Engineering,* 2012.

[79] R. D. Kale, B. K. Sreedhar e K. V. Sreedharan, The history of liquid metal pump development in India, vol. 114, Current Science, 2018, pp. 292-307.

[80] R. Jacob, M. Belusko, A. I. Fernández, L. F. Cabeza, W. Saman and F. Bruno, "Embodied energy and cost of high temperature thermal energy storage systems for use with concentrated solar power plants," ELSEVIER, 2016.

[81] A. Boretti, S. Castelletto and S. Al-Zubaidy, "Concentrating Solar Power Technology: Present Status and Outlook," DE GRUYTER, 2018.

[82] Fraunhofer ISE, "Levelized Cost of Electricity: Renewable Energy Technologies," Fraunhofer Institu for Solar Energy Systems ISE, 2013.

[83] J. Moore, R. Grimes, E. Walsh and A. O'Donovan, "Modelling the thermodynamic performance of a concentrated solar power plant with novel modular air-colled condenser," ELSEVIER, 2014.

[84] V. Solar, "drone image, vast solar - ABC News (Australian Broadcasting Corporation)," Australian Broadcasting Corporation, 5 June 2019. [Online]. Available: https://www.abc.net.au/news/2019-06-06/drone-image,-vast-solar-1/11177756?nw=0. [Accessed 12 may 2021].

[85] C. Hernández, R. Barraza, A. Saez, M. Ibarra and D. Estay, "Potential Map for the Installation of Concentrated Solar Power Towers in Chile," MDPI, Santiago, Chile, 2020.

[86] M. Aminyavari, “Modelling On/Off-Design performance of a concentrated solar power plant using supercritical carbon dioxide as working fluid,” Politecnico di Milano, Milan, 2014.

[87] P. F. t. S. Chapter-10, "Power From the Sun," [Online]. Available: http://www.powerfromthesun.net/Book/chapter10/chapter10.html.

[88] T. Conroy, M. N. Collins and R. Grimes, "Integrated optical-thermal-mechanical model for investigations into high temperature sodium receiver operation," ELSEVIER, 2019.

[89] T. Conroy, M. N. Collins and R. Grimes, "Sodium receiver designs for integration with high temperature power cycles," ELSEVIER, 2019.

[90] N. Española, "UNE-EN 10216-2:2014," 2014.

[91] L. Vant-Hull, "Issues with beam-down concepts," ELSEVIER, 2014.

Appendix

A. Cost of Vast Solar Components

$$c_{SF} = 699[heliostats] \cdot 3.6[m^2/helisotat] \cdot 200[\$/m^2]$$

$$c_{SF} = \$504.678$$

$$IC_{ref} = c_{SF}/0.36$$

$$IC_{ref} = \$1.401.883$$

$$c_{Receiver\_ref} = \$70.094$$

$$c_{Receiver\_ref\_base} = \$70.094$$

$$c_{Receiver\_ref\_tubes} = \$7.009$$

$$Cost\ scaling = 5$$

$$c_{ReceiverA} = c_{Receiver\_ref\_base} - c_{Receiver\_ref\_tubes}$$

$$c_{ReceiverA} = \$63.085$$

$$c_{ReceiverB} = c_{Receiver\_ref\_tubes} \cdot 5$$

$$c_{ReceiverB} = \$35.047$$

$$c_{Receiver\_new} = (c_{ReceiverA} + c_{ReceiverB}) \cdot A_{receiver}$$

$$c_{Receiver\_new} = \$220.797$$

$$IC_{new} = IC_{ref} + c_{Receiver\_new} - c_{Receiver\_ref}$$

$$IC_{new} = \$1.552.586$$

$$c_{Tower} = IC_{new} * 10\%$$

$$c_{Tower} = \$140.188$$

B. Sodium Polar Receivers

a. $5\ MWth$

Table 0-1: (5MWth Sodium Polar Receiver) Parametric Analysis Range for the Initial Guess and the Narrower Optimization.

	Initial Parametric Analysis		*Second Parametric Analysis*	
	Min	Max	Min	Max
Receiver Height [m]	1.5	6.5	2.75	4.35
Step [m]	1.25		0.4	
Aspect Ratio [-]	0.5	2	0.5	2
Step [-]	0.25		0.25	
Tower Height [m]	50	87.5	50	56
Step [m]	12.5		5	

Table 0-2: (5MWth Sodium Polar Receiver) Summary of Results from both parametric analyses, showing the top 4 choices for each parametric analysis.

		Initial Parametric Analysis				*Second Parametric Analysis*			
		1	2	3	4	1	2	3	4
Receiver Height	**m**	**2.75**	**2.75**	**2.75**	**2.75**	**2.75**	**3.15**	**3.55**	**4.35**
Receiver Diameter	**m**	**2.2**	**1.83**	**1.57**	**1.38**	**1.57**	**1.58**	**1.78**	**1.57**
Tower Height	**m**	**50**	**50**	**50**	**50**	**50**	**50**	**50**	**50**
Receiver Area	m^2	6.05	5.0325	4.3175	3.795	4.3175	4.977	6.319	6.8295
Total plant cost	**$**	**$3,007, 241**	**$3,011, 488**	**$3,050, 909**	**$3,118, 913**	**$3,059, 053**	**$3,075, 577**	**$3,075, 620**	**$3,165, 394**
Cost/Energy metric	-	**2.221**	**2.144**	**2.082**	**2.046**	**2.082**	**2.11**	**2.182**	**2.17**
Simulated heliostat area	m^2	8262.8	8485.7	8875.9	9412.3	8928.1	8907.2	8649.4	9126.7
Simulated heliostat count	-	2372	2436	2548	2702	2563	2557	2483	2620
Power incident on field	kW	7849.6	8061.4	8432.1	8941.7	8481.7	8461.9	8217	8670.3
Power absorbed by the receiver	kW	4865.3	4858	4886.3	4905.8	4892.2	4960	5036.9	5203
Power absorbed by the HTF	**kW**	**4480.2**	**4537.6**	**4611.5**	**4664.3**	**4617.4**	**4643.2**	**4634.7**	**4768.3**
Cloudiness efficiency	%	100	100	100	100	100	100	100	100
Shading efficiency	%	100	100	100	100	100	100	100	100
Cosine efficiency	%	92.7	92.7	92.5	92.4	92.4	92.4	92.5	92.4
Reflection efficiency	%	90.2	90.2	90.2	90.2	90.2	90.2	90.3	90.2
Blocking efficiency	%	100	100	99.9	99.9	99.9	99.9	99.9	99.9
Attenuation efficiency	%	98.2	98.2	98.2	98.1	98.1	98.1	98.1	98.1
Image intercept efficiency	%	80.3	78.1	75.2	71.4	75	76.2	79.6	78.1
Absorption efficiency	%	94	94	94	94	94	94	94	94
Solar Field Optical Efficiency	**%**	**66.0%**	**64.1%**	**61.6%**	**58.4%**	**61.4%**	**62.3%**	**65.2%**	**63.8%**
Thermal Efficiency	**%**	**86.6%**	**87.8%**	**88.7%**	**89.4%**	**88.7%**	**88.0%**	**86.5%**	**86.1%**
Average incident flux	kW/ m2	855.5	1026.9	1204	1375.2	1205.4	1060.2	848	810.5
Peak incident flux	kW/ m2	1121.9	1360.5	1656.5	1925.6	1669	1413.7	1113.4	1061.9

Azimuth \ Elevation	0	5	10	15	20	25	30	35	40	45	50	55	60	65	70	75	80	85	90
-130	1.3%	10.7%	27.3%	35.9%	41.6%	45.6%	48.6%	50.6%	52.7%	54.5%	56.3%	58.2%	59.6%	61.0%	62.4%	63.6%	64.8%	66.0%	66.9%
-120	1.2%	10.0%	28.7%	38.1%	43.8%	47.9%	51.1%	53.0%	54.8%	56.5%	57.9%	59.6%	61.0%	62.2%	63.4%	64.3%	65.2%	66.2%	66.9%
-110	1.2%	8.9%	29.4%	40.1%	46.4%	50.5%	53.7%	55.5%	57.1%	58.6%	59.9%	61.1%	62.2%	63.4%	64.3%	64.9%	65.7%	66.4%	66.9%
-100	1.2%	7.9%	30.2%	42.2%	49.1%	53.3%	56.5%	58.0%	59.4%	60.7%	61.8%	62.9%	63.8%	64.5%	65.2%	65.7%	66.3%	66.6%	66.9%
-90	1.3%	7.1%	31.3%	43.9%	51.5%	56.2%	59.3%	60.6%	61.7%	62.8%	63.7%	64.5%	65.1%	65.9%	66.1%	66.5%	66.7%	66.8%	66.9%
-80	1.4%	6.1%	31.6%	45.4%	53.7%	59.0%	61.9%	63.0%	64.0%	64.8%	65.4%	66.2%	66.6%	66.9%	67.1%	67.2%	67.2%	67.0%	66.9%
-70	1.5%	5.1%	31.7%	47.1%	56.0%	61.6%	64.4%	65.4%	66.2%	66.8%	67.2%	67.6%	68.0%	68.0%	68.1%	67.9%	67.7%	67.3%	66.9%
-60	1.6%	4.3%	32.0%	48.6%	57.8%	64.0%	66.9%	67.3%	68.0%	68.5%	68.8%	69.0%	69.1%	68.9%	68.8%	68.5%	68.1%	67.6%	66.9%
-50	1.7%	3.9%	31.9%	49.6%	59.5%	66.1%	68.6%	69.5%	69.9%	70.2%	70.3%	70.3%	70.1%	69.9%	69.6%	69.1%	68.5%	67.8%	66.9%
-40	1.7%	3.4%	31.8%	50.3%	61.1%	67.9%	70.4%	71.1%	71.3%	71.6%	71.4%	71.3%	71.1%	70.7%	70.2%	69.6%	68.8%	67.9%	66.9%
-30	1.7%	3.3%	32.7%	51.6%	62.3%	69.4%	71.8%	72.2%	72.4%	72.4%	72.4%	72.1%	71.7%	71.4%	70.7%	69.9%	69.1%	68.1%	66.9%
-20	1.7%	3.2%	33.2%	52.8%	63.7%	70.5%	72.8%	73.3%	73.4%	73.3%	73.3%	72.9%	72.6%	71.8%	71.2%	70.2%	69.3%	68.2%	66.9%
-10	1.9%	3.2%	33.3%	53.3%	64.1%	71.4%	73.5%	73.8%	73.9%	73.8%	73.5%	73.2%	72.8%	72.1%	71.3%	70.3%	69.5%	68.2%	66.9%
0	1.9%	3.2%	33.3%	53.7%	64.6%	71.7%	73.7%	73.9%	74.0%	74.0%	73.7%	73.4%	72.9%	72.2%	71.5%	70.5%	69.4%	68.3%	66.9%
10	1.9%	3.3%	33.1%	53.2%	64.3%	71.5%	73.5%	73.8%	73.9%	73.7%	73.5%	73.3%	72.8%	72.0%	71.4%	70.4%	69.4%	68.3%	66.9%
20	1.8%	3.3%	33.2%	52.7%	63.6%	70.7%	73.0%	73.3%	73.4%	73.3%	73.2%	73.0%	72.6%	71.8%	71.2%	70.2%	69.1%	68.2%	66.9%
30	1.7%	3.3%	32.7%	51.5%	62.7%	69.5%	72.0%	72.3%	72.6%	72.6%	72.3%	72.2%	71.8%	71.4%	70.7%	70.0%	69.0%	68.0%	66.9%
40	1.7%	3.4%	31.7%	50.3%	60.9%	68.0%	70.6%	71.1%	71.5%	71.5%	71.6%	71.4%	71.2%	70.7%	70.2%	69.6%	68.8%	67.9%	66.9%
50	1.8%	3.9%	31.9%	49.6%	59.6%	66.2%	68.7%	69.5%	69.8%	70.2%	70.3%	70.3%	70.2%	70.0%	69.7%	69.1%	68.5%	67.8%	66.9%
60	1.7%	4.5%	32.0%	48.4%	57.8%	64.0%	66.7%	67.6%	68.2%	68.6%	68.8%	69.0%	69.1%	69.1%	68.9%	68.6%	68.1%	67.6%	66.9%
70	1.6%	5.2%	31.7%	47.1%	55.9%	61.7%	64.6%	65.4%	66.2%	66.8%	67.2%	67.6%	68.0%	68.0%	68.1%	67.9%	67.7%	67.3%	66.9%
80	1.5%	6.2%	31.6%	45.4%	53.8%	59.0%	62.0%	63.2%	64.0%	64.9%	65.5%	66.2%	66.6%	66.9%	67.0%	67.2%	67.2%	67.0%	66.9%
90	1.3%	7.1%	31.2%	43.9%	51.6%	56.3%	59.4%	60.6%	61.8%	62.8%	63.7%	64.6%	65.2%	65.9%	66.2%	66.5%	66.7%	66.8%	66.9%
100	1.2%	7.9%	30.0%	42.2%	49.1%	53.3%	56.5%	58.1%	59.5%	60.7%	61.9%	62.9%	63.6%	64.5%	65.2%	65.7%	66.3%	66.6%	66.9%
110	1.2%	8.9%	29.3%	40.0%	46.3%	50.5%	53.8%	55.5%	57.1%	58.6%	60.0%	61.3%	62.3%	63.3%	64.1%	65.0%	65.7%	66.4%	66.9%
120	1.3%	9.9%	28.5%	38.0%	43.7%	48.0%	51.1%	53.0%	54.8%	56.5%	58.0%	59.5%	60.9%	62.2%	63.3%	64.3%	65.2%	66.2%	66.9%
130	1.3%	10.6%	27.1%	35.7%	41.5%	45.6%	48.6%	50.6%	52.7%	54.6%	56.2%	57.9%	59.4%	61.1%	62.3%	63.6%	64.9%	65.9%	66.9%
135	1.2%	10.6%	26.4%	34.7%	40.4%	44.6%	47.4%	49.6%	51.7%	53.7%	55.6%	57.4%	59.1%	60.5%	62.1%	63.4%	64.7%	65.9%	66.9%

Figure 0-1: (5MWth Sodium Polar Receiver) Optical Efficiency Map, without reflectivity losses.

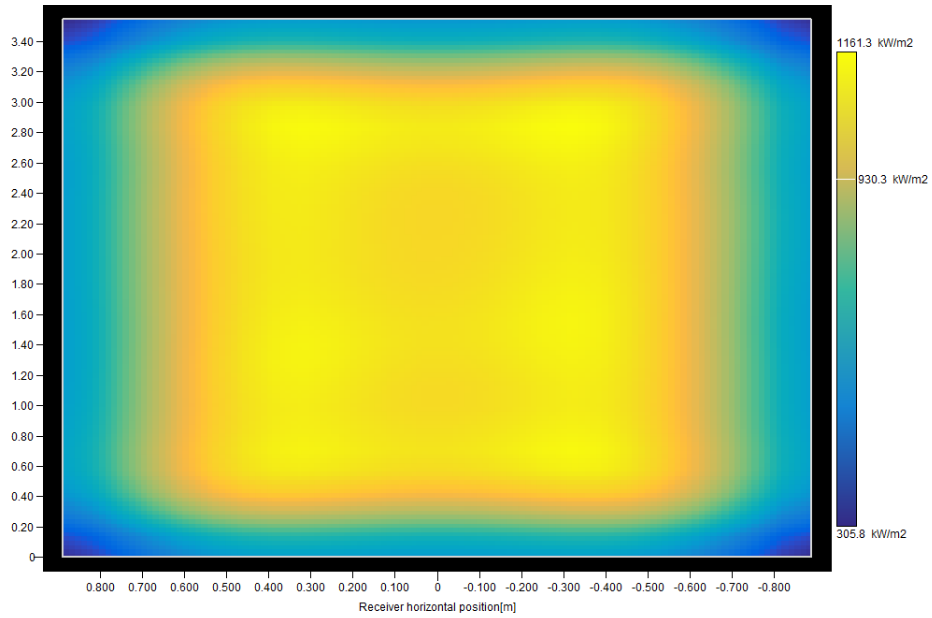

Figure 0-2: (5MWth Sodium Polar Receiver) Flux distribution at Autumnal Equinox.

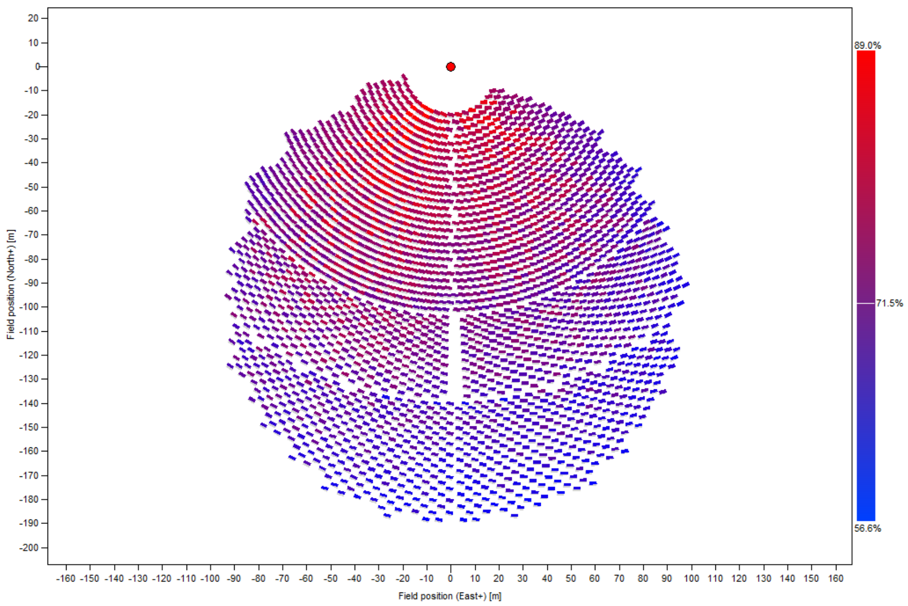

Figure 0-3: (5MWth Sodium Polar Receiver) Layout.

b. $\mathbf{10}\ \boldsymbol{MWth}$

Table 0-3: (10MWth Sodium Polar Receiver) Parametric Analysis Range for the Initial Guess and the Narrower Optimization.

	Initial Parametric Analysis			*Second Parametric Analysis*		
	Min		Max	Min		Max
Receiver Height [m]	1.75		4.15	2.35		3.35
Step [m]		0.6			0.25	
Aspect Ratio [-]	0.5		2	0.5		2
Step [-]		0.25			0.25	
Tower Height [m]	50		68	56		62
Step [m]		6			2	

Table 0-4: (10MWth Sodium Polar Receiver) Summary of Results from both parametric analyses, showing the top 4 choices for each parametric analysis.

		Initial Parametric Analysis				*Second Parametric Analysis*			
		1	2	3	4	1	2	3	4
Receiver Height	**m**	**2.35**	**2.95**	**3.55**	**2.35**	**2.35**	**2.6**	**2.35**	**2.35**
Receiver Diameter	**m**	**4.7**	**3.37**	**2.84**	**4.7**	**4.7**	**2.97**	**4.7**	**4.7**
Tower Height	**m**	**50**	**50**	**50**	**56**	**56**	**56**	**58**	**60**
Receiver Area	m^2	11.045	9.9415	10.082	11.045	11.045	7.722	11.045	11.045
Total plant cost	**$**	**$ 4,706,920**	**$ 4,559,701**	**$ 4,589,999**	**$ 4,735,674**	**$ 4,735,674**	**$ 4,607,186**	**$ 4,763,504**	**$ 4,785,255**
Cost/Energy metric	**-**	**1.35**	**1.36**	**1.364**	**1.392**	**1.392**	**1.35**	**1.406**	**1.418**
Simulated heliostat area	m^2	18197.6	17466.1	17633.3	17946.8	17946.8	17762.2	17960.7	17925.9
Simulated heliostat count	-	5224	5014	5062	5152	5152	5099	5156	5146
Power incident on field	kW	17287.7	16592.8	16751.6	17049.5	17049.5	16874.1	17062.7	17029.6
Power absorbed by the receiver	kW	10269.7	9837.8	9863.9	10227.1	10227.1	9700.8	10234.7	10252.2
Power absorbed by the HTF	**kW**	**9566.7**	**9205.1**	**9222.1**	**9524.1**	**9524.1**	**9209.3**	**9531.7**	**9549.2**
Cloudiness efficiency	%	100	100	100	100	100	100	100	100
Shading efficiency	%	100	100	100	100	100	100	100	100
Cosine efficiency	%	89.7	90	90	90.6	90.6	90.8	90.8	91.1
Reflection efficiency	%	90.2	90.2	90.2	90.3	90.3	90.3	90.2	90.3
Blocking efficiency	%	99.9	99.8	99.8	99.9	99.9	99.9	99.9	99.9
Attenuation efficiency	%	97.8	97.8	97.7	97.8	97.8	97.8	97.8	97.7
Image intercept efficiency	%	79.9	79.5	79	79.9	79.9	76.5	79.7	79.8
Absorption efficiency	%	94	94	94	94	94	94	94	94
Solar Field Optical Efficiency	**%**	**63.2%**	**63.1%**	**62.7%**	**63.8%**	**63.8%**	**61.2%**	**63.8%**	**64.0%**
Thermal Efficiency	**%**	**87.6%**	**88.0%**	**87.9%**	**87.5%**	**87.5%**	**89.2%**	**87.5%**	**87.6%**
Average incident flux	kW/m2	989.2	1052.7	1040.8	985.1	985.1	1336.4	985.8	987.5
Peak incident flux	kW/m2	1275.2	1322.1	1292.3	1322.3	1322.3	1752.3	1339.1	1363

Azimuth \ Elevation	0	5	10	15	20	25	30	35	40	45	50	55	60	65	70	75	80	85	90
-130	1.0%	12.2%	28.2%	35.9%	40.5%	43.7%	46.2%	48.0%	49.7%	51.3%	52.9%	54.4%	55.9%	57.2%	58.5%	59.7%	60.9%	61.9%	62.9%
-120	1.0%	11.8%	29.6%	38.2%	43.2%	46.4%	48.7%	50.3%	51.8%	53.2%	54.5%	55.7%	57.0%	58.2%	59.4%	60.3%	61.3%	62.1%	62.9%
-110	1.0%	11.3%	30.6%	40.4%	46.0%	49.3%	51.6%	52.8%	54.0%	55.2%	56.3%	57.3%	58.3%	59.3%	60.2%	61.0%	61.7%	62.3%	62.9%
-100	1.0%	10.3%	31.8%	42.8%	48.8%	52.3%	54.5%	55.5%	56.5%	57.3%	58.2%	59.0%	59.8%	60.4%	61.2%	61.7%	62.1%	62.6%	62.9%
-90	1.1%	9.6%	33.0%	44.6%	51.5%	55.3%	57.3%	58.2%	58.9%	59.6%	60.2%	60.7%	61.2%	61.7%	62.1%	62.3%	62.7%	62.8%	62.9%
-80	1.1%	8.5%	33.5%	46.3%	53.8%	58.2%	60.1%	60.7%	61.3%	61.7%	62.1%	62.4%	62.7%	62.9%	63.0%	63.1%	63.1%	63.0%	62.9%
-70	1.1%	7.6%	34.0%	48.0%	56.0%	60.6%	62.6%	63.1%	63.5%	63.7%	63.9%	64.0%	64.0%	64.0%	63.9%	63.8%	63.6%	63.2%	62.9%
-60	1.1%	6.7%	34.7%	49.5%	58.0%	62.9%	64.7%	65.2%	65.4%	65.5%	65.5%	65.5%	65.3%	65.1%	64.8%	64.5%	64.0%	63.4%	62.9%
-50	1.2%	6.2%	35.2%	51.0%	59.7%	64.8%	66.6%	66.9%	67.1%	67.1%	67.0%	66.8%	66.5%	66.1%	65.6%	65.0%	64.4%	63.6%	62.9%
-40	1.4%	5.7%	35.4%	51.9%	61.0%	66.4%	68.2%	68.4%	68.5%	68.4%	68.2%	67.9%	67.4%	66.9%	66.3%	65.5%	64.7%	63.8%	62.9%
-30	1.4%	5.2%	35.7%	52.9%	62.1%	67.6%	69.4%	69.6%	69.6%	69.5%	69.1%	68.7%	68.2%	67.6%	66.8%	66.0%	65.0%	63.9%	62.9%
-20	1.5%	5.0%	36.0%	53.3%	62.9%	68.4%	70.2%	70.4%	70.4%	70.2%	69.8%	69.4%	68.7%	68.0%	67.1%	66.3%	65.2%	64.0%	62.9%
-10	1.5%	4.8%	35.9%	53.4%	63.2%	68.8%	70.6%	71.0%	70.9%	70.5%	70.2%	69.7%	69.0%	68.3%	67.4%	66.4%	65.3%	64.1%	62.9%
0	1.5%	4.7%	35.7%	53.4%	63.3%	69.0%	70.9%	71.1%	71.1%	70.7%	70.3%	69.8%	69.1%	68.3%	67.4%	66.4%	65.3%	64.1%	62.9%
10	1.6%	4.8%	35.9%	53.4%	63.2%	68.8%	70.7%	71.0%	70.9%	70.5%	70.2%	69.7%	69.0%	68.3%	67.3%	66.4%	65.3%	64.0%	62.9%
20	1.5%	5.0%	36.0%	53.3%	62.9%	68.3%	70.2%	70.4%	70.3%	70.1%	69.8%	69.3%	68.7%	68.0%	67.1%	66.2%	65.2%	64.0%	62.9%
30	1.4%	5.2%	35.7%	52.9%	62.1%	67.6%	69.4%	69.6%	69.6%	69.5%	69.1%	68.7%	68.2%	67.6%	66.8%	66.0%	65.0%	63.9%	62.9%
40	1.4%	5.9%	35.4%	51.9%	61.0%	66.4%	68.1%	68.4%	68.5%	68.4%	68.2%	67.9%	67.4%	66.9%	66.3%	65.5%	64.7%	63.8%	62.9%
50	1.3%	6.3%	35.1%	50.9%	59.6%	64.8%	66.6%	66.9%	67.0%	67.0%	66.9%	66.7%	66.5%	66.1%	65.5%	65.0%	64.4%	63.6%	62.9%
60	1.1%	6.8%	34.6%	49.5%	57.9%	62.9%	64.7%	65.1%	65.3%	65.5%	65.5%	65.4%	65.3%	65.1%	64.8%	64.5%	63.9%	63.4%	62.9%
70	1.1%	7.7%	33.9%	47.9%	55.9%	60.6%	62.4%	63.0%	63.4%	63.7%	63.8%	64.0%	64.0%	64.0%	63.9%	63.8%	63.5%	63.2%	62.9%
80	1.1%	8.6%	33.4%	46.2%	53.7%	58.1%	60.0%	60.7%	61.2%	61.7%	62.1%	62.3%	62.7%	62.8%	63.0%	63.1%	63.1%	63.0%	62.9%
90	1.0%	9.7%	32.8%	44.5%	51.4%	55.2%	57.2%	58.1%	58.8%	59.5%	60.1%	60.6%	61.2%	61.6%	62.0%	62.3%	62.7%	62.8%	62.9%
100	1.0%	10.3%	31.7%	42.6%	48.7%	52.2%	54.4%	55.4%	56.4%	57.2%	58.1%	58.9%	59.7%	60.4%	61.1%	61.6%	62.1%	62.6%	62.9%
110	1.0%	11.3%	30.5%	40.3%	45.9%	49.1%	51.4%	52.7%	53.9%	55.1%	56.2%	57.2%	58.3%	59.3%	60.2%	61.0%	61.7%	62.3%	62.9%
120	1.0%	11.8%	29.4%	38.0%	43.0%	46.2%	48.6%	50.2%	51.6%	53.0%	54.4%	55.7%	57.0%	58.2%	59.3%	60.3%	61.3%	62.1%	62.9%
130	1.0%	12.1%	28.0%	35.6%	40.4%	43.5%	46.1%	47.8%	49.5%	51.2%	52.8%	54.4%	55.7%	57.2%	58.5%	59.7%	60.9%	61.9%	62.9%
135	1.0%	12.2%	27.2%	34.6%	39.1%	42.3%	44.8%	46.7%	48.5%	50.3%	52.0%	53.7%	55.2%	56.7%	58.1%	59.5%	60.6%	61.8%	62.9%

Figure 0-4: (10MWth Sodium Polar Receiver) Optical Efficiency Map, without reflectivity losses.

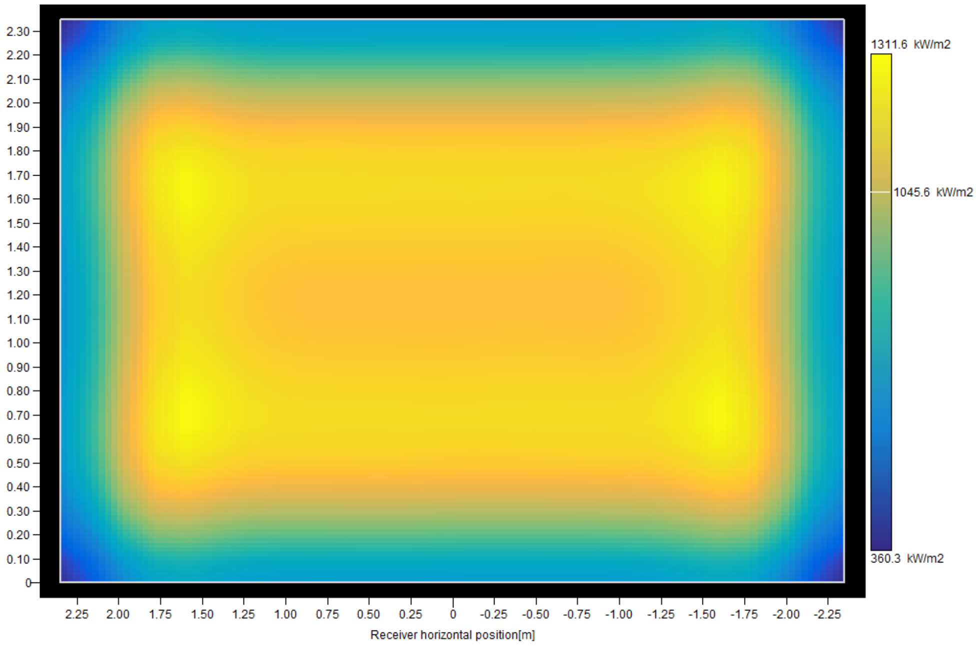

Figure 0-5: (10MWth Sodium Polar Receiver) Flux distribution at Autumnal Equinox.

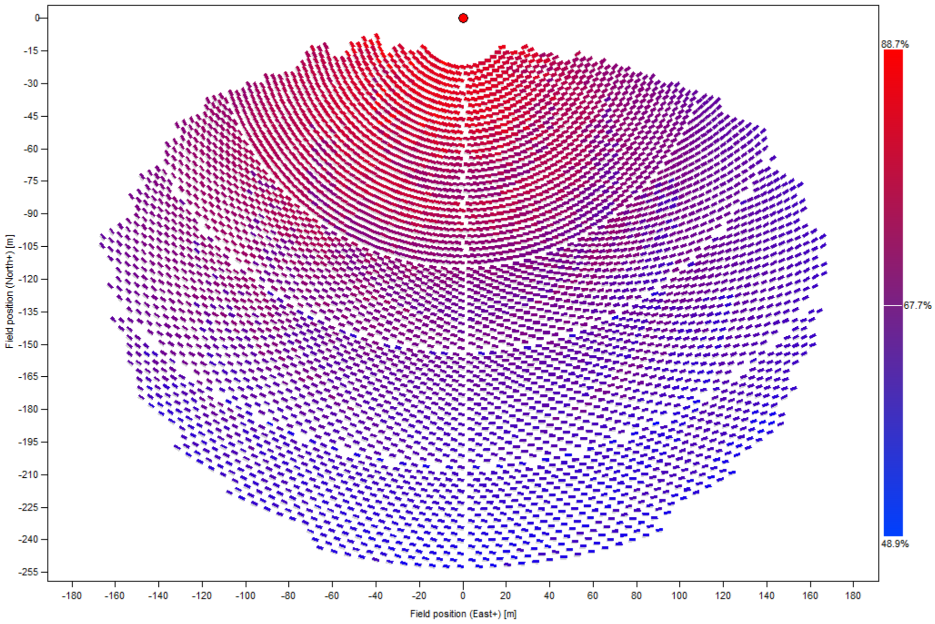

Figure 0-6: (10MWth Sodium Polar Receiver) Layout

c. $20\ MWth$

Table 0-5: (20MWth Sodium Polar Receiver) Parametric Analysis Range for the Initial Guess and the Narrower Optimization.

	Initial Parametric Analysis		Second Parametric Analysis	
	Min	Max	Min	Max
Receiver Height [m]	3.3	6.5	3.3	4.9
Step [m]	0.8		0.4	
Aspect Ratio [-]	0.5	2	0.5	2
Step [-]	0.25		0.25	
Tower Height [m]	70	88	70	76
Step [m]	6		2	

Table 0-6: (20MWth Sodium Polar Receiver) Summary of Results from both parametric analyses, showing the top 4 choices for each parametric analysis.

		Initial Parametric Analysis				Second Parametric Analysis			
		1	2	3	4	1	2	3	4
Receiver Height	**m**	**3.3**	**4.1**	**4.9**	**3.3**	**3.3**	**3.7**	**4.1**	**3.3**
Receiver Diameter	**m**	**6.6**	**4.69**	**3.92**	**6.6**	**6.6**	**4.23**	**4.69**	**6.6**
Tower Height	**m**	**70**	**70**	**70**	**76**	**70**	**70**	**70**	**72**
Receiver Area	m^2	21.78	19.229	19.208	21.78	21.78	15.651	19.229	21.78
Total plant cost	**$**	**$8,216, 207**	**$7,919, 608**	**$7,986, 542**	**$8,294, 875**	**$8,216, 207**	**$8,013, 025**	**$7,919, 608**	**$8,237, 049**
Cost/Energy metric	**-**	**1.027**	**1.024**	**1.027**	**1.052**	**1.027**	**0.991**	**1.024**	**1.035**
Simulated heliostat area	m^2	36837.7	35427	35860.1	36615	36837.7	36713.9	35427	36738.7
Simulated heliostat count	-	2977	2863	2898	2959	2977	2967	2863	2969
Power incident on field	kW	34995.8	33655.7	34067.1	34784.2	34995.8	34878.2	33655.7	34901.8
Power absorbed by the receiver	kW	20575.4	19721.6	19760.6	20539.3	20575.4	19662.1	19721.6	20554.4
Power absorbed by the HTF	**kW**	**19189.1**	**18497.7**	**18538**	**19153**	**19189.1**	**18666**	**18497.7**	**19168.1**
Cloudiness efficiency	%	100	100	100	100	100	100	100	100
Shading efficiency	%	100	100	100	100	100	100	100	100
Cosine efficiency	%	89.7	90	90	90.3	89.7	89.9	90	89.9
Reflection efficiency	%	90.2	90.2	90.2	90.2	90.2	90.2	90.2	90.2
Blocking efficiency	%	99.7	99.7	99.7	99.8	99.7	99.7	99.7	99.8
Attenuation efficiency	%	97.2	97.2	97.1	97.1	97.2	97.1	97.2	97.1
Image intercept efficiency	%	79.7	79.2	78.4	79.5	79.7	76.4	79.2	79.6
Absorption efficiency	%	94	94	94	94	94	94	94	94
Solar Field Optical Efficiency	**%**	**62.6%**	**62.3%**	**61.7%**	**62.8%**	**62.6%**	**60.0%**	**62.3%**	**62.7%**
Thermal Efficiency	**%**	**87.7%**	**88.2%**	**88.2%**	**87.7%**	**87.7%**	**89.2%**	**88.2%**	**87.7%**
Average incident flux	kW/ m2	1005	1091.1	1094.4	1003.2	1005	1336.5	1091.1	1004
Peak incident flux	kW/ m2	1296.6	1365.3	1353.6	1321.6	1296.6	1710.1	1365.3	1310.9

Azimuth \ Elevation	0	5	10	15	20	25	30	35	40	45	50	55	60	65	70	75	80	85	90
-130	1.5%	13.2%	27.0%	34.5%	38.9%	42.1%	45.0%	46.9%	48.7%	50.4%	52.1%	53.7%	55.1%	56.7%	58.2%	59.3%	60.3%	61.4%	62.3%
-120	1.5%	13.0%	28.4%	36.7%	41.5%	44.8%	47.6%	49.1%	50.9%	52.3%	53.8%	55.1%	56.5%	57.7%	58.4%	59.9%	60.6%	61.6%	62.3%
-110	1.5%	12.9%	29.8%	39.0%	44.3%	47.7%	50.3%	51.8%	53.1%	54.4%	55.6%	56.8%	57.8%	58.8%	59.4%	60.5%	61.1%	61.8%	62.3%
-100	1.4%	12.3%	31.2%	41.4%	47.0%	50.5%	53.2%	54.4%	55.5%	56.6%	57.6%	58.5%	59.3%	59.9%	60.6%	61.2%	61.6%	62.0%	62.3%
-90	1.4%	11.8%	32.4%	43.3%	49.8%	53.7%	56.3%	57.1%	58.1%	58.8%	59.5%	60.1%	60.9%	61.4%	61.6%	61.9%	62.1%	62.2%	62.3%
-80	1.5%	11.0%	33.2%	45.4%	52.1%	56.4%	59.0%	59.8%	60.5%	61.0%	61.5%	62.0%	61.9%	62.7%	62.6%	62.7%	62.7%	62.6%	62.3%
-70	1.5%	10.3%	34.0%	47.2%	54.5%	58.9%	61.7%	62.1%	62.8%	63.2%	63.4%	63.5%	63.4%	63.9%	63.4%	63.3%	63.1%	62.8%	62.3%
-60	1.6%	9.8%	35.5%	48.9%	56.7%	61.1%	63.4%	64.3%	64.6%	64.7%	65.2%	64.9%	64.8%	64.7%	64.3%	63.9%	63.5%	63.0%	62.3%
-50	1.8%	9.7%	36.3%	50.7%	58.5%	63.0%	65.6%	66.0%	66.5%	66.6%	66.5%	66.4%	66.1%	65.6%	65.2%	64.6%	63.9%	63.2%	62.3%
-40	1.9%	9.4%	36.8%	51.9%	60.1%	64.4%	67.2%	67.8%	67.9%	67.8%	67.7%	67.4%	67.0%	66.5%	65.6%	65.1%	64.3%	63.3%	62.3%
-30	2.0%	8.9%	37.0%	52.7%	60.6%	65.6%	68.6%	68.4%	69.0%	68.8%	69.0%	68.3%	68.0%	67.1%	66.5%	65.6%	64.5%	63.4%	62.3%
-20	2.0%	8.7%	37.3%	53.3%	62.2%	66.5%	68.9%	69.3%	69.4%	69.3%	68.9%	69.1%	68.5%	67.8%	66.9%	65.5%	64.6%	63.6%	62.3%
-10	2.0%	8.3%	36.9%	53.5%	62.0%	67.4%	69.6%	70.6%	70.0%	69.8%	69.9%	69.1%	68.5%	67.9%	66.8%	66.2%	64.9%	63.6%	62.3%
0	2.0%	8.0%	36.5%	53.4%	62.2%	67.7%	70.4%	70.4%	70.5%	70.2%	69.9%	69.4%	68.7%	67.9%	67.1%	66.0%	64.9%	63.6%	62.3%
10	2.0%	8.3%	37.0%	53.6%	62.3%	66.8%	70.3%	70.7%	70.0%	70.4%	70.0%	69.4%	68.6%	68.0%	66.9%	66.1%	64.9%	63.6%	62.3%
20	2.0%	8.6%	36.9%	53.1%	61.4%	66.4%	68.9%	70.2%	69.4%	69.1%	68.8%	68.5%	68.0%	67.7%	66.4%	65.7%	64.8%	63.7%	62.3%
30	2.0%	9.3%	36.8%	52.7%	61.4%	65.3%	68.6%	68.5%	69.4%	68.5%	68.3%	68.2%	67.7%	67.0%	66.3%	65.5%	64.6%	63.3%	62.3%
40	1.8%	9.5%	36.4%	51.8%	59.3%	64.6%	67.0%	67.4%	67.9%	67.7%	67.7%	67.4%	66.9%	66.4%	65.7%	65.1%	64.3%	63.3%	62.3%
50	1.8%	9.6%	36.2%	50.7%	58.1%	62.8%	65.5%	66.3%	66.2%	66.6%	66.2%	66.3%	65.9%	65.5%	65.1%	64.5%	63.9%	63.1%	62.3%
60	1.5%	9.9%	34.8%	48.7%	56.4%	60.9%	63.6%	64.3%	64.6%	64.7%	64.8%	65.0%	64.8%	64.4%	64.1%	63.9%	63.5%	63.0%	62.3%
70	1.5%	10.5%	33.8%	47.1%	54.1%	58.6%	61.3%	62.0%	62.4%	63.0%	63.3%	63.4%	63.5%	63.8%	63.4%	63.3%	63.1%	62.8%	62.3%
80	1.4%	11.2%	33.3%	45.2%	51.8%	56.1%	58.8%	59.5%	60.3%	60.9%	61.4%	61.7%	62.0%	62.3%	62.4%	62.6%	62.6%	62.4%	62.3%
90	1.4%	11.9%	32.3%	43.2%	49.4%	53.4%	56.0%	57.0%	57.9%	58.6%	59.5%	60.0%	60.6%	61.2%	61.5%	61.8%	62.1%	62.2%	62.3%
100	1.4%	12.2%	30.9%	41.2%	46.9%	50.4%	53.1%	54.3%	55.3%	56.4%	57.3%	58.3%	59.0%	59.9%	60.7%	61.1%	61.6%	62.0%	62.3%
110	1.5%	12.9%	29.6%	38.8%	43.9%	47.4%	50.1%	51.5%	52.9%	54.1%	55.4%	56.6%	57.7%	58.9%	59.4%	60.4%	61.2%	61.7%	62.3%
120	1.5%	13.0%	28.3%	36.5%	41.3%	44.6%	47.2%	48.9%	50.6%	52.1%	53.6%	55.0%	56.4%	57.9%	58.9%	59.8%	60.7%	61.6%	62.3%
130	1.5%	13.2%	26.8%	34.1%	38.6%	41.9%	44.7%	46.6%	48.5%	50.3%	51.9%	53.5%	55.2%	56.2%	57.6%	58.8%	60.3%	61.4%	62.3%
135	1.5%	13.0%	26.0%	33.0%	37.4%	40.7%	43.5%	45.4%	47.6%	49.4%	51.2%	52.8%	54.8%	56.4%	57.2%	58.9%	60.1%	61.3%	62.3%

Figure 0-7: (20MWth Sodium Polar Receiver) Optical Efficiency Map, without reflectivity losses.

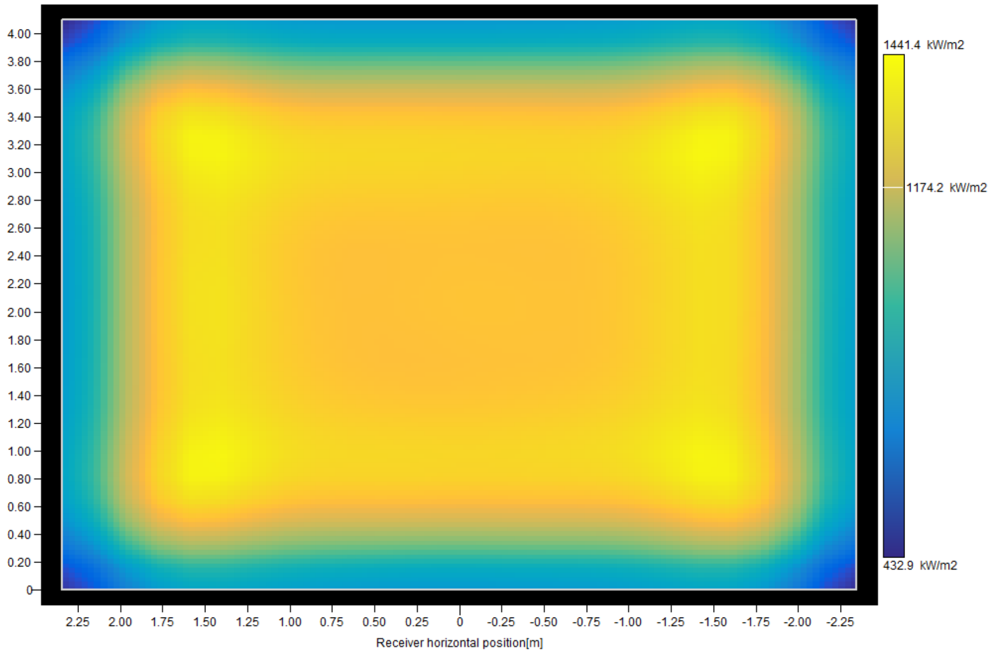

Figure 0-8: (20MWth Sodium Polar Receiver) Flux distribution at Autumnal Equinox.

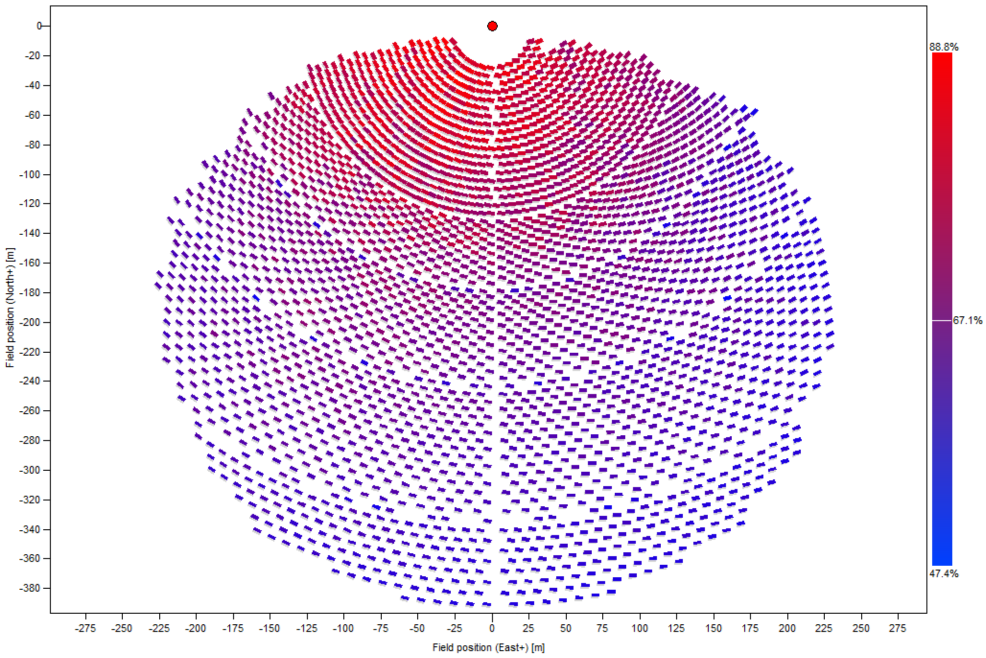

Figure 0-9: (20MWth Sodium Polar Receiver) Layout

d. $30\ MWth$

Table 0-7: (30MWth Sodium Polar Receiver) Parametric Analysis Range for the Initial Guess and the Narrower Optimization.

	Initial Parametric Analysis		*Second Parametric Analysis*	
	Min	Max	Min	Max
Receiver Height [m]	4	6.8	4.7	5.5
Step [m]	0.7		0.2	
Aspect Ratio [-]	0.5	2	0.5	2
Step [-]	0.25		0.25	
Tower Height [m]	70	88	70	82
Step [m]	6		2	

Table 0-8: (30MWth Sodium Polar Receiver) Summary of Results from both parametric analyses, showing the top 4 choices for each parametric analysis.

		Initial Parametric Analysis				*Second Parametric Analysis*			
		1	2	3	4	1	2	3	4
Receiver Height	**m**	**5.4**	**4.7**	**5.4**	**4.7**	**4.9**	**5.1**	**4.9**	**5.1**
Receiver Diameter	**m**	**6.17**	**5.37**	**6.17**	**5.37**	**5.6**	**5.83**	**5.6**	**5.83**
Tower Height	**m**	**70**	**76**	**76**	**82**	**78**	**78**	**82**	**82**
Receiver Area	m^2	33.318	25.239	33.318	25.239	27.44	29.733	27.44	29.733
Total plant cost	**$**	**$11,440,516**	**$11,479,489**	**$11,374,401**	**$11,340,172**	**$11,356,648**	**$11,338,577**	**$11,300,029**	**$11,289,680**
Cost/Energy metric	-	**0.886**	**0.859**	**0.901**	**0.875**	**0.875**	**0.887**	**0.886**	**0.897**
Simulated heliostat area	m^2	55287.5	56364	54136.7	54656.4	54891.5	54334.7	53975.8	53468.5
Simulated heliostat count	-	4468	4555	4375	4417	4436	4391	4362	4321
Power incident on field	kW	52523.1	53545.8	51429.8	51923.6	52146.9	51617.9	51277	50795
Power absorbed by the receiver	kW	30242.9	29791.4	30045.1	29481.2	29728	29815.8	29568.4	29679
Power absorbed by the HTF	**kW**	**28122.2**	**28185**	**27924.4**	**27874.8**	**27981.4**	**27923.3**	**27821.9**	**27786.5**
Cloudiness efficiency	%	100	100	100	100	100	100	100	100
Shading efficiency	%	100	100	100	100	100	100	100	100
Cosine efficiency	%	88.4	88.9	89	89.6	89.1	89.2	89.7	89.7
Reflection efficiency	%	90.3	90.2	90.2	90.3	90.3	90.3	90.3	90.3
Blocking efficiency	%	99.7	99.6	99.7	99.7	99.7	99.7	99.8	99.8
Attenuation efficiency	%	96.6	96.6	96.6	96.7	96.6	96.6	96.7	96.7
Image intercept efficiency	%	79.8	76.7	80.3	77.5	78.3	79.2	78.6	79.6
Absorption efficiency	%	94	94	94	94	94	94	94	94
Solar Field Optical Efficiency	**%**	**61.3%**	**59.1%**	**62.1%**	**60.4%**	**60.6%**	**61.5%**	**61.4%**	**62.1%**
Thermal Efficiency	**%**	**87.4%**	**88.9%**	**87.4%**	**88.9%**	**88.5%**	**88.0%**	**88.4%**	**88.0%**
Average incident flux	kW/m2	965.6	1255.7	959.3	1242.6	1152.5	1066.8	1146.3	1061.9
Peak incident flux	kW/m2	1183.4	1556	1180.4	1558	1425.1	1313.4	1431.3	1321.3

		Elevation																		
		0	5	10	15	20	25	30	35	40	45	50	55	60	65	70	75	80	85	90
Azimuth	-130	1.3%	14.0%	27.3%	34.3%	38.4%	41.3%	43.8%	45.7%	47.4%	49.1%	50.5%	51.9%	53.9%	55.0%	56.0%	57.4%	58.5%	59.6%	60.5%
	-120	1.3%	14.3%	28.9%	36.6%	41.0%	43.8%	46.4%	48.0%	49.6%	51.0%	52.2%	53.7%	54.6%	55.6%	57.2%	58.0%	58.9%	59.8%	60.5%
	-110	1.3%	14.4%	30.5%	39.1%	43.6%	46.8%	49.1%	50.5%	51.8%	52.9%	54.0%	55.0%	56.2%	57.2%	57.8%	58.6%	59.4%	60.0%	60.5%
	-100	1.2%	14.0%	31.9%	41.3%	46.4%	49.7%	51.9%	53.1%	54.1%	55.1%	56.1%	56.5%	57.8%	58.4%	58.8%	59.4%	59.8%	60.2%	60.5%
	-90	1.3%	13.8%	33.3%	43.4%	49.1%	52.7%	54.8%	55.6%	56.6%	57.3%	58.0%	58.8%	58.8%	59.7%	59.6%	60.1%	60.3%	60.4%	60.5%
	-80	1.2%	13.1%	34.6%	45.5%	51.5%	55.3%	57.6%	58.5%	58.8%	59.6%	59.9%	60.1%	60.4%	61.0%	60.5%	60.7%	60.7%	60.7%	60.5%
	-70	1.3%	12.4%	35.6%	47.6%	53.5%	57.8%	59.9%	60.6%	61.3%	61.1%	62.0%	61.6%	61.8%	61.8%	61.5%	61.4%	61.3%	61.0%	60.5%
	-60	1.4%	12.0%	36.4%	49.3%	55.7%	60.1%	61.8%	62.7%	62.6%	63.3%	63.7%	62.9%	63.1%	62.9%	62.4%	62.0%	61.7%	61.2%	60.5%
	-50	1.4%	12.2%	37.4%	51.2%	57.6%	62.0%	64.1%	65.1%	64.7%	64.8%	64.6%	64.6%	64.1%	63.9%	63.3%	62.8%	62.2%	61.4%	60.5%
	-40	1.6%	12.2%	38.8%	53.0%	59.5%	63.2%	65.3%	66.2%	66.3%	65.7%	65.5%	65.3%	65.1%	64.6%	63.7%	63.1%	62.3%	61.5%	60.5%
	-30	1.7%	11.7%	39.5%	53.9%	60.6%	64.4%	66.6%	67.7%	66.8%	67.3%	66.5%	66.1%	65.9%	65.1%	64.8%	63.4%	62.9%	61.8%	60.5%
	-20	1.7%	11.4%	39.3%	54.3%	61.9%	65.2%	67.3%	68.5%	67.6%	67.3%	67.0%	67.4%	66.7%	66.0%	64.9%	63.9%	62.9%	61.6%	60.5%
	-10	1.7%	10.3%	38.1%	54.0%	62.1%	65.9%	68.9%	68.2%	69.0%	67.9%	68.3%	67.7%	66.8%	66.0%	65.3%	64.4%	63.1%	62.0%	60.5%
	0	1.8%	10.2%	38.0%	53.6%	61.9%	66.4%	68.6%	69.1%	68.6%	68.4%	67.9%	67.6%	66.9%	66.2%	65.2%	64.1%	63.0%	61.9%	60.5%
	10	1.7%	10.5%	38.6%	53.3%	62.2%	65.7%	68.9%	69.1%	68.2%	67.9%	68.3%	67.7%	66.8%	66.1%	65.1%	64.1%	62.8%	61.8%	60.5%
	20	1.7%	11.5%	39.4%	53.4%	61.8%	66.2%	68.4%	68.6%	68.6%	68.4%	68.0%	67.4%	66.4%	65.7%	64.9%	64.0%	63.0%	61.8%	60.5%
	30	1.6%	11.7%	38.8%	53.2%	60.1%	65.2%	66.5%	67.7%	67.7%	66.6%	66.4%	66.8%	66.0%	65.2%	64.7%	63.4%	62.4%	61.5%	60.5%
	40	1.6%	12.1%	38.8%	52.2%	58.9%	63.5%	66.2%	65.5%	65.9%	66.0%	66.4%	66.0%	65.1%	64.4%	64.0%	63.4%	62.3%	61.5%	60.5%
	50	1.4%	12.1%	37.3%	51.6%	58.0%	62.3%	64.6%	63.9%	64.3%	64.9%	65.1%	64.8%	64.1%	63.7%	63.2%	62.7%	62.1%	61.3%	60.5%
	60	1.4%	12.0%	36.5%	49.9%	55.9%	60.0%	62.1%	62.7%	62.6%	63.1%	62.9%	62.8%	63.1%	62.8%	62.6%	62.3%	61.7%	61.2%	60.5%
	70	1.3%	12.7%	35.5%	47.4%	54.3%	57.7%	59.9%	60.6%	61.0%	61.1%	61.2%	61.9%	61.7%	61.5%	61.9%	61.7%	61.3%	61.0%	60.5%
	80	1.2%	13.3%	34.4%	45.3%	51.3%	55.2%	57.4%	58.2%	58.8%	59.6%	59.9%	60.0%	60.3%	60.3%	61.0%	60.9%	60.7%	60.6%	60.5%
	90	1.3%	14.0%	33.1%	43.3%	49.0%	52.6%	54.7%	55.6%	56.5%	57.1%	57.9%	58.4%	58.6%	59.7%	59.9%	60.0%	60.3%	60.4%	60.5%
	100	1.3%	13.9%	31.7%	41.1%	46.4%	49.5%	51.7%	53.1%	54.0%	55.0%	56.0%	56.5%	57.2%	58.0%	58.9%	59.4%	59.8%	60.2%	60.5%
	110	1.3%	14.3%	30.2%	38.9%	43.4%	46.6%	48.9%	50.3%	51.6%	52.8%	53.9%	55.1%	56.0%	56.9%	57.9%	58.6%	59.4%	60.0%	60.5%
	120	1.3%	14.3%	28.7%	36.4%	40.7%	43.7%	46.3%	47.9%	49.4%	50.9%	52.1%	53.5%	54.5%	56.2%	57.2%	58.0%	58.9%	59.8%	60.5%
	130	1.3%	14.0%	27.1%	34.1%	38.2%	41.1%	43.7%	45.5%	47.4%	49.0%	50.6%	51.8%	53.3%	54.7%	56.2%	57.4%	58.5%	59.6%	60.5%
	135	1.3%	13.8%	26.4%	33.1%	36.8%	40.0%	42.4%	44.5%	46.5%	48.3%	49.8%	51.2%	53.3%	54.1%	55.6%	57.0%	58.4%	59.4%	60.5%

Figure 0-10: (30MWth Sodium Polar Receiver) Optical Efficiency Map, without reflectivity losses.

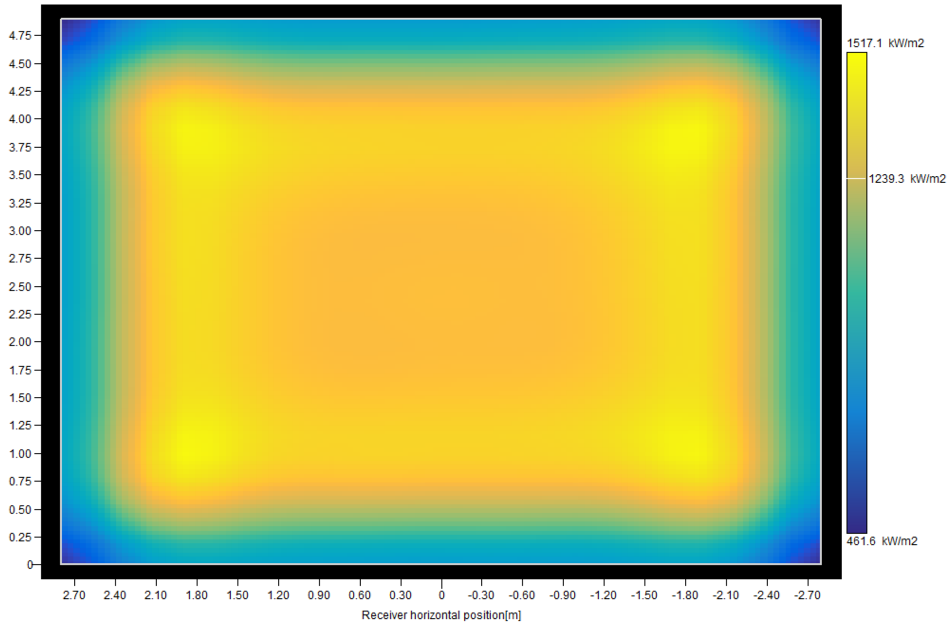

Figure 0-11: (30MWth Sodium Polar Receiver) Flux distribution at Autumnal Equinox.

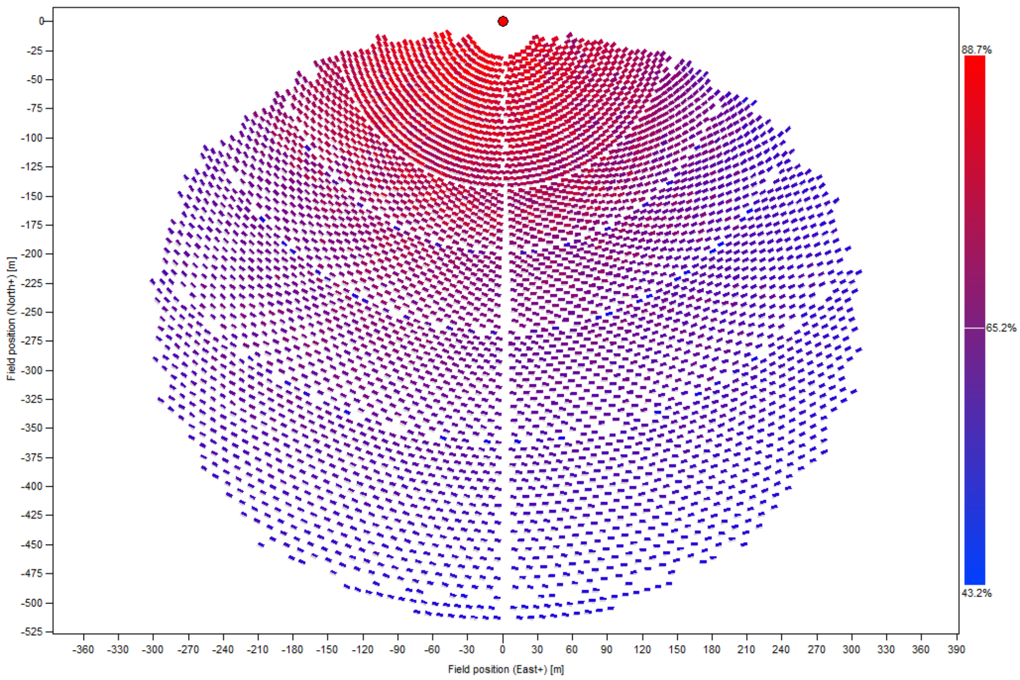

Figure 0-12: (30MWth Sodium Polar Receiver) Layout

e. $50\ MWth$

Table 0-9: (50MWth Sodium Polar Receiver) Parametric Analysis Range for the Initial Guess and the Narrower Optimization.

	Initial Parametric Analysis		*Second Parametric Analysis*	
	Min	Max	Min	Max
Receiver Height [m]	5.5	8.3	6.2	7
Step [m]	0.7		0.2	
Aspect Ratio [-]	0.5	2	0.5	2
Step [-]	0.25		0.25	
Tower Height [m]	80	102.5	95	107
Step [m]	7.5		4	

Table 0-10: (50MWth Sodium Polar Receiver) Summary of Results from both parametric analyses, showing the top 4 choices for each parametric analysis.

		Initial Parametric Analysis				*Second Parametric Analysis*			
		1	2	3	4	1	2	3	4
Receiver Height	**m**	**6.2**	**6.9**	**6.2**	**6.9**	**6.2**	**6.4**	**6.6**	**6.4**
Receiver Diameter	**m**	**7.09**	**7.89**	**7.09**	**7.89**	**7.09**	**7.31**	**7.54**	**7.31**
Tower Height	**m**	**95**	**95**	**102.5**	**102.5**	**99**	**99**	**99**	**103**
Receiver Area	m^2	43.958	54.441	43.958	54.441	43.958	46.784	49.764	46.784
Total plant cost	**$**	**$18,391 ,406**	**$18,279 ,283**	**$18,214 ,586**	**$18,187 ,405**	**$18,262 ,151**	**$18,217 ,592**	**$18,191 ,162**	**$18,171 ,612**
Cost/Energy metric	-	**0.76**	**0.785**	**0.772**	**0.799**	**0.765**	**0.772**	**0.779**	**0.779**
Simulated heliostat area	m^2	94191.6	91456.9	91679.7	89489.5	92644.9	91815.8	91073.3	90764
Simulated heliostat count	-	7612	7391	7409	7232	7487	7420	7360	7335
Power incident on field	kW	89482	86884.1	87095.7	85015	88012.6	87225	86519.7	86225.8
Power absorbed by the receiver	kW	49622.7	50051.3	49227.7	49748.3	49435.8	49542.9	49656.7	49369.2
Power absorbed by the HTF	**kW**	**46824.7**	**46586.2**	**46429. 8**	**46283. 1**	**46637. 9**	**46565. 1**	**46489. 2**	**46391. 4**
Cloudiness efficiency	%	100	100	100	100	100	100	100	100
Shading efficiency	%	100	100	100	100	100	100	100	100
Cosine efficiency	%	88.7	88.8	89.3	89.4	89	89.1	89.1	89.4
Reflection efficiency	%	90.3	90.3	90.3	90.3	90.2	90.2	90.2	90.2
Blocking efficiency	%	99.7	99.8	99.7	99.8	99.7	99.8	99.8	99.8
Attenuation efficiency	%	95.8	95.9	95.9	95.9	95.9	95.9	95.9	95.9
Image intercept efficiency	%	77.2	80	77.9	80.5	77.8	78.6	79.3	78.9
Absorption efficiency	%	94	94	94	94	94	94	94	94
Solar Field Optical Efficiency	**%**	**59.0%**	**61.3%**	**60.1%**	**62.2%**	**59.8%**	**60.4%**	**61.1%**	**61.0%**
Thermal Efficiency	**%**	**88.7%**	**87.5%**	**88.7%**	**87.5%**	**88.7%**	**88.4%**	**88.0%**	**88.3%**
Average incident flux	kW/ m2	1200.9	978.1	1191.4	972.1	1196.4	1126.6	1061.5	1122.6
Peak incident flux	kW/ m2	1478.6	1196.5	1486.5	1198.3	1482.9	1392.8	1313.1	1400.6

Azimuth	Elevation: 0	5	10	15	20	25	30	35	40	45	50	55	60	65	70	75	80	85	90
-130	1.0%	14.3%	27.7%	34.7%	38.5%	41.5%	44.0%	45.9%	47.6%	48.9%	50.9%	52.3%	53.6%	54.9%	56.1%	57.2%	58.3%	59.4%	60.3%
-120	1.0%	14.6%	29.1%	36.8%	41.2%	44.1%	46.6%	48.2%	49.6%	51.1%	52.1%	53.3%	54.6%	56.1%	56.7%	57.8%	58.7%	59.6%	60.3%
-110	1.0%	14.5%	30.6%	39.1%	43.9%	47.0%	49.3%	50.4%	51.7%	53.0%	54.3%	54.8%	55.7%	56.7%	58.0%	58.5%	59.1%	59.8%	60.3%
-100	1.0%	14.0%	32.1%	41.6%	46.7%	49.8%	52.1%	53.2%	54.1%	55.0%	56.0%	56.9%	57.8%	57.8%	58.7%	59.3%	59.7%	60.0%	60.3%
-90	1.0%	14.0%	33.5%	43.5%	49.4%	52.8%	54.9%	55.7%	56.6%	57.4%	57.9%	58.5%	59.0%	59.5%	59.7%	60.0%	60.0%	60.2%	60.3%
-80	1.0%	13.2%	34.5%	45.6%	51.8%	55.5%	57.6%	58.3%	58.8%	59.4%	59.4%	60.0%	60.4%	60.4%	60.5%	60.9%	60.9%	60.4%	60.3%
-70	1.0%	12.8%	36.0%	47.4%	54.0%	57.8%	59.5%	60.4%	61.3%	61.6%	61.8%	61.7%	62.0%	61.6%	61.5%	61.3%	61.3%	60.7%	60.3%
-60	1.1%	12.3%	37.2%	49.4%	55.9%	59.6%	62.2%	62.7%	63.3%	62.6%	62.7%	63.4%	62.4%	62.9%	62.4%	62.0%	61.5%	60.9%	60.3%
-50	1.1%	12.1%	37.9%	51.9%	58.1%	61.6%	63.6%	63.9%	65.0%	64.1%	65.0%	63.8%	64.4%	63.8%	63.2%	62.7%	61.7%	61.3%	60.3%
-40	1.2%	11.9%	38.3%	52.3%	59.9%	64.0%	66.1%	66.0%	66.4%	66.0%	65.2%	65.6%	65.3%	64.4%	63.7%	63.0%	62.4%	61.5%	60.3%
-30	1.3%	11.7%	38.8%	53.9%	61.1%	65.2%	66.5%	67.6%	67.4%	67.3%	66.1%	66.2%	66.0%	65.0%	64.5%	63.6%	62.7%	61.2%	60.3%
-20	1.3%	11.4%	39.4%	53.4%	60.9%	65.2%	68.2%	68.5%	67.3%	67.1%	66.7%	67.2%	65.7%	65.4%	64.6%	63.6%	62.7%	61.6%	60.3%
-10	1.3%	10.2%	38.7%	53.3%	61.3%	65.6%	67.9%	68.9%	68.8%	68.5%	68.1%	67.6%	66.8%	65.9%	64.8%	63.9%	62.8%	61.8%	60.3%
0	1.4%	10.1%	38.1%	53.9%	61.9%	66.4%	68.2%	68.9%	68.2%	68.5%	68.0%	67.0%	66.5%	65.9%	65.0%	63.9%	62.8%	61.5%	60.3%
10	1.4%	10.5%	38.2%	54.1%	62.1%	65.7%	67.9%	68.0%	67.9%	68.6%	68.1%	66.7%	66.6%	65.9%	65.0%	63.8%	62.8%	61.7%	60.3%
20	1.3%	11.5%	38.7%	53.4%	60.9%	65.1%	68.3%	68.5%	67.3%	68.1%	66.7%	66.3%	65.6%	65.4%	64.6%	63.7%	62.7%	61.8%	60.3%
30	1.3%	11.9%	39.5%	53.9%	60.1%	64.3%	67.3%	66.6%	67.1%	67.3%	67.0%	65.7%	65.3%	64.8%	64.5%	63.6%	62.7%	61.6%	60.3%
40	1.2%	12.0%	38.8%	52.2%	58.9%	63.9%	65.2%	66.4%	65.7%	66.3%	66.1%	64.9%	65.3%	64.4%	63.7%	63.2%	62.4%	61.3%	60.3%
50	1.2%	12.3%	38.1%	51.1%	58.5%	61.5%	63.5%	63.9%	65.0%	65.0%	65.0%	64.7%	63.5%	63.8%	63.1%	62.2%	61.7%	61.1%	60.3%
60	1.1%	12.3%	37.1%	50.1%	56.5%	60.3%	62.4%	62.9%	63.3%	63.2%	63.4%	63.1%	63.2%	62.3%	62.4%	62.0%	61.4%	60.9%	60.3%
70	1.1%	12.7%	35.2%	47.3%	53.9%	57.8%	60.3%	60.3%	60.9%	61.6%	61.4%	61.9%	61.9%	61.5%	61.5%	61.3%	60.9%	60.7%	60.3%
80	1.0%	13.2%	34.4%	45.9%	51.9%	55.0%	57.4%	58.1%	58.7%	59.3%	59.4%	59.7%	60.1%	60.4%	60.7%	60.3%	60.6%	60.4%	60.3%
90	1.0%	14.0%	33.3%	43.5%	49.3%	52.7%	54.8%	55.9%	56.5%	57.0%	57.8%	58.3%	58.7%	59.5%	59.7%	60.0%	60.2%	60.2%	60.3%
100	1.0%	13.9%	31.9%	41.5%	46.5%	49.8%	52.0%	53.1%	54.0%	55.0%	55.9%	56.9%	57.0%	57.8%	58.4%	59.3%	59.6%	60.0%	60.3%
110	1.0%	14.4%	30.5%	39.0%	43.7%	46.9%	49.1%	50.5%	51.6%	52.9%	54.1%	55.2%	55.7%	56.9%	57.6%	58.4%	59.1%	59.8%	60.3%
120	1.0%	14.4%	29.0%	36.7%	41.1%	44.0%	46.5%	48.0%	49.5%	50.9%	52.3%	53.6%	54.6%	55.6%	56.7%	57.8%	58.7%	59.6%	60.3%
130	1.0%	14.1%	27.4%	34.5%	38.6%	41.6%	43.9%	45.6%	47.6%	49.1%	50.7%	52.2%	53.6%	55.1%	56.1%	57.2%	58.3%	59.4%	60.3%
135	1.1%	13.9%	26.7%	33.3%	37.4%	40.4%	42.8%	44.8%	46.6%	48.4%	50.1%	51.2%	53.0%	54.4%	55.7%	56.9%	58.2%	59.3%	60.3%

Figure 0-13: (50MWth Sodium Polar Receiver) Optical Efficiency Map, without reflectivity losses.

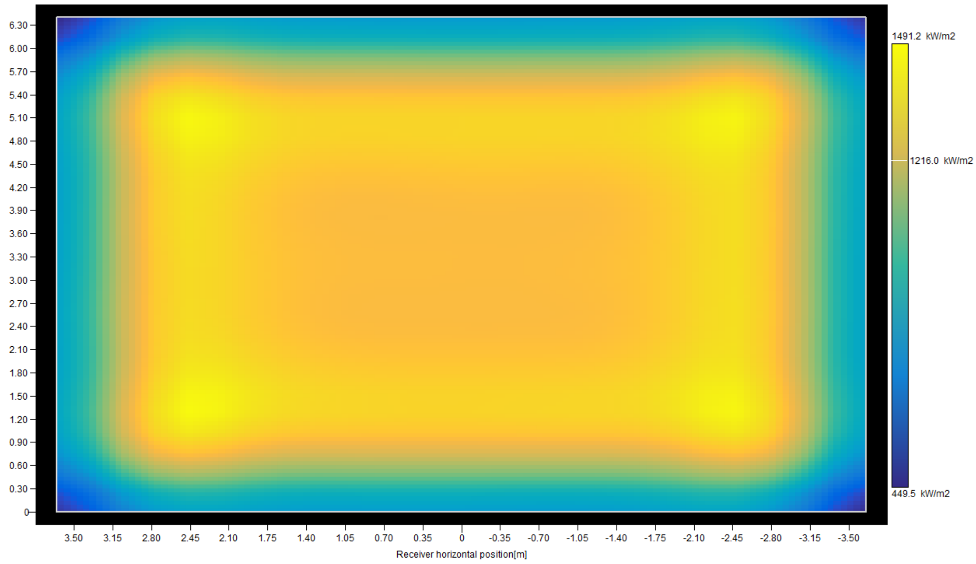

Figure 0-14: (50MWth Sodium Polar Receiver) Flux distribution at Autumnal Equinox.

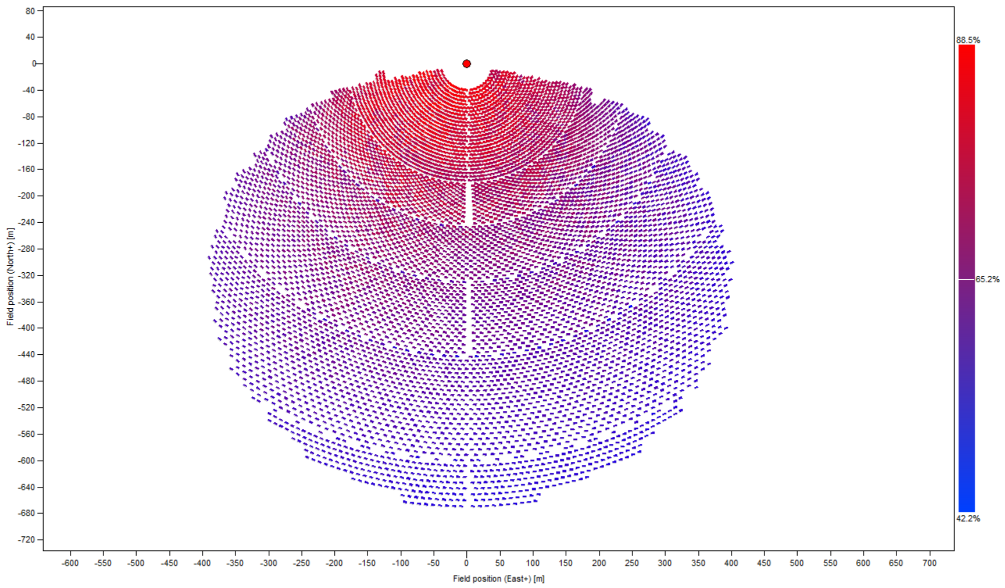

Figure 0-15: (50MWth Sodium Polar Receiver) Layout

C. Sodium Central Receivers

a. 150 $MWth$

Table 0-11: (150MWth Sodium Central Receiver) Parametric Analysis Range for the Initial Guess and the Narrower Optimization.

	Initial Parametric Analysis		*Second Parametric Analysis*	
	Min	Max	Min	Max
Receiver Height [m]	8	10	8	8.8
Step [m]	0.5		0.2	
Aspect Ratio [-]	1	2	1	2
Step [-]	0.25		0.25	
Tower Height [m]	140	155	140	146
Step [m]	5		2	

Table 0-12: (150MWth Sodium Central Receiver) Summary of Results from both parametric analyses, showing the top 4 choices for each parametric analysis.

		Initial Parametric Analysis				*Second Parametric Analysis*			
		1	2	3	4	1	2	3	4
Receiver Height	**m**	**8**	**8.5**	**8.5**	**8.5**	**8**	**8**	**8.2**	**8**
Receiver Diameter	**m**	**6.4**	**5.67**	**6.8**	**6.8**	**6.4**	**6.4**	**6.56**	**6.4**
Tower Height	**m**	**140**	**140**	**145**	**155**	**140**	**142**	**142**	**144**
Receiver Area	m^2	161	151	182	182	161	161	169	161
Total plant cost	**$**	**$53,637,947**	**$53,765,149**	**$54,321,784**	**$54,363,515**	**$53,637,947**	**$53,547,592**	**$53,814,919**	**$53,618,530**
Cost/Energy metric	**-**	**0.572**	**0.573**	**0.587**	**0.596**	**0.572**	**0.573**	**0.577**	**0.576**
Simulated heliostat area	m^2	266707.3	270548.5	262994.2	260177.3	266707.3	265555	264658.7	265426.9
Simulated heliostat count	-	2083	2113	2054	2032	2083	2074	2067	2073
Power incident on field	kW	253372	257021.1	249844.5	247168.4	253372	252277.2	251425.7	252155.6
Power absorbed by the receiver	kW	157930.2	156569.4	159551.2	159595.5	157930.2	157850.9	158500.9	157719.7
Power absorbed by the HTF	**kW**	**147692**	**146932**	**147993**	**148038**	**147692**	**147613**	**147745**	**147482**
Cloudiness efficiency	%	100	100	100	100	100	100	100	100
Shading efficiency	%	100	100	100	100	100	100	100	100
Cosine efficiency	%	83.7	83.6	84.2	84.9	83.7	83.8	83.9	83.9
Reflection efficiency	%	90.3	90.3	90.3	90.3	90.3	90.2	90.3	90.2
Blocking efficiency	%	99.1	99	99.2	99.2	99.1	99.1	99.1	99.1
Attenuation efficiency	%	95.6	95.6	95.6	95.6	95.6	95.6	95.6	95.6
Image intercept efficiency	%	92.7	90.8	94.3	94.6	92.7	92.9	93.5	92.8
Absorption efficiency	%	94	94	94	94	94	94	94	94
Solar Field Optical Efficiency	**%**	**66.3%**	**64.8%**	**68.0%**	**68.7%**	**66.3%**	**66.6%**	**67.0%**	**66.5%**
Thermal Efficiency	**%**	**87.9%**	**88.2%**	**87.2%**	**87.2%**	**87.9%**	**87.9%**	**87.6%**	**87.9%**
Average incident flux	kW/m2	1044.5	1100.1	934.7	935	1044.5	1044	997.8	1043.1
Peak incident flux	kW/m2	2142.3	2106.2	1967.7	2048.7	2142.3	2177.8	2091.5	2168.6

Azimuth \ Elevation	0	5	10	15	20	25	30	35	40	45	50	55	60	65	70	75	80	85	90
-130	1.6%	8.9%	26.9%	39.0%	45.9%	50.7%	54.4%	57.0%	59.1%	60.7%	62.0%	63.1%	63.9%	64.8%	65.5%	66.3%	66.7%	67.1%	67.4%
-120	1.7%	9.0%	27.1%	39.3%	46.3%	51.2%	54.8%	57.4%	59.5%	61.2%	62.3%	63.3%	64.3%	65.0%	65.7%	66.4%	66.8%	67.2%	67.4%
-110	1.7%	9.1%	27.4%	39.8%	46.7%	51.6%	55.3%	58.0%	60.0%	61.5%	62.7%	63.6%	64.5%	65.2%	66.0%	66.5%	66.9%	67.2%	67.4%
-100	1.7%	9.1%	27.9%	40.3%	47.2%	52.1%	55.9%	58.5%	60.4%	61.9%	63.1%	64.0%	64.8%	65.5%	66.1%	66.6%	67.0%	67.3%	67.4%
-90	1.8%	9.0%	28.4%	40.9%	47.8%	52.7%	56.4%	58.9%	61.0%	62.3%	63.4%	64.4%	65.1%	65.7%	66.3%	66.8%	67.1%	67.3%	67.4%
-80	1.7%	9.1%	28.6%	41.3%	48.3%	53.2%	56.9%	59.5%	61.4%	62.8%	63.8%	64.7%	65.3%	66.0%	66.5%	66.9%	67.2%	67.4%	67.4%
-70	1.8%	9.3%	28.8%	41.5%	48.7%	53.7%	57.3%	59.9%	61.8%	63.2%	64.1%	65.0%	65.6%	66.2%	66.7%	67.0%	67.3%	67.4%	67.4%
-60	1.8%	9.1%	29.1%	42.0%	49.1%	54.3%	57.9%	60.3%	62.1%	63.5%	64.5%	65.2%	65.9%	66.4%	66.8%	67.2%	67.4%	67.4%	67.4%
-50	1.8%	9.0%	29.7%	42.6%	49.7%	54.7%	58.3%	60.7%	62.6%	63.8%	64.8%	65.5%	66.1%	66.6%	67.0%	67.3%	67.4%	67.6%	67.4%
-40	1.8%	9.1%	29.9%	42.8%	49.9%	55.0%	58.5%	61.0%	62.8%	64.1%	65.0%	65.7%	66.3%	66.7%	67.1%	67.3%	67.6%	67.6%	67.4%
-30	1.9%	8.8%	29.8%	43.0%	50.1%	55.2%	58.8%	61.3%	63.0%	64.4%	65.2%	65.9%	66.4%	66.8%	67.1%	67.4%	67.6%	67.6%	67.4%
-20	1.9%	9.0%	29.9%	43.0%	50.2%	55.3%	58.9%	61.4%	63.2%	64.5%	65.3%	66.0%	66.5%	66.9%	67.2%	67.4%	67.6%	67.6%	67.4%
-10	1.9%	8.9%	29.8%	43.0%	50.2%	55.4%	59.0%	61.5%	63.2%	64.5%	65.3%	66.0%	66.5%	66.9%	67.2%	67.6%	67.7%	67.6%	67.4%
0	1.9%	8.9%	29.9%	43.1%	50.2%	55.4%	58.9%	61.4%	63.2%	64.5%	65.3%	66.0%	66.5%	66.9%	67.2%	67.6%	67.7%	67.6%	67.4%
10	1.9%	8.9%	29.7%	42.9%	50.1%	55.3%	58.9%	61.4%	63.1%	64.4%	65.2%	66.0%	66.5%	66.9%	67.2%	67.4%	67.6%	67.6%	67.4%
20	1.8%	9.0%	29.8%	42.9%	50.0%	55.1%	58.7%	61.2%	63.0%	64.3%	65.1%	65.9%	66.4%	66.8%	67.1%	67.4%	67.6%	67.6%	67.4%
30	1.8%	8.9%	29.6%	42.7%	49.8%	54.9%	58.5%	61.0%	62.8%	64.0%	64.9%	65.6%	66.2%	66.7%	67.0%	67.3%	67.6%	67.6%	67.4%
40	1.8%	9.1%	29.6%	42.3%	49.5%	54.5%	58.1%	60.5%	62.4%	63.7%	64.7%	65.4%	66.1%	66.5%	66.9%	67.2%	67.4%	67.6%	67.4%
50	1.7%	9.0%	29.3%	42.0%	49.1%	54.1%	57.7%	60.2%	62.0%	63.4%	64.4%	65.2%	65.7%	66.3%	66.8%	67.1%	67.3%	67.4%	67.4%
60	1.7%	9.1%	28.7%	41.5%	48.6%	53.6%	57.2%	59.8%	61.6%	63.1%	64.0%	64.9%	65.5%	66.2%	66.6%	67.0%	67.3%	67.4%	67.4%
70	1.8%	9.3%	28.4%	41.0%	48.1%	53.1%	56.7%	59.3%	61.2%	62.7%	63.7%	64.6%	65.3%	65.9%	66.4%	66.9%	67.2%	67.3%	67.4%
80	1.7%	9.1%	28.2%	40.6%	47.7%	52.6%	56.2%	58.8%	60.7%	62.2%	63.3%	64.3%	65.0%	65.6%	66.3%	66.7%	67.1%	67.3%	67.4%
90	1.8%	9.0%	27.9%	40.2%	47.1%	52.0%	55.6%	58.3%	60.3%	61.8%	63.0%	63.9%	64.7%	65.4%	66.1%	66.6%	67.0%	67.3%	67.4%
100	1.7%	9.1%	27.3%	39.7%	46.6%	51.5%	55.2%	57.8%	59.8%	61.4%	62.6%	63.5%	64.5%	65.2%	65.9%	66.5%	66.9%	67.2%	67.4%
110	1.7%	9.0%	27.0%	39.1%	46.1%	51.0%	54.7%	57.3%	59.4%	61.1%	62.2%	63.3%	64.1%	64.9%	65.6%	66.3%	66.8%	67.2%	67.4%
120	1.7%	9.0%	26.7%	38.8%	45.6%	50.5%	54.3%	56.9%	59.0%	60.6%	61.9%	63.0%	63.9%	64.7%	65.5%	66.2%	66.7%	67.1%	67.4%
130	1.6%	9.0%	26.7%	38.6%	45.4%	50.2%	53.8%	56.6%	58.6%	60.3%	61.6%	62.7%	63.7%	64.6%	65.3%	66.1%	66.7%	67.1%	67.4%
135	1.7%	9.0%	26.7%	38.5%	45.2%	50.0%	53.7%	56.4%	58.5%	60.2%	61.5%	62.6%	63.6%	64.5%	65.3%	66.1%	66.6%	67.1%	67.4%

Figure 0-16: (150MWth Sodium Central Receiver) Efficiency Map without reflectivity losses

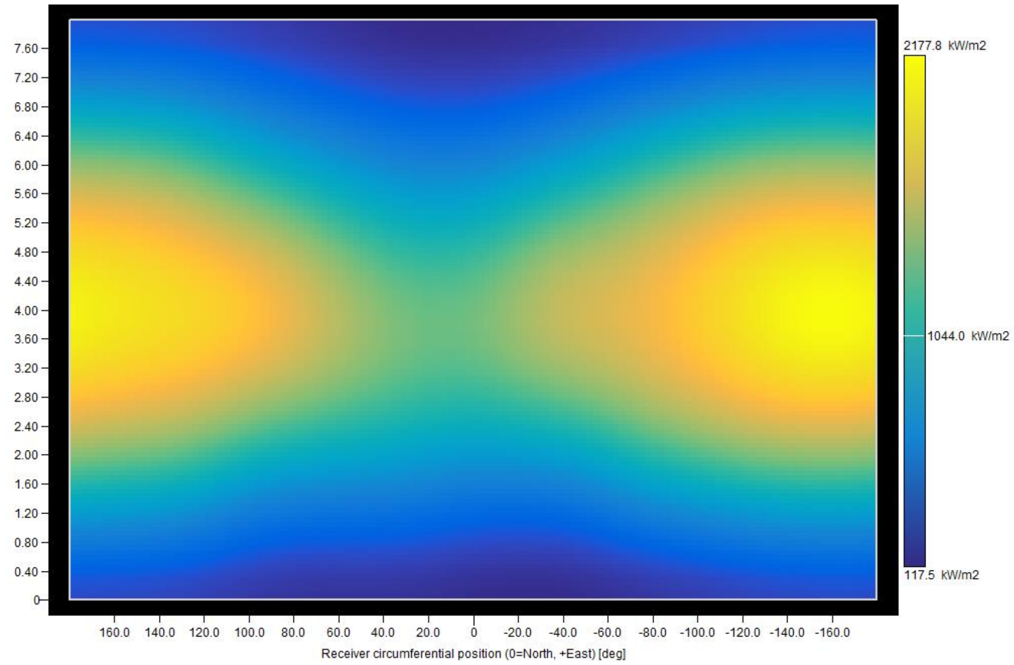

Figure 0-17: (150MWth Sodium Central Receiver) Flux distribution at Equinox.

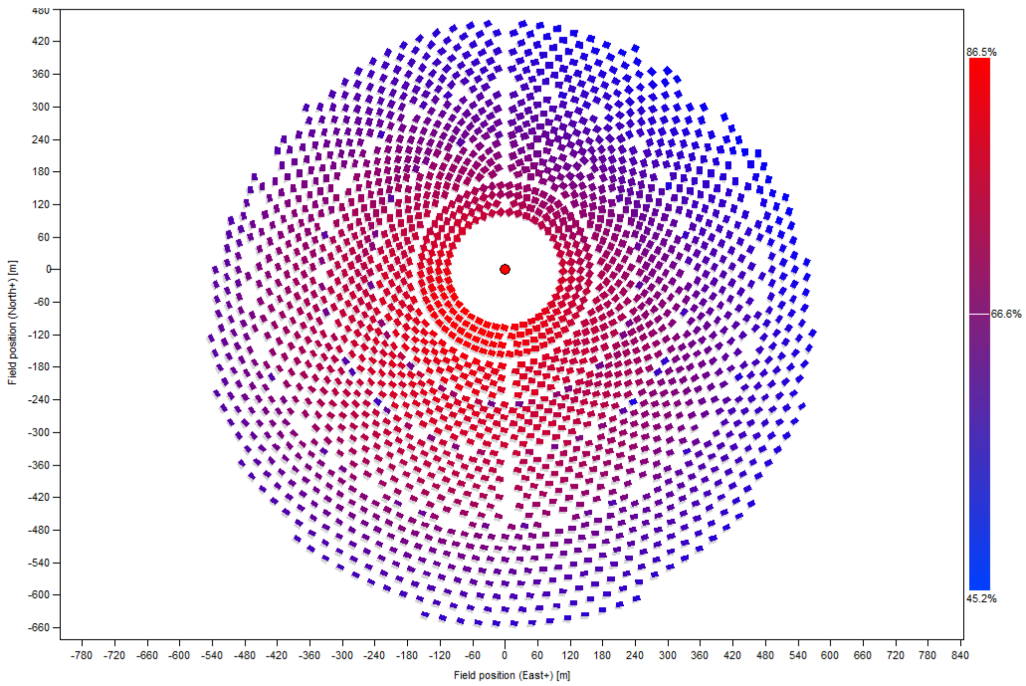

Figure 0-18: (150MWth Sodium Central Receiver) Layout.

b. $250\ MWth$

Table 0-13: (250MWth Sodium Central Receiver) Parametric Analysis Range for the Initial Guess and the Narrower Optimization.

	Initial Parametric Analysis		Second Parametric Analysis	
	Min	Max	Min	Max
Receiver Height [m]	9	12	9	10.2
Step [m]	0.75		0.3	
Aspect Ratio [-]	1	2	1	2
Step [-]	0.25		0.25	
Tower Height [m]	150	177	162	174
Step [m]	9		4	

Table 0-14: (250MWth Sodium Central Receiver) Summary of Results from both parametric analyses, showing the top 4 choices for each parametric analysis.

		Initial Parametric Analysis				Second Parametric Analysis			
		1	2	3	4	1	2	3	4
Receiver Height	**m**	**9**	**9.75**	**9**	**10.5**	**9.9**	**9**	**9.9**	**9.9**
Receiver Diameter	**m**	**9**	**7.8**	**9**	**8.4**	**7.92**	**9**	**7.92**	**7.92**
Tower Height	**m**	**159**	**159**	**168**	**177**	**162**	**166**	**166**	**170**
Receiver Area	m^2	254	239	254	277	246	254	246	246
Total plant cost	**$**	**$89,170,925**	**$88,692,994**	**$88,811,154**	**$89,093,765**	**$88,620,463**	**$88,761,940**	**$88,374,773**	**$88,334,880**
Cost/Energy metric	**-**	**0.529**	**0.527**	**0.534**	**0.544**	**0.529**	**0.531**	**0.53**	**0.533**
Simulated heliostat area	m^2	458639	460560	453262	444555	456719	453646	453774	452109
Simulated heliostat count	-	3582	3597	3540	3472	3567	3543	3544	3531
Power incident on field	kW	435707.3	437531.9	430598.5	422327.1	433882.7	430963.4	431085.1	429503.8
Power absorbed by the receiver	kW	261754.7	259586.5	261408.8	263012	260248.5	261755.4	260299.1	260167.1
Power absorbed by the HTF	**kW**	**245557.8**	**244379.3**	**245211.8**	**245375.4**	**244569.9**	**245558.5**	**244620.4**	**244488.5**
Cloudiness efficiency	%	100	100	100	100	100	100	100	100
Shading efficiency	%	100	100	100	100	100	100	100	100
Cosine efficiency	%	82.1	82	82.5	83.3	82.2	82.5	82.5	82.6
Reflection efficiency	%	90.3	90.3	90.3	90.3	90.2	90.2	90.2	90.3
Blocking efficiency	%	98.9	98.8	99.1	99.3	98.9	98.9	98.8	99.1
Attenuation efficiency	%	94.5	94.5	94.6	94.6	94.6	94.6	94.6	94.6
Image intercept efficiency	%	92.3	91.3	92.6	93.9	92	92.8	92.3	92.3
Absorption efficiency	%	94	94	94	94	94	94	94	94
Solar Field Optical Efficiency	**%**	**63.9%**	**63.1%**	**64.6%**	**66.3%**	**63.8%**	**64.6%**	**64.3%**	**64.5%**
Thermal Efficiency	**%**	**88.2%**	**88.5%**	**88.2%**	**87.7%**	**88.3%**	**88.2%**	**88.3%**	**88.3%**
Average incident flux	kW/m2	1094.3	1155.9	1092.8	1009.8	1124	1094.3	1124.2	1123.6
Peak incident flux	kW/m2	2157.1	2128.2	2191.5	1994.5	2095.4	2192	2121.7	2195.6

Azimuth \ Elevation	0	5	10	15	20	25	30	35	40	45	50	55	60	65	70	75	80	85	90
-130	1.4%	9.9%	28.2%	39.9%	46.4%	51.1%	54.4%	56.7%	58.5%	59.8%	60.9%	61.7%	62.4%	63.2%	63.8%	64.4%	64.9%	65.2%	65.4%
-120	1.4%	10.0%	28.4%	40.1%	46.7%	51.4%	54.7%	57.0%	58.7%	60.1%	61.1%	61.9%	62.7%	63.3%	63.9%	64.5%	64.9%	65.2%	65.4%
-110	1.5%	10.1%	28.6%	40.4%	47.0%	51.7%	55.0%	57.3%	59.0%	60.3%	61.3%	62.1%	62.8%	63.5%	64.0%	64.6%	65.0%	65.3%	65.4%
-100	1.5%	10.1%	29.0%	40.9%	47.3%	52.0%	55.3%	57.7%	59.4%	60.6%	61.5%	62.3%	63.0%	63.6%	64.1%	64.7%	65.0%	65.3%	65.4%
-90	1.5%	10.2%	29.4%	41.2%	47.8%	52.4%	55.7%	58.0%	59.7%	60.9%	61.8%	62.6%	63.2%	63.7%	64.3%	64.8%	65.1%	65.3%	65.4%
-80	1.5%	10.2%	29.6%	41.5%	48.1%	52.8%	56.1%	58.3%	60.0%	61.2%	62.0%	62.8%	63.4%	63.9%	64.4%	64.8%	65.2%	65.4%	65.4%
-70	1.5%	10.3%	29.7%	41.7%	48.4%	53.2%	56.4%	58.6%	60.2%	61.4%	62.2%	63.0%	63.5%	64.0%	64.5%	64.9%	65.2%	65.4%	65.4%
-60	1.5%	10.3%	30.0%	42.0%	48.8%	53.5%	56.7%	58.9%	60.5%	61.6%	62.4%	63.1%	63.7%	64.1%	64.6%	65.0%	65.3%	65.4%	65.4%
-50	1.6%	10.3%	30.3%	42.4%	49.1%	53.8%	57.0%	59.1%	60.7%	61.8%	62.7%	63.3%	63.8%	64.3%	64.7%	65.1%	65.3%	65.4%	65.4%
-40	1.6%	10.2%	30.4%	42.6%	49.3%	53.9%	57.1%	59.4%	61.0%	62.0%	62.8%	63.4%	63.9%	64.4%	64.8%	65.1%	65.3%	65.4%	65.4%
-30	1.6%	10.2%	30.4%	42.7%	49.4%	54.0%	57.3%	59.5%	61.1%	62.1%	62.9%	63.5%	64.0%	64.5%	64.8%	65.1%	65.4%	65.5%	65.4%
-20	1.6%	10.2%	30.4%	42.7%	49.5%	54.1%	57.4%	59.6%	61.2%	62.2%	63.0%	63.6%	64.0%	64.5%	64.9%	65.2%	65.4%	65.5%	65.4%
-10	1.6%	10.2%	30.3%	42.7%	49.5%	54.3%	57.4%	59.6%	61.2%	62.2%	63.0%	63.6%	64.1%	64.6%	64.9%	65.2%	65.4%	65.5%	65.4%
0	1.6%	10.0%	30.3%	42.7%	49.5%	54.1%	57.4%	59.6%	61.2%	62.2%	63.0%	63.6%	64.0%	64.5%	64.9%	65.2%	65.4%	65.5%	65.4%
10	1.6%	10.2%	30.3%	42.7%	49.5%	54.1%	57.3%	59.6%	61.1%	62.1%	62.9%	63.5%	64.0%	64.5%	64.9%	65.2%	65.4%	65.5%	65.4%
20	1.6%	10.3%	30.3%	42.6%	49.3%	54.0%	57.2%	59.4%	61.0%	62.0%	62.9%	63.4%	63.9%	64.5%	64.8%	65.1%	65.3%	65.5%	65.4%
30	1.6%	10.2%	30.3%	42.4%	49.1%	53.8%	57.0%	59.3%	60.9%	61.9%	62.7%	63.3%	63.8%	64.4%	64.8%	65.1%	65.3%	65.4%	65.4%
40	1.6%	10.2%	30.1%	42.1%	48.8%	53.6%	56.8%	59.0%	60.6%	61.7%	62.6%	63.2%	63.7%	64.3%	64.7%	65.0%	65.3%	65.4%	65.4%
50	1.6%	10.2%	29.9%	42.0%	48.6%	53.3%	56.5%	58.7%	60.3%	61.5%	62.3%	63.0%	63.6%	64.1%	64.6%	65.0%	65.2%	65.4%	65.4%
60	1.5%	10.2%	29.5%	41.6%	48.3%	53.0%	56.2%	58.4%	60.1%	61.3%	62.1%	62.9%	63.4%	63.9%	64.5%	64.9%	65.2%	65.4%	65.4%
70	1.5%	10.2%	29.3%	41.2%	47.9%	52.6%	55.9%	58.1%	59.8%	61.0%	61.9%	62.7%	63.3%	63.8%	64.4%	64.8%	65.1%	65.3%	65.4%
80	1.5%	10.2%	29.1%	41.0%	47.6%	52.2%	55.5%	57.8%	59.5%	60.7%	61.6%	62.4%	63.1%	63.7%	64.3%	64.7%	65.1%	65.3%	65.4%
90	1.5%	10.1%	28.9%	40.6%	47.1%	51.8%	55.1%	57.4%	59.3%	60.4%	61.4%	62.2%	62.9%	63.5%	64.0%	64.6%	65.0%	65.3%	65.4%
100	1.5%	10.0%	28.5%	40.2%	46.8%	51.5%	54.8%	57.1%	58.9%	60.2%	61.2%	62.0%	62.7%	63.4%	63.9%	64.5%	65.0%	65.3%	65.4%
110	1.5%	10.1%	28.2%	39.9%	46.5%	51.2%	54.5%	56.8%	58.6%	59.9%	61.0%	61.8%	62.6%	63.2%	63.8%	64.4%	64.9%	65.2%	65.4%
120	1.4%	10.0%	28.0%	39.7%	46.3%	50.9%	54.3%	56.6%	58.3%	59.7%	60.7%	61.6%	62.3%	63.1%	63.7%	64.4%	64.8%	65.2%	65.4%
130	1.5%	9.9%	28.0%	39.6%	46.1%	50.6%	53.9%	56.4%	58.1%	59.5%	60.5%	61.4%	62.2%	63.0%	63.6%	64.3%	64.8%	65.2%	65.4%
135	1.4%	9.9%	28.0%	39.5%	46.0%	50.5%	53.8%	56.3%	58.1%	59.4%	60.4%	61.4%	62.1%	62.9%	63.6%	64.3%	64.8%	65.2%	65.4%

Figure 0-19: (250MWth Sodium Central Receiver) Efficiency Map without reflectivity losses

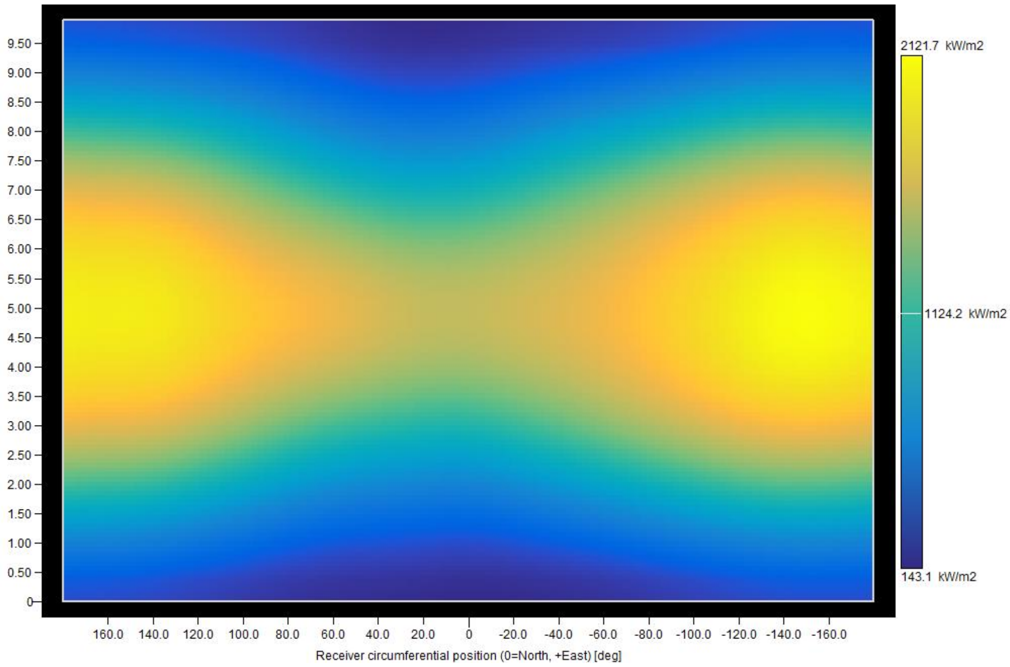

Figure 0-20: (250MWth Sodium Central Receiver) Flux distribution at Equinox.

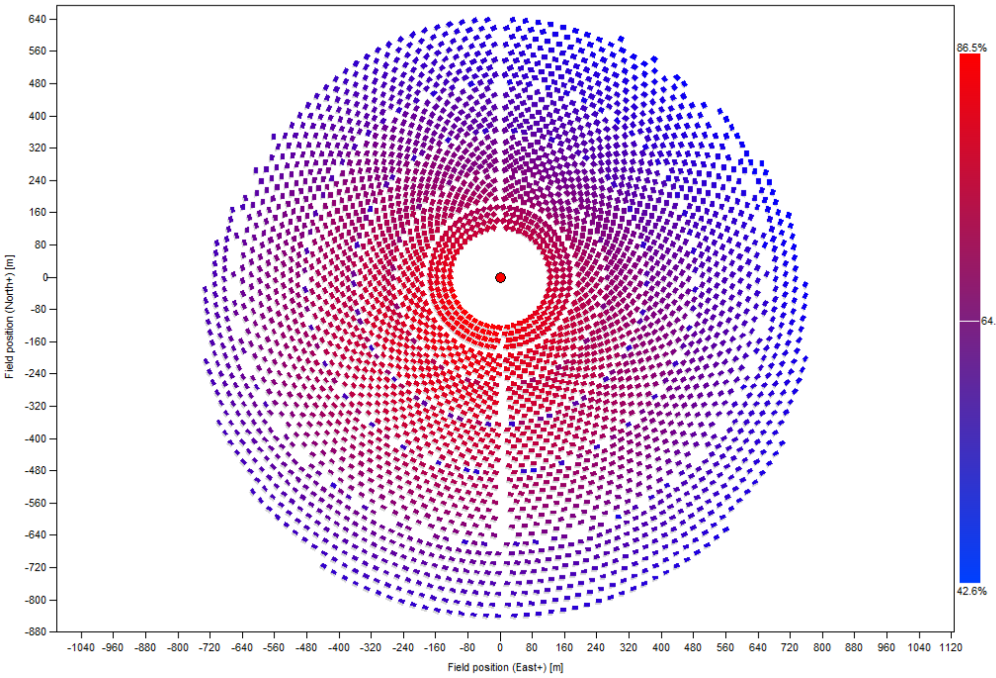

Figure 0-21: (250MWth Sodium Central Receiver) Layout

c. 500 $MWth$

Table 0-15: (500MWth Sodium Central Receiver) Parametric Analysis Range for the Initial Guess and the Narrower Optimization.

	Initial Parametric Analysis		*Second Parametric Analysis*	
	Min	Max	Min	Max
Receiver Height [m]	11	15	13	14.2
Step [m]	1		0.3	
Aspect Ratio [-]	1	2	1	2
Step [-]	0.25		0.25	
Tower Height [m]	190	212.5	197.5	209.5
Step [m]	12.5		5	

Table 0-16: (500MWth Sodium Central Receiver) Summary of Results from both parametric analyses, showing the top 4 choices for each parametric analysis.

		Initial Parametric Analysis				*Second Parametric Analysis*			
		1	2	3	4	1	2	3	4
Receiver Height	**m**	**13**	**13**	**14**	**14**	**14.2**	**13**	**13.3**	**13.3**
Receiver Diameter	**m**	**10.4**	**10.4**	**9.33**	**11.2**	**8.67**	**10.4**	**10.64**	**10.64**
Tower Height	**m**	**197.5**	**205**	**205**	**212.5**	**197.5**	**205.5**	**205.5**	**209.5**
Receiver Area	m^2	425	425	410	493	387	425	445	445
Total plant cost	**$**	**###########**	**###########**	**###########**	**###########**	**###########**	**###########**	**###########**	**###########**
Cost/Energy metric	**-**	**0.503**	**0.503**	**0.508**	**0.507**	**0.516**	**0.503**	**0.503**	**0.504**
Simulated heliostat area	m^2	983987	968751	986164	937765	1028289	968623	960684	954794
Simulated heliostat count	-	7685	7566	7702	7324	8031	7565	7503	7457
Power incident on field	kW	934788	920313.1	936855.9	890876.7	976874.8	920191.5	912649.9	907054.6
Power absorbed by the receiver	kW	514135.6	513587.2	511358.7	518323.2	509222.8	513610.3	515022.5	514862.6
Power absorbed by the HTF	**kW**	**487100.7**	**486552.3**	**485239.6**	**486969.1**	**484604.6**	**486575.4**	**486725.5**	**486565.6**
Cloudiness efficiency	%	100	100	100	100	100	100	100	100
Shading efficiency	%	100	100	100	100	100	100	100	100
Cosine efficiency	%	80.3	80.6	80.5	81.1	80	80.6	80.7	80.8
Reflection efficiency	%	90.2	90.3	90.2	90.2	90.3	90.3	90.3	90.2
Blocking efficiency	%	98.6	98.8	98.7	99	98.6	98.8	98.9	98.9
Attenuation efficiency	%	92.5	92.6	92.5	92.7	92.3	92.6	92.6	92.7
Image intercept efficiency	%	88.5	89.2	87.4	92.1	84.3	89.2	90	90.3
Absorption efficiency	%	94	94	94	94	94	94	94	94
Solar Field Optical Efficiency	**%**	**58.5%**	**59.4%**	**58.1%**	**61.9%**	**55.4%**	**59.4%**	**60.0%**	**60.4%**
Thermal Efficiency	**%**	**89.1%**	**89.1%**	**89.2%**	**88.3%**	**89.5%**	**89.1%**	**88.8%**	**88.8%**
Average incident flux	kW/m2	1287.7	1286.4	1325.7	1119.4	1400.6	1286.4	1232.4	1232
Peak incident flux	kW/m2	2159.9	2198.8	2189.7	1916.5	2190.8	2199.9	2091.7	2110.6

Azimuth \ Elevation	0	5	10	15	20	25	30	35	40	45	50	55	60	65	70	75	80	85	90
-130	1.0%	11.9%	27.8%	37.0%	42.2%	45.9%	48.3%	50.0%	51.4%	52.3%	53.2%	53.9%	54.6%	55.1%	55.6%	56.2%	56.5%	56.8%	56.9%
-120	1.0%	12.0%	27.9%	37.0%	42.3%	46.0%	48.4%	50.2%	51.5%	52.4%	53.3%	53.9%	54.6%	55.2%	55.7%	56.2%	56.5%	56.8%	56.9%
-110	1.0%	12.0%	28.0%	37.2%	42.4%	46.1%	48.6%	50.3%	51.6%	52.6%	53.4%	54.0%	54.7%	55.2%	55.7%	56.2%	56.6%	56.8%	56.9%
-100	1.0%	12.1%	28.2%	37.4%	42.7%	46.2%	48.7%	50.4%	51.7%	52.7%	53.5%	54.1%	54.8%	55.3%	55.7%	56.3%	56.6%	56.8%	56.9%
-90	1.0%	12.1%	28.4%	37.6%	42.8%	46.4%	48.8%	50.5%	51.8%	52.8%	53.6%	54.3%	54.8%	55.3%	55.9%	56.3%	56.6%	56.8%	56.9%
-80	1.0%	12.1%	28.4%	37.7%	43.0%	46.5%	49.0%	50.7%	51.9%	52.9%	53.6%	54.4%	54.9%	55.4%	55.9%	56.3%	56.6%	56.8%	56.9%
-70	1.0%	12.2%	28.4%	37.8%	43.1%	46.7%	49.1%	50.9%	52.0%	53.0%	53.7%	54.4%	55.0%	55.4%	56.0%	56.4%	56.6%	56.8%	56.9%
-60	1.0%	12.2%	28.6%	38.0%	43.2%	46.8%	49.3%	51.0%	52.1%	53.1%	53.8%	54.5%	55.0%	55.5%	56.0%	56.4%	56.7%	56.8%	56.9%
-50	1.0%	12.2%	28.7%	38.1%	43.4%	46.9%	49.4%	51.1%	52.2%	53.2%	53.9%	54.6%	55.1%	55.5%	56.0%	56.4%	56.7%	56.8%	56.9%
-40	1.1%	12.3%	28.8%	38.2%	43.4%	47.0%	49.5%	51.1%	52.3%	53.3%	53.9%	54.6%	55.1%	55.6%	56.1%	56.4%	56.7%	56.8%	56.9%
-30	1.0%	12.3%	28.9%	38.3%	43.5%	47.0%	49.5%	51.2%	52.3%	53.3%	54.0%	54.6%	55.1%	55.6%	56.1%	56.4%	56.7%	56.8%	56.9%
-20	1.0%	12.3%	28.9%	38.3%	43.5%	47.1%	49.6%	51.2%	52.4%	53.3%	54.0%	54.7%	55.2%	55.6%	56.1%	56.4%	56.7%	56.9%	56.9%
-10	1.1%	12.2%	28.8%	38.3%	43.5%	47.1%	49.6%	51.3%	52.4%	53.3%	54.0%	54.7%	55.2%	55.6%	56.1%	56.5%	56.7%	56.9%	56.9%
0	1.1%	12.2%	28.8%	38.2%	43.5%	47.1%	49.6%	51.2%	52.4%	53.3%	54.0%	54.7%	55.2%	55.6%	56.1%	56.5%	56.7%	56.9%	56.9%
10	1.1%	12.2%	28.8%	38.2%	43.5%	47.0%	49.5%	51.2%	52.4%	53.3%	54.0%	54.7%	55.1%	55.6%	56.1%	56.4%	56.7%	56.8%	56.9%
20	1.0%	12.2%	28.8%	38.2%	43.4%	47.0%	49.5%	51.2%	52.3%	53.3%	53.9%	54.6%	55.1%	55.6%	56.1%	56.4%	56.7%	56.8%	56.9%
30	1.0%	12.2%	28.8%	38.1%	43.4%	46.9%	49.4%	51.1%	52.2%	53.2%	53.9%	54.6%	55.1%	55.5%	56.1%	56.4%	56.7%	56.8%	56.9%
40	1.0%	12.2%	28.7%	38.0%	43.2%	46.8%	49.3%	51.0%	52.2%	53.1%	53.8%	54.5%	55.0%	55.5%	56.0%	56.4%	56.7%	56.8%	56.9%
50	1.0%	12.1%	28.5%	37.9%	43.2%	46.7%	49.1%	50.9%	52.1%	53.0%	53.7%	54.4%	55.0%	55.5%	56.0%	56.4%	56.6%	56.8%	56.9%
60	1.0%	12.1%	28.4%	37.7%	43.0%	46.6%	49.0%	50.7%	52.0%	53.0%	53.7%	54.4%	54.9%	55.4%	55.9%	56.3%	56.6%	56.8%	56.9%
70	1.0%	12.1%	28.2%	37.4%	42.8%	46.4%	48.8%	50.5%	51.8%	52.9%	53.6%	54.3%	54.8%	55.3%	55.9%	56.3%	56.6%	56.8%	56.9%
80	1.0%	12.0%	28.2%	37.4%	42.7%	46.3%	48.7%	50.4%	51.7%	52.8%	53.5%	54.1%	54.8%	55.3%	55.9%	56.3%	56.6%	56.8%	56.9%
90	1.0%	12.0%	28.2%	37.3%	42.4%	46.1%	48.6%	50.3%	51.6%	52.7%	53.4%	54.0%	54.7%	55.2%	55.7%	56.2%	56.6%	56.8%	56.9%
100	1.0%	12.0%	27.9%	37.1%	42.3%	46.0%	48.4%	50.2%	51.5%	52.4%	53.3%	54.0%	54.6%	55.2%	55.7%	56.2%	56.5%	56.8%	56.9%
110	1.0%	11.9%	27.8%	36.9%	42.2%	45.9%	48.3%	50.1%	51.4%	52.4%	53.2%	53.9%	54.6%	55.1%	55.6%	56.2%	56.5%	56.8%	56.9%
120	1.0%	11.9%	27.7%	36.8%	42.1%	45.7%	48.2%	50.0%	51.3%	52.3%	53.1%	53.8%	54.5%	55.1%	55.6%	56.1%	56.5%	56.7%	56.9%
130	1.0%	11.8%	27.7%	36.7%	41.9%	45.6%	48.1%	49.9%	51.2%	52.2%	53.1%	53.8%	54.5%	55.0%	55.5%	56.1%	56.5%	56.7%	56.9%
135	0.9%	11.8%	27.6%	36.7%	41.9%	45.5%	48.1%	49.8%	51.2%	52.2%	53.0%	53.7%	54.4%	55.0%	55.5%	56.1%	56.5%	56.7%	56.9%

Figure 0-22: (500MWth Sodium Central Receiver) Optical Efficiency Map, without reflectivity losses.

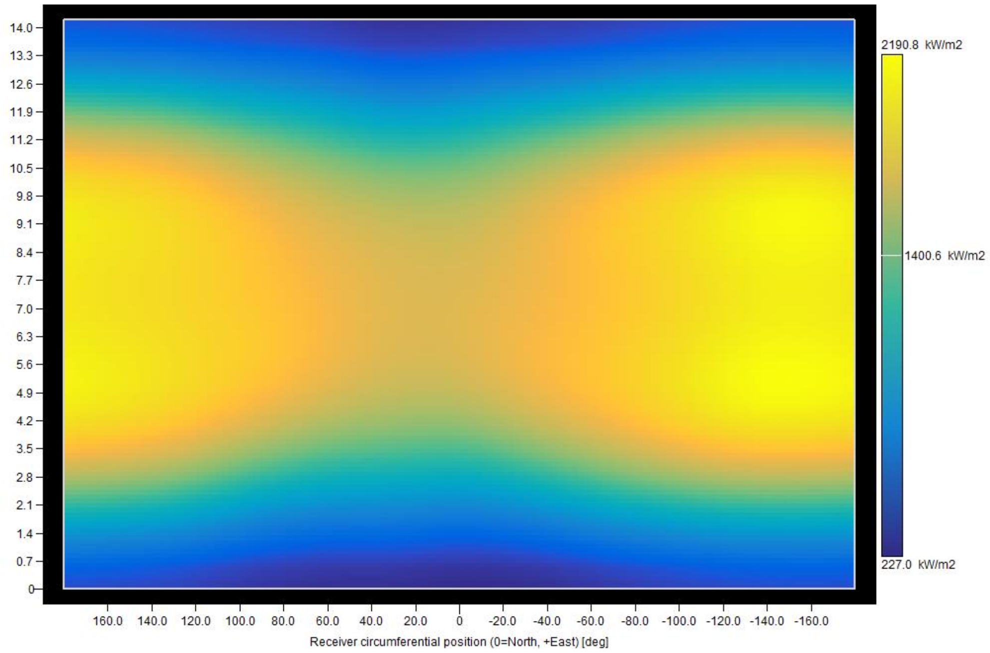

Figure 0-23: (500MWth Sodium Central Receiver) Flux distribution at Autumnal Equinox.

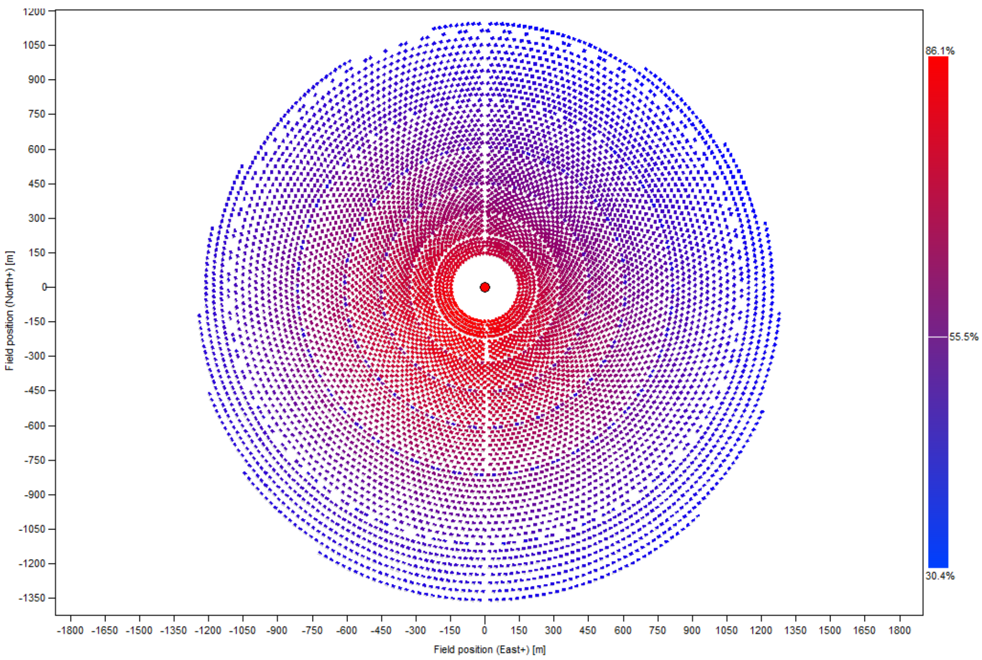

Figure 0-24: (500MWth Sodium Central Receiver) Layout